Chapter 6

Kinematic Analysis

At first glance it may seem surprising how rich and deep the study of mechanism kinematics has become considering how commonplace four-bar linkages are. A mechanical system typically comprises a power source and a linkage that transforms the power into a desired motion in a controlled, predictable, and repeatable way. Our focus will be on the linkage itself, and how to design and analyse the resulting motion. The motion design employs the many techniques of kinematic synthesis, while the study of the generated motion requires the tools and techniques of kinematic analysis, some of which will be examined in this chapter.

Modern day kinematic analysis and synthesis are rooted in the geometry of antiquity: in both the axiomatic structure of synthetic geometry and the metric structure of analytic geometry. Indeed, the modern understanding of axiomatic and non-Euclidean geometries arose from careful reflection on Euclid's work [1] over the course of the last 2300 years. Consider the following quote from [2], page 11:

> The Greeks called an axiomatic approach *synthetic* because it synthesizes (proves) new results from statements already known. The Greeks often used a process they called *analysis* to find new results that they then proved. They analyzed a problem by assuming the desired solution and worked backward to something known. We mimic this procedure in what we call analytic geometry and algebra by assuming that there is an answer, the unknown x, and solving for it. In modern times synthetic geometry has come to mean geometry without coordinates because coordinates are central to analytic geometry.

6.1 Planar Mechanisms

In this section we will examine the elementary kinematics of planar four-bar mechanisms from an advanced standpoint. The last sentence, while true, is a grammatical nod to Felix Klein [3]. Kinematic constraints will first be discussed, followed by a novel development of the input-output (I-O) equation for planar 4R mechanisms, which turns out to represent the I-O equation for any planar four-bar topology.

6.1.1 Kinematic Constraints

In the context of mechanism kinematics, a *dyad* is a binary link coupled to two other rigid bodies with two kinematic pairs [4]. In a planar four-bar linkage the two other rigid bodies are a relatively non-moving ground link, while the other is the coupler when coupled to another dyad. For planar displacements there are only two types of lower pair that can be used to generate a planar motion: R- and P-pairs. This means there are only four practical planar dyads

$$RR,\ PR,\ RP, \text{ and } PP.$$

These 3-link serially connected open kinematic chains of rigid bodies are the building blocks of every planar mechanism. They are designated according to the type of joints connecting the rigid links, and listed in series starting with the joint connected to ground, each illustrated in Figure 6.1.

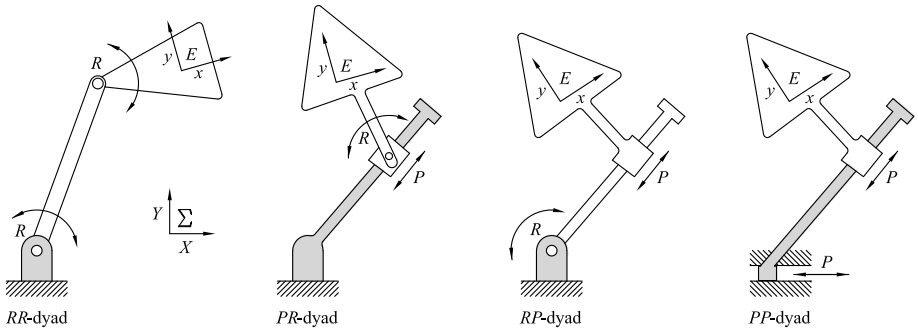

Figure 6.1: Types of dyads.

When a pair of dyads are joined, a four-bar linkage is obtained. However, the designation of the *output* dyad changes. For example, consider a planar four-bar linkage composed of an RR-dyad on the *left-hand side* of the mechanism, and

a PR-dyad on the *right-hand side*, where the *input* link is the *grounded* link in the RR-dyad, see Figure 6.2.

Suppose revolute joint R_1 is actuated by some form of torque supplied by an electric rotary motor transferred by a transmission, in turn driving the input link, a_1. The linkage is designated by listing the joints in sequence from the ground fixed actuated joint, starting with the input link listing the joints in order. Thus, the mechanism composed of a driving RR-dyad, and an output PR-dyad is called an $RRRP$ linkage, where the order of PR is switched to RP. If the output were an RP-dyad, the mechanism would be an $RRPR$ linkage. If the input were an RP-dyad while the output was an RR-dyad, the resulting mechanism would be an $RPRR$ linkage, with no noticeable alteration in the designation.

Since there are only two linearly independent translations and a single rotation available for the displacement of a rigid body in the plane, the maximum number of relative degrees of freedom (DOF) is three. Many mechanical systems are designed to provide only a single DOF meaning that only one motor is needed. Regardless, a planar four-bar linkage can be designed to generate coupled translations and rotations, as in the rigid body guidance problem. In this case the motion of the coupler is considered, link a_2 in Figure 6.3. Alternately, only a fixed axis rotation, or displacement along a fixed line may be the required output. In this case, the linkage is generally termed a *function gener-*

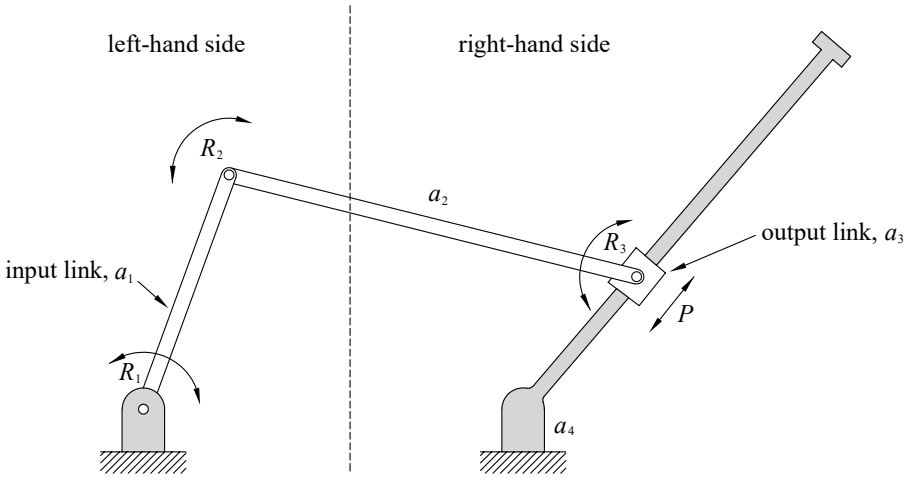

Figure 6.2: An RR-dyad on the left-hand side and PR-dyad on the right-hand side connected by the coupler, a_3, combine to form an $RRRP$ four-bar linkage.

ator, since it typically uses the linkage geometry to move the output link, link a_3, for example, in Figure 6.3, as a function of the motion of the input, link a_1 in this case. The function is generally expressed as the output angle in terms of the input angle, $\theta_4 = f(\theta_1)$. The function is inverted if link a_3 is the input while link a_1 is the output.

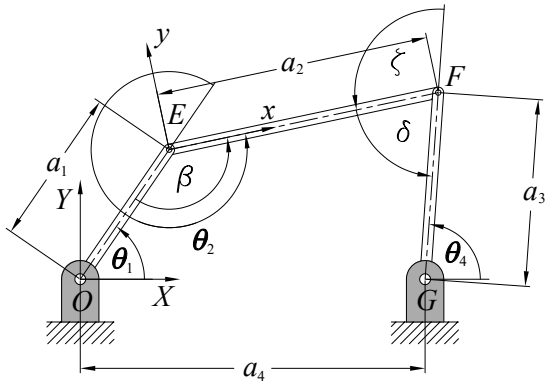

Figure 6.3: 4R four-bar mechanism parameters.

6.1.2 Grashof Condition

A Grashof planar four-bar 4R linkage is one in which the sum of the lengths of the longest and shortest links is less than the sum of the lengths of the other two [5]. A Grashof planar 4R mechanism contains at least one link that can fully rotate if

$$l + s \quad < \quad p + q, \tag{6.1}$$

where l and s refer to the lengths of the longest and shortest links, while p and q are the lengths of the two intermediate links.

There are three classes of mechanisms according to the Grashof condition, two of which contain several cases. The first four cases are the possible Grashof planar 4R mechanisms for which the following relations, stated without proof, are valid.

1. The four possible Grashof planar 4R mechanisms.

   (a) Link a_1 is a crank if it is the shortest link, and the output link a_3 is a rocker.

(b) Link a_3 is a crank if it is the shortest link, and the input link a_1 is a rocker.

(c) If the relatively non-moving link, the base, is the shortest link, then both the input and output links a_1 and a_3 are cranks.

(d) If the coupler is the shortest link, then both the input and output links a_1 and a_3 are rockers.

2. If $l + s > p + q$ then there are four different inversions of double rocker mechanisms that result, which are all non-Grashof linkages.

3. If $l + s = p + q$ the mechanism is known as a non-Grashof *change-point mechanism*, because it can fold. In the folded configuration all four links align on the line joining the centres of the two ground fixed revolute joints. They are called change-point mechanisms since, in the absence of inertial effects, the linkage can come out of the folded configuration in either of it's two assembly modes, see Section 6.5.3. There are two special cases.

   (a) If all four links are of equal length, $a_1 = a_2 = a_3 = a_4$, the change-point linkage is known as a *parallelogram linkage*. All four inversions are double cranks.

   (b) The *deltoid linkage* is the other special case where two equal length short links are connected to two equal length long links.

6.2 Coupler Angle

The goal of this section is to obtain an expression for the angle θ_2 the coupler a_2 makes with respect to the input link a_1 in terms of the input and output angles, θ_1 and θ_4, and the link lengths a_1, a_2, a_3, and a_4, using traditional methods of plane trigonometry, see Figure 6.3. However, as will be shown in Section 6.5.5, such expressions can be determined using relative Denavit-Hartenberg joint angle parameters and methods of algebraic geometry without any explicit trigonometry whatsoever.

This material is partly based on the approach presented in [6]. Let θ_2 denote the angle of the coupler a_2 measured about point E relative to the input link a_1. Hence, the angle $\theta_1 + \theta_2$ measures the angle the coupler a_2 makes with respect to the X-axis of the relatively fixed coordinate system centred at O. The coordinates of point F can be defined in terms of θ_2 as

$$\begin{bmatrix} F_X \\ F_Y \end{bmatrix} = \begin{bmatrix} a_1 \cos\theta_1 + a_2 \cos(\theta_1 + \theta_2) \\ a_1 \sin\theta_1 + a_2 \sin(\theta_1 + \theta_2) \end{bmatrix}. \tag{6.2}$$

But, the coordinates of F can also be defined in terms of the output link a_3 as

$$\begin{bmatrix} F_X \\ F_Y \end{bmatrix} = \begin{bmatrix} a_4 + a_3 \cos\theta_4 \\ a_3 \sin\theta_4 \end{bmatrix}. \tag{6.3}$$

Equation Equations (6.2) and (6.3) yields the kinematic closure equations for the four-bar linkage:

$$a_1 \cos\theta_1 + a_2 \cos(\theta_1 + \theta_2) = a_4 + a_3 \cos\theta_4, \tag{6.4}$$

$$a_1 \sin\theta_1 + a_2 \sin(\theta_1 + \theta_2) = a_3 \sin\theta_4. \tag{6.5}$$

For any value of the input angle θ_1 we can write

$$\left.\begin{aligned} \cos(\theta_1 + \theta_2) &= \frac{a_4 + a_3\cos\theta_4 - a_1\cos\theta_1}{a_2}, \\ \sin(\theta_1 + \theta_2) &= \frac{a_3\sin\theta_4 - a_1\sin\theta_1}{a_2}. \end{aligned}\right\} \tag{6.6}$$

We can solve Equation (6.6) for θ_2 revealing

$$\theta_2 = \tan^{-1}\left(\frac{a_3\sin\theta_4 - a_1\sin\theta_1}{a_4 + a_3\cos\theta_4 - a_1\cos\theta_1}\right) - \theta_1. \tag{6.7}$$

6.3 Performance Metrics

Various angles and ratios of a four-bar mechanism act as performance metrics that can be used to evaluate how well a mechanism performs the task it is intended for, or to compare the performance of different linkages at carrying out the same task. While there is no single performance metric, or index of merit [7, 8] for all mechanisms, several have emerged as particularly useful. The *transmission angle* between the coupler a_2 and output link a_3, ζ in Figures 6.3 and 6.4, is a standard four-bar mechanism performance metric that can be used as a measure of the *mechanical advantage* and *velocity ratio* of a particular linkage. These three metrics will be discussed in the following two subsections.

6.3.1 Transmission Angle

If the only external loads on linkage are generated by torques on the input and output links, then the forces $\mathbf{F}_E$ and $\mathbf{F}_F$ acting on the coupler at the centres of the revolute joints connecting it to the input and output links must act in opposite directions acting along the line connecting the two moving joint centres. Hence, in general only a component of force $\mathbf{F}_F$ is transferred to the output link

as output torque via the coupler depending on the transmission angle ζ. The component of $\mathbf{F}_F$ transmitted to the output link as torque is proportional to $\sin\zeta$. The component proportional to $\cos\zeta$ is transferred to the centre of the ground fixed revolute joint at G and must be absorbed as a reaction force.

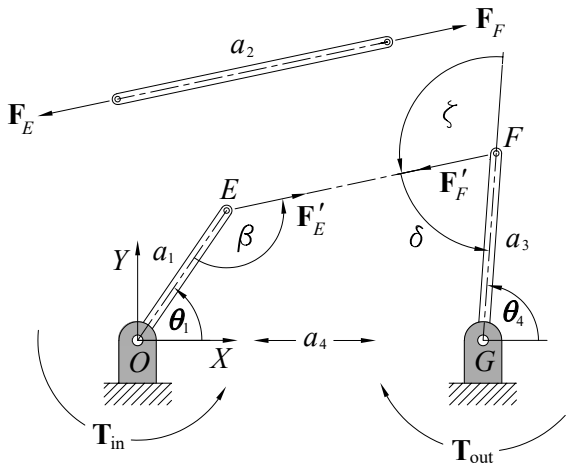

Figure 6.4: 4R four-bar mechanism parameters.

It is useful to have the transmission angle ζ expressed in terms of the input angle θ_1. To do this we can equate the cosine laws for the triangles $\triangle OGE$ and $\triangle GFE$ along the diagonal EG of the quadrangle formed by the revolute joint centres $OGFE$. Referring to Figure 6.4, because ζ is an exterior angle this gives

$$(|\mathbf{E}-\mathbf{G}|)^2 = a_4^2 + a_1^2 - 2a_1a_4\cos\theta_1 = a_2^2 + a_3^2 + 2a_2a_3\cos\zeta. \tag{6.8}$$

Solving for the transmission angle ζ yields

$$\zeta = \cos^{-1}\left(\frac{a_4^2 + a_1^2 - a_2^2 - a_3^2 - 2a_1a_4\cos\theta_1}{2a_2a_3}\right). \tag{6.9}$$

6.3.2 Mechanical Advantage and Velocity Ratio

Consider Figures 6.3 and 6.4 once again. If friction and inertia forces are small compared to the actuation forces then the power supplied to the input link a_1 is the negative of the power applied to the output link a_3 by the load. Since power can be defined as the inner (dot) product of torque and angular velocity vectors it must be that

$$\mathbf{T}_{\text{in}} \cdot \dot{\boldsymbol{\theta}}_1 \quad = \quad \mathbf{T}_{\text{out}} \cdot \dot{\boldsymbol{\theta}}_4. \tag{6.10}$$

We can consider only the magnitudes of these vectors and re-express this relation as the following equivalent ratios:

$$\frac{T_{\text{out}}}{T_{\text{in}}} = \frac{\dot{\theta}_1}{\dot{\theta}_4}. \tag{6.11}$$

The first ratio in Equation (6.11) is the *mechanical advantage* of the linkage, which is equivalent to the negative reciprocal of the *velocity ratio*. The velocity ratio in Equation (6.11) can be expressed in terms of the two angles δ and β illustrated in Figure 6.3. Since δ is $\pi - \zeta$ we additionally have

$$\frac{T_{\text{out}}}{T_{\text{in}}} = \frac{\dot{\theta}_1}{\dot{\theta}_4} = \frac{a_3 \sin\delta}{a_1 \sin\beta}. \tag{6.12}$$

Equation (6.12) shows that the mechanical advantage approaches infinity when the angle β approaches 0 or π. These configurations are called *toggle* configurations, and are illustrated in Figure 6.5. The two toggle configurations for the linkage in Figure 6.5 correspond to $\beta = 0$ and $\beta = \pi$. Moreover, Equation (6.12) also shows that issues arise when $\delta \to 0$ and $\delta \to \pi$. These two extremes for the transmission angle correspond to when $\zeta \to \pi$ and $\zeta \to 0$. In these configurations the mechanical advantage of the linkage becomes very small, and then even a very small amount of friction or misalignment will cause the mechanism to jam or lock. Hence, a design rule-of-thumb is that the best four-bar linkage will have a transmission angle which deviates from a right angle by the smallest amount [7, 8].

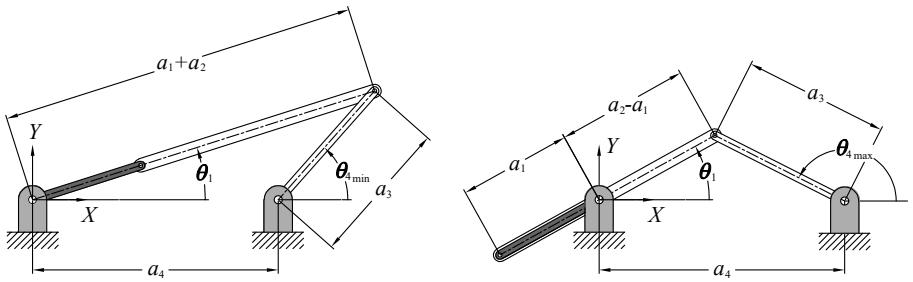

Figure 6.5: The angular limits of the output link, if they exist, are $\theta_{4_{\min/\max}}$.

6.4 Coupler Point Curves

One of the earliest recorded examples of mechanical system design for guiding a point along a curve belongs to Archimedes (ca. 287-212 BC). He was born in

Syracuse in the ancient Greek colony of Sicily, but he studied mathematics at the Museum in Alexandria [9] between 250-240 BC under the direction of Conon of Samos. Conon was a mathematician who was a pupil of Euclid and became the custodian of the library of Alexandria after Euclid's death. Archimedes work is the first recorded systematic study of mechanism design and analysis, although undoubtedly these concepts were widely studied earlier everywhere there were humans who could formulate abstract thoughts. However, the very first patent [10] for a mechanism designed to move a point along a desired curve belongs to James Watt (1736-1819) awarded more than 2000 years after Archimedes death.

The point equation for the coupler curve of a selected coupler point which is generated by a planar 4R mechanism that is presented here is largely based on the way it was originally derived by Samuel Roberts in [11] and reported in [12], and subtly modified in [6]. Referring to Figure 6.6, the ground fixed stationary reference coordinate system has it's origin O at the centre of the left ground fixed R-pair and uses coordinates (X, Y). Let the coordinate system that moves with the coupler be centred at E, with x-axis on the line between E and F. Let the coordinates of any particular coupler reference point C be (x_C, y_C). Since the coupler angle θ_2 is a function of the input angle θ_1 we will express

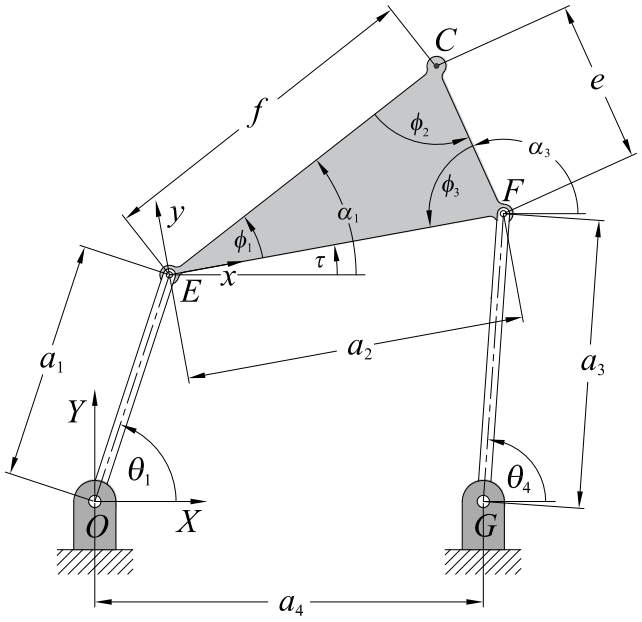

Figure 6.6: 4R four-bar point coupler curve parameters.

the equation of the coupler curve that point C traces as θ_1 changes in terms of the input angle all expressed in the non-moving coordinate system. Since the location of point C has constant coordinates (x_C, y_C) in the moving coordinate system, we can always transform these coordinates to the non-moving frame coordinates (X_C, Y_C) with the coordinate transformation

$$\begin{bmatrix} 1 \\ X_C(\theta_1) \\ Y_C(\theta_1) \end{bmatrix} = \begin{bmatrix} 0 & 0 & 1 \\ \cos(\theta_1+\theta_2) & -\sin(\theta_1+\theta_2) & a_1\cos\theta_1 \\ \sin(\theta_1+\theta_2) & \cos(\theta_1+\theta_2) & a_1\sin\theta_1 \end{bmatrix} \begin{bmatrix} 1 \\ x_C \\ y_C \end{bmatrix}. \quad (6.13)$$

The coupler geometry is fixed with the angle at the coupler reference point C between sides f and e indicated by the constant angle ϕ_2. Hence, by eliminating θ_1 from the equation, we can obtain a quasi-algebraic form of the coupler curve. However, the equation is still essentially transcendental in terms of $\cos\phi_2$ and $\sin\phi_2$, so we call it quasi-algebraic. We will define the coordinates of the coupler point C in two ways. Let the coupler triangle $\triangle CEF$ in Figure 6.6 have lengths a_2, e and f, where e and f are determined by the choice of coupler point C. These two sides are determined by

$$f = |\mathbf{C}-\mathbf{E}| = (x_C^2+y_C^2)^{\frac{1}{2}}, \quad \text{and} \quad e = |\mathbf{C}-\mathbf{F}| = \left((x_C-a_2)^2+y_C^2\right)^{\frac{1}{2}}. \quad (6.14)$$

The angle α_1 is defined in the non-moving frame centred at O as the angle that side f makes with respect to the X-axis, counter-clockwise being positive, while the angle α_3 is the angle between the X-axis and side e. We therefore write

$$\mathbf{C}-\mathbf{E} = \begin{bmatrix} 1 \\ f\cos\alpha_1 \\ f\sin\alpha_1 \end{bmatrix}, \quad \text{and} \quad \mathbf{C}-\mathbf{F} = \begin{bmatrix} 1 \\ e\cos\alpha_3 \\ e\sin\alpha_3 \end{bmatrix}. \quad (6.15)$$

Now de-homogenise and rearrange Equations (6.15) to isolate $\mathbf{E}$ and $\mathbf{F}$:

$$\mathbf{E} = \begin{bmatrix} X_C - f\cos\alpha_1 \\ Y_C - f\sin\alpha_1 \end{bmatrix}, \quad \text{and} \quad \mathbf{F} = \begin{bmatrix} X_C - e\cos\alpha_3 \\ Y_C - e\sin\alpha_3 \end{bmatrix}. \quad (6.16)$$

Substitute these results into the identities defined in the fixed frame

$$\mathbf{E}\cdot\mathbf{E} = a_1^2, \quad \text{and} \quad (\mathbf{F}-\mathbf{G})\cdot(\mathbf{F}-\mathbf{G}) = a_3^2.$$

The first dot product gives

$$\mathbf{E}\cdot\mathbf{E} \;=\; (X_C - f\cos\alpha_1)^2 + (Y_C - f\sin\alpha_1)^2 \;=\; a_1^2.$$

After collecting terms and using the identity $\cos^2\alpha_1 + \sin^2\alpha_1 = 1$, and rearranging the terms this simplifies to

$$\mathbf{E}\cdot\mathbf{E} \;=\; X_C^2 + Y_C^2 - 2fX_C\cos\alpha_1 - 2fY_C\sin\alpha_1 + f^2 - a_1^2 \;=\; 0. \quad (6.17)$$

Since our fixed coordinate system is selected such that the X-axis is directed from point O to point G, with the origin located at O, the difference of the two vectors in the second dot product is

$$\mathbf{F} - \mathbf{G} \quad = \quad \begin{bmatrix} X_C - e\cos\alpha_3 - a_4 \\ Y_C - e\sin\alpha_3 \end{bmatrix}.$$

Using the same approach, the second dot product simplifies to

$$\begin{aligned}(\mathbf{F} - \mathbf{G}) \cdot (\mathbf{F} - \mathbf{G}) \; &= \; X_C^2 + Y_C^2 - 2eX_C\cos\alpha_3 - 2eY_C\sin\alpha_3 + \\ &2a_4e\cos\alpha_3 - 2a_4X_C + a_4^2 + e^2 - a_3^2 \quad = \quad 0. \end{aligned} \tag{6.18}$$

It will be convenient to express α_3 in terms of α_1 and ϕ_2. For this we can use the triangle interior/exterior angle rule [1]. Consider the triangle illustrated in Figure 6.7a. Consider that

$$\phi_1 + \phi_2 + \phi_3 \quad = \quad \pi,$$

and

$$\phi_3 + \phi_4 \quad = \quad \pi.$$

Then we can say that

$$\phi_4 \quad = \quad \pi - \phi_3,$$

and

$$\phi_1 + \phi_2 \quad = \quad \pi - \phi_3.$$

Therefore

$$\phi_1 + \phi_2 \quad = \quad \phi_4. \tag{6.19}$$

The same rule holds for the triangle shown in Figure 6.7b, that is τ can be added to both sides of Equation (6.19) without changing it's validity:

$$\underbrace{(\phi_1 + \tau)}_{\alpha_1} + \phi_2 \quad = \quad \underbrace{(\phi_4 + \tau)}_{\alpha_3}.$$

Therefore

$$\alpha_1 + \phi_2 \quad = \quad \alpha_3. \tag{6.20}$$

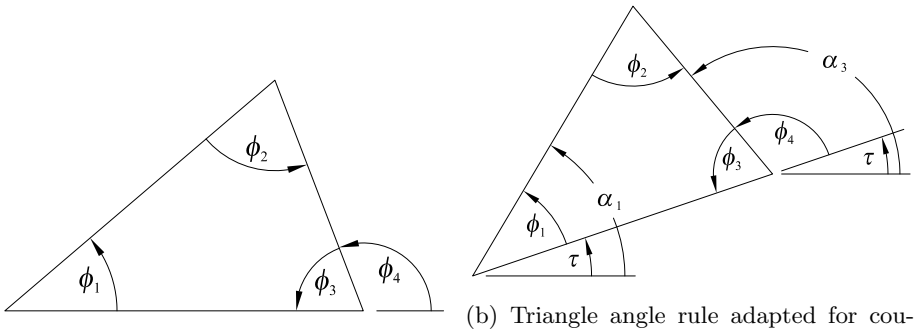

(a) Triangle angle rule.

(b) Triangle angle rule adapted for coupler.

Figure 6.7: Triangle angle rules.

Making this substitution in Equation (6.18) and using the addition identities for sine and cosine functions

$$\begin{aligned}\cos(\phi_2+\alpha_1) &= \cos\phi_2\cos\alpha_1 - \sin\phi_2\sin\alpha_1,\\ \sin(\phi_2+\alpha_1) &= \cos\phi_2\sin\alpha_1 + \sin\phi_2\cos\alpha_1,\end{aligned}$$

one can separate the angle functions, and after rearranging the terms as in Equation (6.18) gives

$$\begin{aligned}X_C^2 + Y_C^2 \; - \; & 2e\left((X_C - a_4)\cos\phi_2 + Y_C\sin\phi_2\right)\cos\alpha_1 \; - \\ & 2e\left(Y_C\cos\phi_2 + (a_4 - X_C)\sin\phi_2\right)\sin\alpha_1 + a_4^2 + e^2 - 2X_C a_4 \;=\; a_3^2. \quad (6.21)\end{aligned}$$

The next step towards obtaining the quasi-algebraic point coupler curve expressed in the non-moving coordinate system in terms of X_C and Y_C is to linearly solve Equations (6.17) and (6.21) for $\cos\alpha_1$ and $\sin\alpha_1$ using Cramer's rule [13].

To apply Cramer's rule to this system of equations, the equations must be in the vector-matrix form $\mathbf{Ax} = \mathbf{b}$. Recall that if $\mathbf{Ax} = \mathbf{b}$ represents a system of n equations where all the elements of matrix $\mathbf{A}$ and vector $\mathbf{b}$ are known, and the equations are linear in the unknown elements of vector $\mathbf{x}$. If $\det(\mathbf{A}) \neq 0$ then the system has a unique solution for $\mathbf{x} = [x_1, x_2, \cdots, x_n]^T$ given by [13]

$$x_1 = \frac{\det(\mathbf{A}_1)}{\det(\mathbf{A})}, \quad x_2 = \frac{\det(\mathbf{A}_2)}{\det(\mathbf{A})}, \quad \cdots, \quad x_n = \frac{\det(\mathbf{A}_n)}{\det(\mathbf{A})},$$

where $\det(\mathbf{A}_j)$ is the matrix obtained by replacing the entries in the j^{th} column of $\mathbf{A}$ by the elements in the vector $\mathbf{b} = [b_1, b_2, \cdots, b_n]^T$.

To apply Cramer's rule, we first simplify Equations (6.17) and (6.21) by collecting the terms that are scaled by $\cos\alpha_1$ and $\sin\alpha_1$, and those that are independent of the angles as

$$\left.\begin{array}{rcl} P_1\cos\alpha_1 + Q_1\sin\alpha_1 &=& R_1, \\ P_2\cos\alpha_1 + Q_2\sin\alpha_1 &=& R_2, \end{array}\right\} \tag{6.22}$$

where

$$\begin{array}{rcl|rcl} P_1 &=& 2X_C f, & P_2 &=& 2e\left((X_C - a_4)\cos\phi_2 + Y_C\sin\phi_2\right), \\ Q_1 &=& 2Y_C f, & Q_2 &=& 2e\left(Y_C\cos\phi_2 - (X_C - a_4)\sin\phi_2\right), \\ R_1 &=& X_C^2 + Y_C^2 + f^2 - a_1^2. & R_2 &=& (X_C - a_4)^2 + Y_C^2 + e^2 - a_3^2. \end{array}$$

We can now arrange these equations in the desired form as

$$\begin{bmatrix} P_1 & Q_1 \\ P_2 & Q_2 \end{bmatrix} \begin{bmatrix} \cos\alpha_1 \\ \sin\alpha_1 \end{bmatrix} = \begin{bmatrix} R_1 \\ R_2 \end{bmatrix}. \tag{6.23}$$

Note that the term $(X_C - a_4)^2$ in the coefficient R_2 in Equations (6.22) is obtained from the three terms $X_C^2 - 2a_4X_C + a_4^2$ in Equation (6.21). Solving Equations (6.22) using Cramer's rule for $\cos\alpha_1$ and $\sin\alpha_1$ yields

$$\cos\alpha_1 = \frac{\begin{vmatrix} R_1 & Q_1 \\ R_2 & Q_2 \end{vmatrix}}{\begin{vmatrix} P_1 & Q_1 \\ P_2 & Q_2 \end{vmatrix}} = \frac{R_1Q_2 - R_2Q_1}{P_1Q_2 - P_2Q_1}, \quad \text{and} \tag{6.24}$$

$$\sin\alpha_1 = \frac{\begin{vmatrix} P_1 & R_1 \\ P_2 & R_2 \end{vmatrix}}{\begin{vmatrix} P_1 & Q_1 \\ P_2 & Q_2 \end{vmatrix}} = \frac{P_1R_2 - P_2R_1}{P_1Q_2 - P_2R_1}. \tag{6.25}$$

Finally we enforce the identity $\cos^2\alpha_1 + \sin^2\alpha_1 = 1$ to obtain

$$(R_1Q_2 - R_2Q_1)^2 + (P_1R_2 - P_2R_1)^2 = (P_1Q_2 - P_2Q_1)^2,$$

or

$$(R_1Q_2 - R_2Q_1)^2 + (P_1R_2 - P_2R_1)^2 - (P_1Q_2 - P_2Q_1)^2 = 0. \tag{6.26}$$

The P_i and Q_i coefficients in Equation (6.26) are linear in the coordinates of the coupler point X_C and Y_C, while the R_i are quadratic. The products P_iR_j and Q_iR_j are therefore of order three $(1+2)$, and the squares of the differences are of order six $(3*2)$. Hence, the point coupler curve of an arbitrary planar 4R mechanism represented by Equation (6.26) is of order six (a *sextic*) agreeing with the well known theory of planar mechanisms [12].

6.4.1 Coupler Curve Examples

The following three examples of coupler curves from different mechanisms are intended to illustrate that the nature of any particular coupler point in any particular 4R linkage is tremendously varied. The first coupler curve plotted in Figure 6.8 (a) is for the non Grashof double π-rocker with link lengths in generic units of length of $a_1 = 9$, $a_3 = 12$, $a_4 = 6$ and a_2 implied by the coupler edge lengths $e = 8$ and $f = 8$, and the angle $\phi_2 = \frac{\pi}{3}$ between sides f and e, giving $a_2 = \sqrt{e^2 + f^2 - 2ef\cos\phi_2} = 8$, obviously, since the coupler triangle must be equilateral. Evaluating the signs of the appropriate coefficient products in Equation (6.83) then consulting Tables 6.7-6.10 reveals the linkage is indeed a non Grashof double π-rocker. Note the coupler curve possesses a single real crunode (real double point).

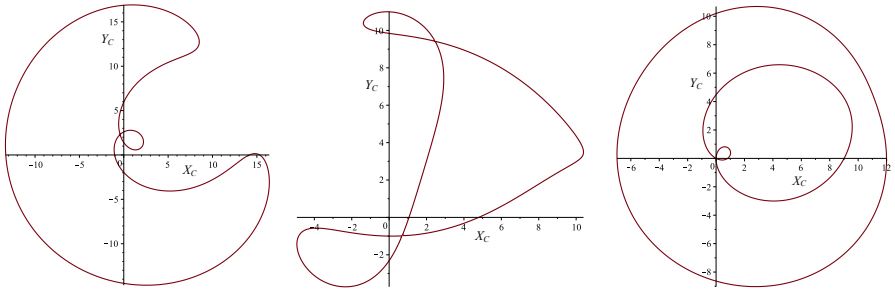

(a) (b) (c)

Figure 6.8: Three different coupler curves.

The second linkage is a non Grashof 0-rocker, π-rocker determined by $a_1 = 6$, $a_3 = 7$, $a_4 = 12$ and a_2 implied by the coupler edge lengths $e = 10$ and $f = 5$, and the angle $\phi_2 = \frac{\pi}{3}$ between sides f and e, giving $c = \sqrt{e^2 + f^2 - 2ef\cos\phi_2} \approx 8.66$. The corresponding coupler curve is plotted in Figure 6.8 (b). This coupler curve possesses two real crunodes.

The third linkage is a Grashof double crank determined by $a_1 = 6$, $a_3 = 7$,

$a_4 = 4$ and a_2 implied by the coupler edge lengths $e = 4$ and $f = 6$, and the angle $\phi_2 = \frac{\pi}{3}$ between sides f and e, giving $c = \sqrt{e^2 + f^2 - 2ef\cos\phi_2} \approx 5.29$. The coupler curve, plotted in Figure 6.8 (c), has two distinct branches, one with a real crunode the other without. This illustrates a synthesis issue known as the *branch defect* because the linkage must be re-assembled in two different ways to reach both branches of the coupler curve.

6.4.2 Algebraic Properties of the Planar Coupler Curve

Discussion of the algebraic properties of the sextic coupler curve requires some knowledge of *plane algebraic curves* and *rational algebraic functions*. This material is discussed in great detail in [14], while the material presented in [15] is, in the author's own words: "intended to give the student a reasonably brief introduction to the subject". Some elementary material will be presented next to highlight the properties of these sextic curves. In particular, it is instructive to consider the *order* of the point equation of a curve as well as it's *circularity*, the *class* of the corresponding line equation of the curve, the number and type of *singular points*, and the *Plücker numbers* that relate them by virtue of the principle of duality. We will consider plane algebraic curves in general and the sextic coupler curve in particular in the following four subsections.

6.4.2.1 Curve Order; Bézout's Theorem; Imaginary Conjugate Circular Points; Circularity

A planar curve is *algebraic* if a point (x_1, x_2) which traces the curve satisfies an equation $f(x_1, x_2) = 0$, where f is a rational integral algebraic function of the coordinates x_1 and x_2. In other words a function is algebraic if

$$f(x_1, x_2) = \sum a_{ij} x_1^i x_2^j = 0$$

and the indices i and j take either finite integer values, or are zero, and a_{ij} is some constant rational coefficient (i.e. a ratio of two integers) for each unique term $x_1^i x_2^j$. The *degree* n of an algebraic planar curve is the highest power of x_1^i and x_2^j combined: $n = (i + j)_{\max}$. Clearly, the degree of a curve is a positive integer. In the study of algebraic curves, the degree of a particular curve is usually called it's *order*. When one, or more of the terms cannot be expressed as a rational number (a ratio of integers) it is said to be *irrational*. For example $x = e^y$, or $y = \cos x$ are *transcendental*, since the expressions for exponential and trigonometric functions represent infinite power series which cannot be represented as ratios of integers.

In 1876 Alfred Bray Kempe, a mathematician best known for his work on linkages, proved a theorem relating the properties of plane algebraic curves to planar linkages, which can contain only P- and R-pairs: it is theoretically possible to design a linkage to guide a point to trace any plane algebraic curve [16]. Regardless, since that time no general method has been discovered for identifying the best, or simplest mechanical system for tracing any particular plane algebraic curve [12]. Hence, there remains keen interest throughout the world for advancing and developing new knowledge in linkage design methods, performance metrics, and optimisation strategies. An excellent comprehensive introduction to plane algebraic curves may be found in [15] but is beyond the scope of this text. Nonetheless some of the concepts germane to planar four-bar analysis and design will now be introduced.

An arbitrary line in the plane cuts an n^{th} order algebraic curve in *at most* n points. A plane algebraic curve can be described by an equation as a locus of points, but it can also be described in a dual way by an equation as an envelope of lines tangent to the curve. In this case, a general point in the plane has *at most* n lines passing through it that are tangent to an algebraic curve of n^{th} class. Hence the distinction between the point equation and the line equation of a curve. Line equations will be discussed in greater detail later and are mentioned now only to hint at the great depth of the study of plane algebraic curves since antiquity. We will focus on point equations for the moment. Generalising the notion of how many times a line cuts a n^{th} order algebraic curve we can eliminate the phrase "at most" from the theorem if we admit the existence of points of intersection that are imaginary and/or infinite.

Because the point equation of a line is linear, it follows that it can intersect an n^{th} order algebraic curve in n points. By extension, Bézout's theorem states that two coplanar algebraic curves of orders n and m which do not share a common component, that is, which do not have infinitely many common points, intersect in general in nm points: the product of their orders. The theorem is named after Étienne Bézout who published a proof in 1779 in a treatise entitled *Théorie Générale des Équations Algébriques* [17], but the theorem was originally essentially stated without proof by Issac Newton in his proof of Lemma 28 in Volume 1 of his Principia in 1687 [18]. Regardless, history has justly recognised Bézout and the theorem bears his name.

It is easy to confirm by inspection that a line can cut a conic section in no more that two real points. Considering the plots in Figure 6.9, it is equally easy to confirm that two general coplanar conics, second order plane algebraic curves, can have four points in common, unless they are coincident. If a right circular

cone is cut by a plane parallel to it's base circle, but not at it's apex, the trace of the cone on the plane is a circle, a conic section, a general plane algebraic curve of order two. In fact, a circle is a special case of an ellipse whose major and minor axes have the same length. Yet two distinct coplanar circles never intersect in more than two real points. A circle cuts any other conic section in as many as four points, but not another circle! How is this so? Does this suggest that our Cartesian representation of the algebraic equation of a circle in the Euclidean plane $\mathbb{E}^2$ is lacking the resolution needed to identify two additional points of intersection? Are there two additional points that are occluded by the representation using Cartesian coordinates? Let's examine the possibilities.

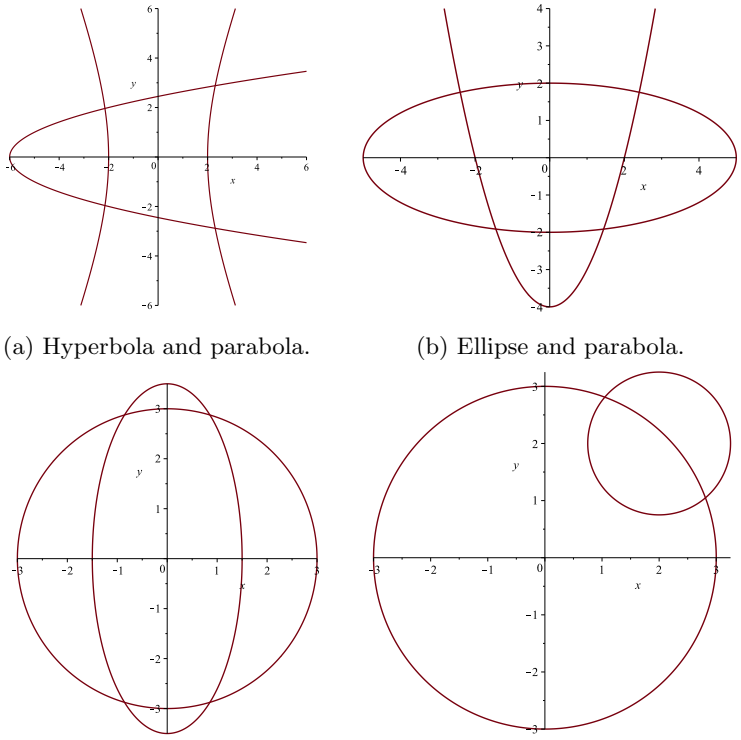

(a) Hyperbola and parabola.

(b) Ellipse and parabola.

(c) Circle and ellipse.

(d) Two circles.

Figure 6.9: Conic section intersections.

Consider the equation of an arbitrary circle, k, in the Euclidean plane $\mathbb{E}^2$ with radius r and centre $\mathcal{C}(x_c, y_c)$:

$$(x - x_c)^2 + (y - y_c)^2 \quad = \quad r^2. \tag{6.27}$$

Expressing Equation (6.27) using homogeneous coordinates $x = \frac{x_1}{x_0}$, $y = \frac{x_2}{x_0}$

produces the corresponding circle in the projective extension of $\mathbb{E}^2$, called $\mathbb{P}^2$:

$$\left(\frac{x_1}{x_0} - x_c\right)^2 + \left(\frac{x_2}{x_0} - y_c\right)^2 \quad = \quad r^2. \tag{6.28}$$

The homogenising coordinate x_0 can be considered a third length coordinate that has the effect of scaling the circle. In the case of a circle the value of x_0 must be a positive number, or zero. When $x_0 = 1$ Equations (6.27) and (6.28) are identical. When the relative magnitude of x_0 increases, the circle becomes smaller and approaches it's centre. As $x_0 \Rightarrow \infty$ the circle diminishes in area until it becomes vanishingly small and ultimately degenerates to a single point: the centre. As x_0 diminishes, the area of the circle increases, with the limiting case being $x_0 = 0$. Equation (6.28) is now said to be *homogeneous* in x_0, x_1, and x_2. This is seen more readily if we multiply it by x_0^2 giving

$$(x_1 - x_c x_0)^2 + (x_2 - y_c x_0)^2 \quad = \quad r^2 x_0^2. \tag{6.29}$$

Now, every term in Equation (6.29) is homogeneously of degree two. When $x_0 = 1$ then $x_1 = 0$ and $x_2 = 0$ are the coordinate axes, but what happens when $x_0 = 0$ while x_1, x_2, x_c, y_c, and r remain finite? Just as lines $x_1 = 0$ and $x_2 = 0$ always intersect the circle in two real, or imaginary points, it must also be that the line $x_0 = 0$ intersects the circle in two points. Since the effect of setting $x_0 = 0$ gives the circle an infinitely large area and because $x_0 = 0$ is a line, it must be that $x_0 = 0$ is a line at infinity. Because we are considering a circle in a plane, there can only be one line at infinity that bounds the finite locations in the plane. Hence, $x_0 = 0$ is called *the line at infinity.*

The intersection of a circle with the line at infinity $x_0 = 0$ is given by the equations

$$x_0 = 0, \quad x_1^2 + x_2^2 = 0. \tag{6.30}$$

In this case Equation (6.29) becomes

$$x_1^2 + x_2^2 \quad = \quad 0. \tag{6.31}$$

Equation (6.31) factors into a degenerate conic section consisting of a pair of complex conjugate imaginary lines

$$(x_1 + ix_2)(x_1 - ix_2) \quad = \quad 0 \tag{6.32}$$

which possess one real point of intersection, namely $(x_1, x_2) = (0, 0)$. Therefore, the line at infinity intersects the circle where the complex conjugate lines

represented by Equation (6.32) meet the line at infinity, namely at the complex conjugate points I_1 and I_2:

$$(x_0 : x_1 : x_2) \quad = \quad \begin{cases} I_1(0 : i : 1), \\ I_2(0 : -i : 1). \end{cases} \tag{6.33}$$

The constants r, x_c and y_c which characterise the circle do not appear in the result. Thus, every circle represented in the projective extension of the Euclidean plane intersects the line at infinity in exactly the same two imaginary points, called the *conjugate imaginary circular points* I_1 and I_2. They are also widely called the *imaginary absolute circle points* [3, 12, 19, 20, 21]. It can be shown, in the same way, that every sphere cuts the plane at infinity in the imaginary conic:

$$x_0 = 0, \quad x_1^2 + x_2^2 + x_3^2 = 0, \tag{6.34}$$

which is called the *imaginary*, or *absolute sphere circle*.

These absolute quantities account for the apparent deficiency of Bézout's theorem [12, 22] for the intersections of algebraic curves and surfaces. That is, two curves of order n and m will intersect in nm points; similarly, two surfaces of order n and m will intersect in a curve of order nm. Clearly, two circles can intersect in at most two real points, while two spheres intersect in a circle (a second order curve). Since every circle contains the complex conjugate points I_1 and I_2, two circles can intersect in at most two more real points for a maximum number of four. The same applies for spheres; they intersect in a curve that, if it contains a real circle, always splits into a real and an imaginary conic. Hence Bézout's theorem is seen to be always true.

A *double point*, also known as a *node*, of a plane algebraic curve is a location where the curve intersects itself such that two branches of the curve have distinct tangent lines at that point. Double points are one type of singular point which will be elaborated on in greater detail in Subsection 6.4.2.4. Ordinary double points of plane curves are commonly known as *crunodes*. Ordinary double points of a plane curve given by $f(x_1, x_2) = 0$ must satisfy

$$f(x_1, x_2) = \frac{\partial f}{\partial x_1} = \frac{\partial f}{\partial x_2} = 0.$$

A non-degenerate planar algebraic curve of order n can have at most

$$\frac{1}{2}(n-1)(n-2) \tag{6.35}$$

double points, real and/or imaginary. Hence, a sextic coupler curve can have as many as 10 double points:

$$\frac{1}{2}(6-1)(6-2) = 10. \tag{6.36}$$

Because a circle contains the complex points I_1 and I_2 as two single complex conjugate points, a circle is said to have a *circularity* of one. Curves that contain I_1 and I_2 as double and triple points have circularity two and three, respectively. The circularity of the planar 4R coupler curve is determined by expressing the coordinates of the coupler point C as homogeneous coordinates $\frac{X_C}{W_C}$ and $\frac{Y_C}{W_C}$ in the point coupler curve equation, Equation (6.26). The only terms that remain after setting $W_C = 0$ represent the intersection of the general 4R coupler curve with the line at infinity:

$$\begin{aligned} &4\left((e\cos\phi_2)^2 + (e\sin\phi_2)^2 - 2ef\cos\phi_2 + f^2\right)(X_C^6 + Y_C^6) + \\ &\quad 12\left((e\cos\phi_2)^2 + (e\sin\phi_2)^2 - 2ef\cos\phi_2 + f^2\right)(X_C^4 Y_C^2 + X_C^2 Y_C^4) - \\ &\quad 16(e^2 f^2 \sin\phi_2)^2 (X_C^4 + Y_C^4) - 32(ef\sin\phi_2)^2 (X_C^2 + Y_C^2) = 0. \end{aligned}$$

It is to be understood that we are only considering non-degenerate point coupler curves, in which case the constant coefficients do not vanish. It is shown in [12] that the coupler curve intersects the line at infinity at points where

$$\left.\begin{aligned} W_C &= 0, \\ (X_C^2 + Y_C^2)^3 &= 0, \end{aligned}\right\} \tag{6.37}$$

namely at the complex conjugate circular points I_1 and I_2. We see that a planar 4R non-degenerate coupler curve has the imaginary circular points as triple points. Therefore the coupler curve has a circularity of three and is called a *tricircular sextic*. Since these are complex conjugate points, a 4R coupler curve can have at most four additional finite double points because Equation (6.35) indicates that a sextic curve has at most 10 double points, and six are always complex conjugates.

6.4.2.2 Duality

In the Euclidean plane a general line has the equation

$$Ax + By + C = 0 \tag{6.38}$$

where A, B, and C are arbitrary constants defining the slope and intercepts with the coordinate axes. The x and y that satisfy the equation are points on

the line. Using homogeneous coordinates this linear equation becomes

$$X_0x_0 + X_1x_1 + X_2x_2 \quad = \quad 0 \tag{6.39}$$

where the X_i characterise lines (i.e., $X_0 = C$, $X_1 = A$, $X_2 = B$) and the x_i characterise points. Now Equation (6.39) represents Equation (6.38) as an equation that is linear in the X_i as well as the x_i. Every term in (6.39) is bilinear, or homogeneously linear. This should explain the etymology of the term homogeneous coordinates. The X_i are substituted for the A, B and C to underscore the bilinearity and symmetry. Now Equation (6.39) may be viewed as a range of variable points on a fixed line, or as a pencil of variable lines on a fixed point. The X_i define the line and are hence termed *line coordinates*, indicated by the ratios $[X_0 : X_1 : X_2]$; whereas the x_i define the point and bear the name *point coordinates*, indicated by the ratios $(x_0 : x_1 : x_2)$. Note that $[\cdots]$ are used to delimit line coordinates, while $(\cdots)$ are used to delimit point coordinates. Equation (6.39) is a bilinear equation describing the mutual incidence of point and line in the plane. Thus, point and line are considered as dual elements in the projective plane P_2. The importance of this concept is that any valid theorem concerning points and lines yields another valid theorem by simply exchanging these two words. For example, the proposition

any two distinct points determine one and only one line

is dualised by exchanging the words point and line giving a very different proposition,

any two distinct lines determine one and only one point.

This topic is covered more thoroughly in *Chapter 5: Geometry* in this collection of notes and is introduced here as well for clarity in the description of the important duality between curve order and the next topic: class.

6.4.2.3 Class of a Line Equation

Given an arbitrary point in the plane and a plane algebraic curve that does not contain the point, the *class* of the curve is the number of lines that contain the point and are tangent to the curve. The class of a line equation of a curve is the line dual to the order of the point equation of the same curve. If the class is equal to m, then there are m lines tangent to the curve through the point, again these tangent lines may be real, imaginary, or at infinity. For curves of orders one and two the class is also one and two, respectively. For curves of order greater than two the class is generally a different positive integer. As a

concept class is quite important because sometimes in kinematics a curve may be more efficiently expressed as the envelope of it's tangent lines rather than as the locus of it's points. This can be especially true when P- and R-pairs are both in the kinematic chain.

As an example consider the $PRRP$ linkage illustrated in Figure 6.10. Recall that this linkage is known as an elliptical trammel. When the P-pair longitudinal axes of symmetry are orthogonal the coupler, line AB, envelops a four pointed asteroid. The same asteroid would be traced by a circle of diameter $\frac{AB}{2}$ rolling

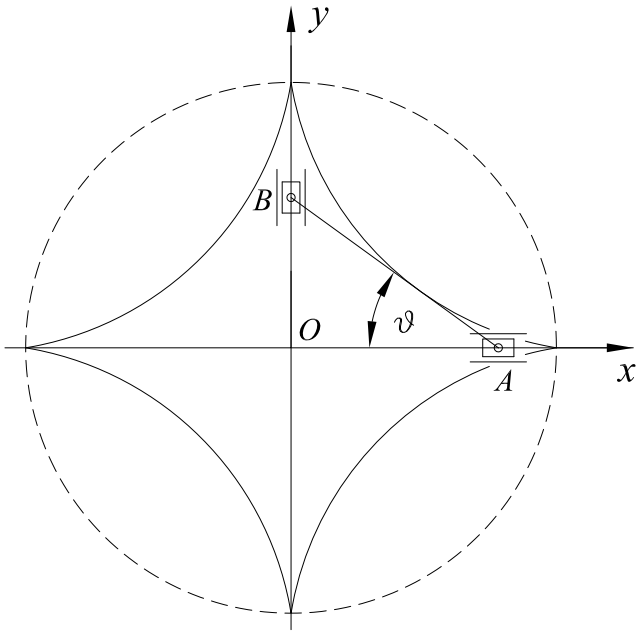

Figure 6.10: An asteroid is generated when the P-pairs in an $PRRP$ linkage are orthogonal.

without slip on the interior of the larger circle defined by the four singular apexes. Line AB has the homogeneous equation

$$\frac{x_1}{a\cos\vartheta} + \frac{x_2}{a\sin\vartheta} - x_0 = 0, \tag{6.40}$$

where a is the length of the coupler AB.

Again, an arbitrary line in the plane has the homogeneous equation

$$X_0x_0 + X_1x_1 + X_2x_2 = 0. \tag{6.41}$$

Comparing and equating the coefficients of x_1 and x_2 in Equations (6.40) and

(6.41) yields

$$\left.\begin{aligned} \frac{X_1}{X_0} &= -\frac{1}{a\cos\vartheta}, \\ \frac{X_2}{X_0} &= -\frac{1}{a\sin\vartheta}. \end{aligned}\right\} \tag{6.42}$$

The angle ϑ can be eliminated from the coefficients in Equation (6.40) with the line coefficients defined as in Equation (6.42) by squaring them and imposing the identity $\cos^2\vartheta + \sin^2\vartheta = 1$ which yields the line equation of the asteroid:

$$a^2X_1^2X_2^2 - X_0^2(X_1^2 + X_2^2) \quad = 0. \tag{6.43}$$

The line equation for the asteroid in Equation (6.43) is of degree four, therefore the class of the asteroid is $m = 4$. The locus of a point on a circle rolling without slip on a plane is known as a *cycloid*. Hence, because the point equation for the four pointed asteroid can be generated by a the locus of a point on the circle rolling without slip inside a circle of larger diameter it is also known as a *hypocycloid*.

Consulting the literature, one finds the point equation for the hypocycloid, or four pointed asteroid is

$$\left(a^2x_0^2 - (x_1^2 + x_2^2)\right)^3 - 27a^2x_0^2x_1^2x_2^2 \quad = \quad 0. \tag{6.44}$$

The point equation for the four pointed asteroid has order six, whereas the line equation for the very same curve is of class four.

6.4.2.4 Singular Points

In the study of kinematic geometry, and algebraic geometry in general, a *singular* point of a curve is a point P that is uniquely defined, hence singular. In the geometric sense, at this point the tangent space of the curve may not be regularly defined. A point that is not singular is a *regular*, or *simple point*. As we have seen in Subsection 6.4.2.1 a curve of order, or class, greater than two can intersect itself. The points where this happens are called *multiple points*. A comprehensive account of multiple points is to be found in [14]. The type of multiple point that occurs for planar 4R coupler curves are called *double points*, or *nodes*. The curve intersects itself a single time at a double point, hence there must be two tangents to the curve at that location. There are three species of double points that arise when the tangents to the curve at the double point are either a pair of distinct real lines, a pair of complex conjugate lines, or a pair of real but coincident lines.

To illustrate the different nature of the three types of double point consider the following cubic equation

$$y^2 = (x-a)(x-b)(x-c) \tag{6.45}$$

where the constant coefficients have rational positive magnitudes such that $a < b < c$. This curve, illustrated in Figure 6.11 (a), is symmetric with respect to the x-axis since every value of x gives equal and opposite values of y. The curve intersects the x-axis at the three points $x = a$, $x = b$, and $x = c$. When $x < a$ the value of y^2 is negative, and y is imaginary. When $a < x < b$ then y^2 is positive, and there are two real, equal and opposite values for y. For values of $b < x < c$ the value for y^2 is again negative, and finally positive again for all values $c < x$. The curve therefore consists of a closed oval between a and b and an open branch beginning at c and extending infinitely in two directions beyond it. The curve illustrated in Figure 6.11 has $a = 2$. $b = 4$, and $c = 5$. These values are then manipulated to yield a crunode, an acnode, and finally a cusp (spinode).

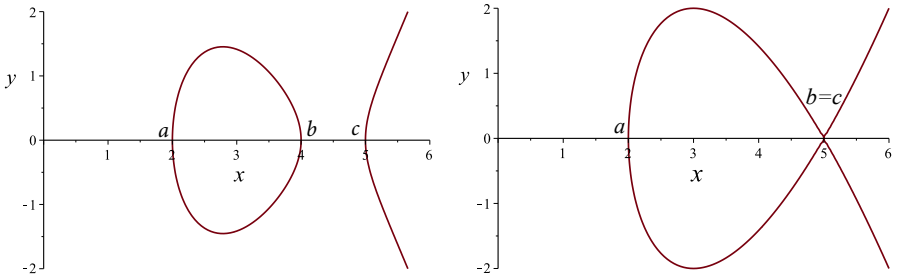

(a) Cubic with two real branches. (b) A crunode.

Figure 6.11: Species of double points: crunode.

6.4.2.4.1 Crunode Now let b vary in magnitude between the range $a \leq b \leq c$. As b increases in value the oval circuit increases in size maintaining it's location at a but growing towards c until $b = c$ and the curve crosses itself. Inspecting the curve illustrated in Figure 6.11 (b) we see that at the double point, or node, the two branches of the curve meet, and each branch has it's own real, distinct tangent. Such a point is called a *crunode*.

6.4.2.4.2 Acnode As b moves in the opposite direction towards a, the original oval circuit in Figure 6.11 (a) now shrinks in size until $b = a$. The cubic now

possesses an isolated double point at $x = a = b$. Isolated points, also known as *hermit* points satisfy the equation of the cubic but do not appear to lie on the curve, see Figure 6.12 (a). Such points are called *acnodes*. The tangents to the curve at an acnode are complex conjugate lines. No real line through the acnode intersects the curve in more than one real point, confirming the necessary condition that a real line cuts a cubic in at most three points.

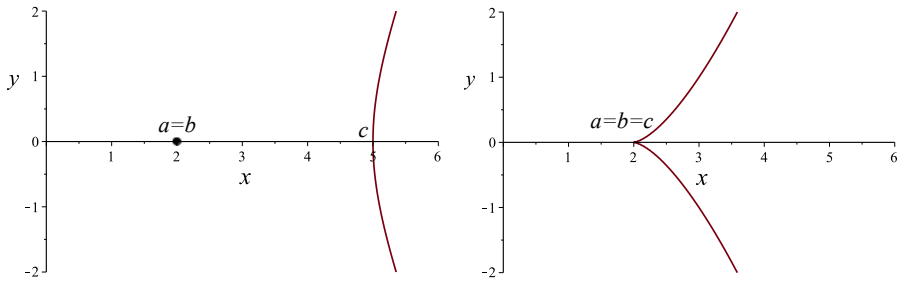

(a) An acnode. (b) A cusp, or spinode.

Figure 6.12: Species of double points: acnode and cusp (spinode).

6.4.2.4.3 Cusp (Spinode) The third species of double point occurs if the equation of the tangent to the curve at a point becomes a perfect square. In this case the tangents at the double point are two real, but coincident lines. In the case of the cubic in Equation (6.45) if we allow both coefficients b and c to approach a, the two distinct branches of the curve merge into a single branch when $a = b = c$ and Equation (6.45) becomes

$$y^2 \quad = (x - a)^3. \tag{6.46}$$

This situation is illustrated in Figure 6.12 (b). The double point where $x = a = b = c$ is called a *cusp*, or a *spinode*. They are also sometimes called *stationary points* because if the curve is generated by the motion of a point then at a cusp the motion of the point in one direction comes to a stop and changes direction. The tangent at the cusp meets the curve in three coincident points at $(a, 0)$ in Figure 6.12 (b). An example we touched on earlier is the four pointed asteroid in Figure 6.10. It contains four real cusps at the coordinates $(\pm a, 0)$ and $(0, \pm a)$.

6.4.2.5 Genus

The *genus* of an algebraic curve is defined as the deficiency between the maximum number of double points for a curve of it's order less the actual number of

double points the curve possesses [12]. The maximum number of double points, $DP_{\max}$, a curve of order n can have is

$$DP_{\max} = \frac{1}{2}(n-1)(n-2). \tag{6.47}$$

Hence, a curve of order $n = 4$ can have a maximum of three double points.

The genus of a curve plays a very important role in the theory of planar algebraic curves [14, 15]. We can define the genus of an algebraic curve, $\mathcal{G}$, as the maximum number of possible double points, $DP_{\max}$, less the actual number, DP_{act} as an equation to make it easier to remember:

$$\mathcal{G} = DP_{\max} - DP_{\text{act}}. \tag{6.48}$$

If $\mathcal{G} = 0$ the curve possesses it's maximum number of double points, in other words $DP_{\text{act}} = DP_{\max}$, then the coordinates of any point on the curve can be expressed as rational algebraic functions of a single variable parameter. This means that an n-dimensional curve with $\mathcal{G} = 0$ can be parametrised and the coordinates may be expressed as rational algebraic functions of parameter t as

$$\begin{aligned} x_1 &= f_1(t) \\ x_2 &= f_2(t) \\ &\vdots \\ x_n &= f_n(t). \end{aligned}$$

If however the genus of the curve is $\mathcal{G} > 0$, then there is no way to parametrise the curve. Because the genus of the algebraic version of the IO curve has genus $\mathcal{G} = 1$, it cannot be parametrised, and it is defined to be an *elliptic* curve [15], see Section 6.5.5. This definition does not mean that the curve has the form of an ellipse, rather it means that the curve can be expressed, with a suitable change of variables, as an elliptic curve. In the plane, every elliptic curve with real coefficients can be put in the standard form

$$x_2^2 = x_1^3 + Ax_1 + B$$

for some real constants A and B.

6.4.2.6 Plücker's Equations

When curves are generated as envelopes of tangent lines using line coordinates there are three dual characteristic numbers for the order of a curve point equation, it's number of cusps, and number of double points that are crunodes and

acnodes. These dual quantities are the *class* of the curve line equation (as we have already discussed in Section 6.4.2.3), the number of *inflection points*, and the number of *bitangent lines*, respectively. The symbols corresponding to these quantities and the corresponding dual quantities pairs:

$$\left.\begin{array}{rcl} \text{order} & = & n \\ \text{class} & = & m \end{array}\right\} \quad \text{dual;}$$

$$\left.\begin{array}{rcl} \text{number of double points} & = & \delta \\ \text{number of bitangent lines} & = & \tau \end{array}\right\} \quad \text{dual;}$$

$$\left.\begin{array}{rcl} \text{number of cusps} & = & \kappa \\ \text{number of inflection points} & = & \iota \end{array}\right\} \quad \text{dual.}$$

The dual of a *cusp* is an *inflection point*. A cusp is generated when a point tracing the curve reaches a limit on it's path and changes direction while an inflection point is generated when a line enveloping a curve reaches a limiting gradient and then reverses. The dual of a *crunode* double point is a single line that is tangent to the curve at two distinct points and is called a *double tangent*, or *bitangent line*. The bitangent line, by analogy to an acnode, may have imaginary conjugate tangent points. In 1839 Julius Plücker published a comprehensive theory of algebraic curves [23] in which he identified five equations relating these six numbers. The versions presented here were derived in detail in [15], while different useful versions are derived in [14]:

$$\left.\begin{array}{rcll} n(n-1) & = & m + 2\delta + 3\kappa; & \text{(a)} \\ m(m-1) & = & n + 2\tau + 3\iota; & \text{(b)} \\ 3n(n-2) & = & \iota + 6\delta + 8\kappa; & \text{(c)} \\ 3m(m-2) & = & \kappa + 6\tau + 8\iota; & \text{(d)} \\ 3(n-m) & = & \kappa - \iota. & \text{(e)} \end{array}\right\} \tag{6.49}$$

In this set of equations, enumerated simply as Equation (6.49), (a) and (b) are duals of each other, as are (c) and (d), while (e) is self-dual [12]. They may be cautiously used to establish limits on some of these numbers given knowledge of others, but they do not always unequivocally give answers. For example, one may compute the class of a curve if the order, number of double points, and number of cusps is known, but doubt may remain because of the need to distinguish between real and imaginary quantities as well as those at infinity.

6.5 Open Kinematic Chains

Recall from *Chapter 1: Introduction* that a kinematic chain is simple if each link in the chain is coupled to at most two other links. The degree of connectivity (DOC) of a link indicates the number of rigid bodies joined to it. If all links are binary ($DOC = 2$) the simple chain is closed. E.g. a four-bar mechanism. Alternately the simple chain is open with the first and last links having $DOC = 1$. Our analysis of planar four-bar mechanisms considered only closed simple kinematic chains, we now turn our attention briefly to the analysis of open chains.

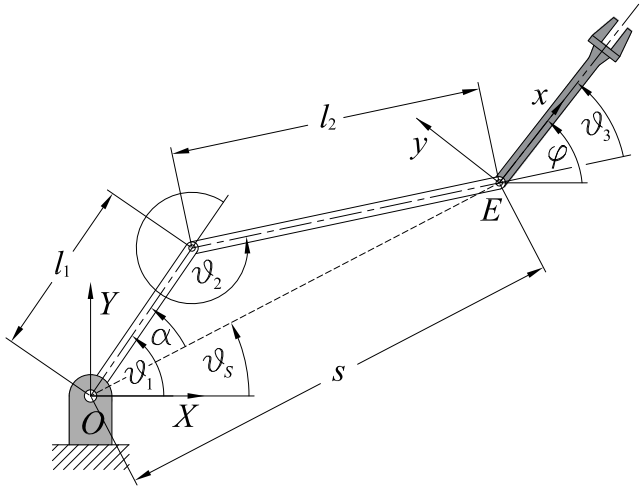

Figure 6.13: A $3R$ planar serial robotic arm.

Over the decades the study of the kinematics and kinetics of open kinematic chains has become largely associated with the study of the dynamics and control of industrial serial robots, see [24] for a comprehensive introduction. Since the focus of these notes is largely on closed kinematic chains the introduction given here is intended only to illustrate the difference between the analysis of closed and open chains. Consider the $3R$ planar serial robotic arm illustrated in Figure 6.13. The two fundamental questions involved in the kinematic analysis of serially jointed robot arms are known as the *forward* and the *inverse* kinematics problems.

6.5.1 Forward Kinematics Problem

The forward kinematics problem involves computing the position and orientation of the end-effector given the individual joint angles. For the planar serial robot in Figure 6.13 this requires determining the location of the origin of the end-effector reference coordinate system, point E in this case, and the angle the x-axis makes with respect to the X-axis of the non-moving ground-fixed reference coordinate system with origin located at point O, given the joint angles, in this case ϑ_1, ϑ_2, and ϑ_3.

Because this is a planar problem, the absolute orientation of the end-effector reference coordinate system with respect to the X-axis, let's call it θ_4, is simply the sum of the three relative joint angles:

$$\theta_4 \quad = \quad \vartheta_1 + \vartheta_2 + \vartheta_3. \tag{6.50}$$

To compute the location of the origin E of the end-effector coordinate system the usual approach is to concatenate the appropriate homogeneous transformation matrices. However, in the planar case we may simply use the law of cosines. Because ϑ_2 is the external angle of edge l_2 with respect to edge l_1 of triangle $\triangle l_1 l_2 s$ we can use the alternate form of the cosine law to compute the distance s between origins O and E as

$$s \quad = \quad \sqrt{l_1^2 + l_2^2 + 2 l_1 l_2 \cos \vartheta_2}. \tag{6.51}$$

The angle that line s makes with respect to the X-axis is ϑ_s, given by

$$\vartheta_s \quad = \quad \vartheta_1 - \alpha \quad = \quad \vartheta_1 - \cos^{-1}\left(\frac{l_1^2 s^2 - l_2^2}{2 l_1 s}\right). \tag{6.52}$$

Finally, the position vector of E in the ground fixed coordinate system with origin at O is

$$\mathbf{E} \quad = \quad \begin{bmatrix} s\cos\vartheta_s \\ s\sin\vartheta_s \end{bmatrix}. \tag{6.53}$$

6.5.2 Inverse Kinematics Problem

The inverse kinematics problem involves computing the joint angles ϑ_1, ϑ_2, and ϑ_3 required to to give the moving coordinate system with origin E a particular position and orientation within the reachable workspace of the arm. Since the position and orientation of the coordinate system that moves with E is given

we know the angle θ_4 and the position vector $\mathbf{E}$, and hence length s, using trigonometry and the cosine law we can compute

$$\vartheta_s = \tan^{-1}\left(\frac{E_Y}{E_X}\right), \quad \text{and} \quad \alpha = \cos^{-1}\left(\frac{l_1^2 + s^2 - l_2^2}{2l_1 s}\right). \tag{6.54}$$

Next we compute

$$\vartheta_1 = \vartheta_s + \alpha. \tag{6.55}$$

We again use the cosine law to obtain

$$\vartheta_2 \quad = \quad \cos^{-1}\left(\frac{l_1^2 + l_2^2 - s^2}{2l_1 l_2}\right). \tag{6.56}$$

Finally, since we are given the angle θ_4 we can determine the last joint angle with Equation (6.50)

$$\vartheta_3 \quad = \quad \theta_4 - \vartheta_1 - \vartheta_2. \tag{6.57}$$

Of course, there are usually more than one solution, and in order for a solution to exist it must be that the goal point given by length s is located within the reachable workspace of the arm such that $s \leq l_1 + l_2$.

6.5.3 Assembly Modes

Planar, spherical, and spatial four-bar mechanisms all possess two *assembly modes* if the link lengths permit the mechanism to have some mobility. This means that for a given input angle there are two possible output angles, one for each assembly mode. For a Grashof linkage, where the sum of the shortest and longest link lengths is less than the sum of the lengths of the other two, to transition between assembly modes requires removing the joint connecting the coupler to the output link, and reassembling the linkage in the other assembly mode. Transition linkages, where the sum of the shortest and longest link lengths is identically equal to the sum of the lengths of the other two, have at least one *folding* configuration where the input link, coupler, and output link are collinear with the non-moving link. The linkage can switch between assembly modes coming out of the folded configuration.

Consider a planar $4R$ mechanism with link lengths $a_1 = 4, a_2 = 12, a_3 = 8, a_4 = 10$ generic units of length. Let the input link be a_1, and let the input angle be $\theta_1 = 21.16135764°$, as illustrated in Figure 6.14. Using the Plücker numbers of the v_1-v_4 IO curve, it can be shown that the genus of a non-degenerate IO curve is always 1, and therefore there is a maximum number of two assembly

modes, see Section 6.5.5.3. This is so because of a theorem on algebraic curves proved by Axel Harnack in 1876 [25] which relates the circuits of an algebraic curve to its genus. Each of the v_i-v_j algebraic IO equations are quartic curves of genus 1, therefore, following Harnack, each can have at most two circuits. Each circuit of a particular v_i-v_j IO curve corresponds to one of the mechanisms assembly modes. In essence, Harnack's theorem states that an algebraic curve of genus n can have at most $n + 1$ circuits. One may therefore immediately conclude that a planar 4R mechanism can never have more than two assembly modes.

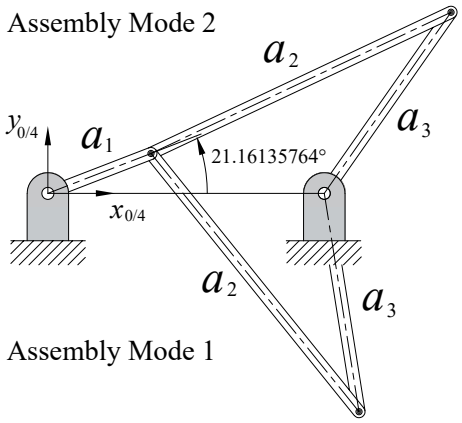

Figure 6.14: 4R assembly modes.

6.5.4 Planar 4R Mechanism Input-output Equations

The first type of linkage that will be analysed contains four rigid links coupled by four R-pairs forming a simple closed kinematic chain. These linkages are generally denoted as 4R mechanisms. In later sections we will examine $RRRP$ and $PRRP$ mechanisms, typically called slider-cranks and elliptical trammels, as well as spherical 4R and some spatial mechanisms.

The new material presented in what follows is from [26, 27], but even newer and more refined results are included as well. Of particular interest is the generalised algorithm for deriving algebraic input-output (IO) equations for planar, spherical, and spatial four-bar mechanisms [28]. However, the algorithm presented in [28], which will be summarised later in this chapter, allows for the analysis of the functional relationship between any of the six joint variable pairs because it uses relative joint angle parameters defined using the Denavit-

Hartenberg rules for assigning coordinate systems to each joint in a kinematic chain, see Section 6.5.5. A planar $4R$ function generator correlates driver and follower angles in a functional relationship. The mechanism can be designed to generate the function $\theta_4 = f(\theta_1)$, or $\theta_1 = f(\theta_4)$, see Figure 6.15. Analysis of the $4R$ mechanism when the four link lengths are specified is greatly facilitated with the algebraic IO equations since every angle pairing in the deformable quadrilateral can be analyses. These equations are equally easy to use for function generation sysntesis.

6.5.4.1 The Freudenstein Trigonometric Input-output Equation

Early analysis and design methods for synthesising function generating linkages typically employ the Freudenstein IO equation, Equation (6.58), to identify link lengths required to generate the function [29, 30]. Exact synthesis uses three IO pairs that satisfy the function which are used to generate three synthesis equations which can be solved linearly for the three k_i, which are ratios of the link lengths, identifying a linkage that generates the function exactly at the three specified input angles. Approximate synthesis uses over-determined sets of prescribed IO angle pairs which generate an over-determined set of synthesis equations which can be solved for using any least squares method to minimise a specified performance error. The identified linkage will, in general, not exactly generate the function at any input angle but will have a smaller overall error than the exact synthesis linkage. While kinematic synthesis is the central topic of Chapter 4, is will be summarised briefly below.

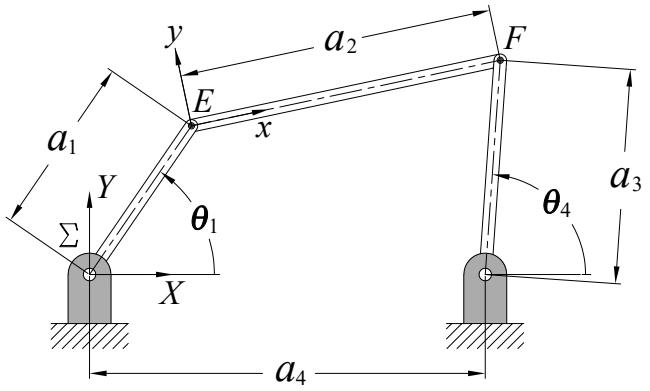

Figure 6.15: 4R four-bar mechanism.

The Freudenstein equation relating the input to the output angles of a planar

$4R$ four-bar mechanism, with link lengths as in Figure 6.15, was first put forward in [31]. In the equation the angle θ_1 is traditionally selected to be the input while θ_4 is the output angle:

$$k_1 + k_2\cos(\theta_{4_i}) - k_3\cos(\theta_{1_i}) \quad = \quad \cos(\theta_{1_i} - \theta_{4_i}). \tag{6.58}$$

Equation (6.58) is linear in the k_i Freudenstein parameters, which are defined in terms of the link length ratios as

$$\left.\begin{array}{rcl} k_1 & \equiv & \dfrac{(a_1^2 + a_3^2 + a_4^2 - a_2^2)}{2a_1a_3}, \\ k_2 & \equiv & \dfrac{a_4}{a_1}, \\ k_3 & \equiv & \dfrac{a_4}{a_3}. \end{array}\right\} \Leftrightarrow \left\{\begin{array}{rcl} a_4 & = & 1, \\ a_1 & = & \dfrac{1}{k_2}, \\ a_3 & = & \dfrac{1}{k_3}, \\ a_2 & = & (a_1^2 + a_3^2 + a_4^2 - 2a_1a_3k_1)^{1/2}. \end{array}\right.$$

For function generation, the scale of the linkage is arbitrary, requiring identification of only three link length ratios. For exact synthesis, this means that three Freudenstein synthesis IO equations must be specified. The system of three equations, linear in the three Freudenstein parameters, is solved for the three unknown Freudenstein parameters, thereby establishing the three link length ratios that will exactly generate the function at the three specified input angles. When a four-bar $4R$ linkage is needed to generate a specified function of the forum $\theta_4 = f(\theta_1)$ the first decision to be made is how to synthesise the linkage: should an exact or approximate synthesis method be employed. If exact synthesis is to be used, then the input angle range must be specified as the set $(\theta_{1_1}, \theta_{1_2}, \theta_{1_3})$, where θ_{1_1} is the minimum value and θ_{1_3} is the maximum value, with θ_{1_2} lying somewhere in between. Next the three Freudenstein synthesis equations are solved, which will identify the values of the link lengths a_1, a_2, and a_3 in terms of a_4.

Once the link lengths have been specified, the design and structural errors are important performance indicators in the assessment and optimisation of function generating linkages arising by means of approximate synthesis. The *design error* indicates the error residual incurred by a specific linkage in satisfying its IO synthesis equations. The *structural error*, in turn, is the difference between the prescribed linkage output value and the actual generated output value for a given input value [32]. From a design point of view it may be successfully

argued that the structural error is the one that really matters, for it is directly related to the performance of the linkage.

It has been observed [33, 34] that as the cardinality of the prescribed discrete IO data set increases, the corresponding four-bar linkages that minimise the Euclidean norm of the design and structural errors tend to converge to the same linkage. The important implication is that minimising the Euclidean norm, or any p-norm, of the structural error can be accomplished indirectly by minimising the same norm of the design error, provided that a suitably large number of IO pairs is prescribed. The importance arises from the fact that the minimisation of the Euclidean norm of the design error leads to a linear least-squares problem whose solution can be obtained directly as opposed to iteratively [35, 36], while the minimisation of the same norm of the structural error leads to a nonlinear least-squares problem, and hence, calls for an iterative solution [32]. In [34] the trigonometric Freudenstein synthesis equations are integrated in the range between minimum and maximum input values, thereby reposing the discrete approximate synthesis problem as a continuous one whereby the objective function is optimised over the entire IO range. Hence, the long-term goal of research in this area is to determine a general method to derive motion constraint based algebraic IO equations that may be used together with the method of continuous approximate synthesis [34] to obtain the very best linkage that can generate an arbitrary function. The goal of what is now presented is to develop one in the hope of providing new insight into the continuous approximate synthesis of function generators, while mitigating numerical integration error. Of course, the same equation will be obtained by making the tangent half-angle substitutions directly into the Freudenstein equation then collecting terms after factoring, normalising, and eliminating non-zero factors. But that must be the case since the geometric relations require that outcome, however this is irrelevant because the goal is to generalise a method to develop constraint based algebraic IO equations for continuous approximate synthesis of planar, spherical, and spatial linkages. Such a generalised method using relative joint angles is presented in Section 6.5.5.

6.5.4.2 Algebraic Input-output Equation Using Absolute Angles

To the best of the authors knowledge, there are no alternative algebraic models of the function generator displacement equations in the accessible literature with the exception of a trigonometric-based derivation by Bottema and Roth [19] relating the angles θ_1 and θ_4. However, in that work absolute measures of angle are used in the derivation, and as we will show in Section 6.5.5, this

eliminates the possibility of representing the IO equations of the remaining five θ_i and θ_j angle pairings, where $i, j \in \{1, 2, 3, 4\}$, of the interior angles of the deformable quadrangle using the same coefficients but in different permutations, see Figure 6.15.

The new idea starts the same as with the Freudenstein and Bottema-Roth methods, writing the displacement constraints in terms of the IO angles. Continuing with tradition of using the absolute angles referenced to the positive X-axis with counter-clockwise considered positive, we select θ_1 to be the input angle and θ_4 to be the output angle, see Figure 6.15. Let Σ be a non moving Cartesian coordinate system with coordinates X and Y whose origin is located at the centre of the ground fixed R-pair connected to the link with length a_1. Let E be a coordinate system that moves with the coupler of length a_2 whose origin is at the centre of the distal R-pair of link a_1, having basis directions x and y.

The displacement constraints for the origin of E can be expressed in terms of Σ as

$$\begin{aligned} X - a_1 \cos\theta_1 &= 0, \\ Y - a_1 \sin\theta_1 &= 0, \end{aligned} \tag{6.59}$$

while those for point F, located at the centre of the distal R-pair on the output link with length a_3 are

$$\begin{aligned} X - a_4 - a_3 \cos\theta_4 &= 0, \\ Y - a_3 \sin\theta_4 &= 0. \end{aligned} \tag{6.60}$$

Next, we use a planar projection of Study's soma coordinates [37] to establish the IO equation. While Study's soma will be explained in detail in *Chapter 5: Geometry*, a few words of introduction are given here. There are several possibilities to parameterise the rigid body displacement group, one of them being the kinematic mapping that was originally formulated by Eduard Study and reported in an appendix of his book "Geometrie der Dynamen" [37] in 1903. It defines every distinct Euclidean displacement as a distinct point on a six-dimensional quadric hyper-surface in a seven-dimensional projective space $\mathbb{P}^7$ now known as the Study quadric, S_6^2. A point on S_6^2 consists of eight homogeneous coordinates, not all zero, $[x_0 : x_1 : x_2 : x_3 : y_0 : y_1 : y_2 : y_3]$ which Study called a "soma", a Greek word meaning "body". The six-dimensional hyper-surface is represented as a bilinear hyper-quadratic equation given by

$$x_0 y_0 + x_1 y_1 + x_2 y_2 + x_3 y_3 = 0, \tag{6.61}$$

excluding the *exceptional generator*, which we call A_∞, where $x_0 = x_1 = x_2 =$

$x_3 = 0$, having the parametric representation

$$[0 : 0 : 0 : 0 : y_0 : y_1 : y_2 : y_3].$$

A_∞ does not represent any real displacement, but it nonetheless plays an important role as a generator space. For a soma to represent a real displacement in the special Euclidean group of displacements in three dimensions, $SE(3)$, it must satisfy two conditions: the first being Equation (6.61); the second being the inequality

$$x_0^2 + x_1^2 + x_2^2 + x_3^2 \quad \neq \quad 0. \tag{6.62}$$

Equation (6.61) contains only bilinear cross terms. This implies that the quadric has been rotated out of its standard position, or normal form. It is straightforward to diagonalise the quadratic form of Equation (6.61) which reveals that this six-dimensional quadric in $\mathbb{P}^7$ has the normal form

$$x_0^2 + x_1^2 + x_2^2 + x_3^2 - y_0^2 - y_1^2 - y_2^2 - y_3^2 = 0, \tag{6.63}$$

which is analogous to the Plücker quadric, P_4^2, of line geometry. The normal form of S_6^2 shows that it is a six-dimensional hyperboloid of one sheet doubly-ruled by special 3-space generators in two opposite reguli, which we call A-planes and B-planes, after [38]. While the generator lines of an hyperboloid of one sheet in Euclidean three dimensional space, $\mathbb{E}^3$, are skew lines in two reguli, the generator spaces of S_6^2 are three dimensional spaces in two opposite reguli. A symbolic sketch of S_6^2 that shows the A-planes as generator spaces is displayed in Figure 6.16.

It can be shown that lines on S_6^2 represent either a one parameter set of translations or rotations. The lines which contain the 1×8 identity array $[1 : 0 : 0 : \ldots : 0]$, which Study called the "protosoma", are either the one parameter rotation or translation subgroups. The exceptional generator A_∞ is an A-plane. In general, two different A-planes do not intersect, nor do two different B-planes, but there are exceptions [39]. An A-plane corresponds to the special orthogonal group of rotations in three dimensions, $SO(3)$, if it contains the identity and its intersection with A_∞ is the empty set, and to the special Euclidean group of displacements in two dimensions, $SE(2)$, if it contains the identity and intersects A_∞ in a line. These two types of A-planes intersect each other in lines on S_6^2. Each of these lines represent rotations about the line orthogonal to the plane of the planar displacement and through the centre point of the spherical displacement [39, 40]. The only B-planes that intersect A_∞

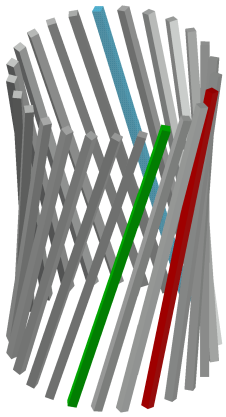

Figure 6.16: Symbolic sketch of the Study quadric S_6^2.

correspond to the subgroup of all translations, while in general the intersection of an A-plane and a B-plane is either a point, or a two dimensional plane [41].

Given a homogeneous transformation matrix $\mathbf{T}$ whose 3×3 rotation submatrix elements are denoted as $\mathbf{A} = (a_{ij})$ with $i, j \in \{1, 2, 3\}$ and whose translation vector $\mathbf{t}$ has elements t_k where $k \in \{1, 2, 3\}$, then the corresponding Study soma coordinates, also known as Study parameters, are obtained in the following way. The homogeneous quadruple $x_0 : x_1 : x_2 : x_3$ can be obtained from at least one of the following ratios:

$$\begin{aligned} x_0 : x_1 : x_2 : x_3 &= 1 + a_{11} + a_{22} + a_{33} : a_{32} - a_{23} : a_{13} - a_{31} : a_{21} - a_{12}; \\ &= a_{32} - a_{23} : 1 + a_{11} - a_{22} - a_{33} : a_{12} + a_{21} : a_{31} + a_{13}; \\ &= a_{13} - a_{31} : a_{12} + a_{21} : 1 - a_{11} + a_{22} - a_{33} : a_{23} + a_{32}; \\ &= a_{21} - a_{12} : a_{31} + a_{13} : a_{23} + a_{32} : 1 - a_{11} - a_{22} + a_{33}. \end{aligned} \tag{6.64}$$

The remaining four coordinates $y_0 : y_1 : y_2 : y_3$ are linear combinations of the x_i and $\mathbf{t} = [t_1, t_2, t_3]^T$ and are computed as

$$\left.\begin{aligned} y_0 &= \tfrac{1}{2}(t_1 x_1 + t_2 x_2 + t_3 x_3), \\ y_1 &= \tfrac{1}{2}(-t_1 x_0 + t_3 x_2 - t_2 x_3), \\ y_2 &= \tfrac{1}{2}(-t_2 x_0 - t_3 x_1 + t_1 x_3), \\ y_3 &= \tfrac{1}{2}(-t_3 x_0 + t_2 x_1 - t_1 x_2). \end{aligned}\right\} \tag{6.65}$$

Study developed the method to compute the four x_i parameters directly from the 3×3 rotation submatrix $\mathbf{A}$ via one of the four sets of ratios expressed in

Equation (6.64). In general each of the four yield the same ratios. But in certain instances, for example when $\mathbf{A}$ describes a rotation through angle π, one or more of the four ratios in Equation (6.64) result in $x_0 : x_1 : x_2 : x_3 = 0 : 0 : 0 : 0$, the exceptional generator. But for every rotation matrix $\mathbf{A}$ at least one of the four ratios does not result in four zeros. Study also showed that the mapping is bijective, meaning that for each point on S_6^2 there is one and only one Euclidean displacement represented by the homogeneous 4×4 transformation matrix $\mathbf{T}$:

$$\mathbf{T} = \frac{1}{\delta}\begin{bmatrix} x_0^2+x_1^2+x_2^2+x_3^2 & 0 & 0 & 0 \\ 2(-x_0y_1+x_1y_0-x_2y_3+x_3y_2) & x_0^2+x_1^2-x_2^2-x_3^2 & 2(-x_0x_3+x_1x_2) & 2(x_0x_2+x_1x_3) \\ 2(-x_0y_2+x_1y_3+x_2y_0-x_3y_1) & 2(x_0x_3+x_1x_2) & x_0^2-x_1^2+x_2^2-x_3^2 & 2(-x_0x_1+x_2x_3) \\ 2(-x_0y_3-x_1y_2+x_2y_1+x_3y_0) & 2(-x_0x_2+x_1x_3) & 2(x_0x_1+x_2x_3) & x_0^2-x_1^2-x_2^2+x_3^2 \end{bmatrix}$$

where $\delta = x_0^2 + x_1^2 + x_2^2 + x_3^2$. The first column is the associated translation of the Euclidean displacement and the elements of the lower right 3×3 submatrix are the nine a_{ij} of the associated rotation matrix $\mathbf{A}$. The order of the rows in $\mathbf{T}$ require the homogeneous coordinate vector to have the homogenising coordinate w be the first element: $[w, x, y, z]^T$.

The transformation matrix $\mathbf{T}$ simplifies considerably when we consider displacements that are restricted to a plane. Three degrees of freedom are lost and hence four Study parameters vanish. The displacements may be restricted to any plane. Without loss in generality, we may select one of the principal planes in Σ. Thus, we arbitrarily select the plane $Z = 0$. Since E and Σ are assumed to be initially coincident, this means

$$\begin{bmatrix} W \\ X \\ Y \\ 0 \end{bmatrix} = \mathbf{T} \begin{bmatrix} w \\ x \\ y \\ 0 \end{bmatrix}. \tag{6.66}$$

This planar case requires that $t_3 = 0$ since $Z = z = 0$ because reference frame E can translate in neither the Z nor z directions. It also requires that $a_{13} = a_{31} = a_{32} = a_{23} = 0$ because any rotation must occur about an axis parallel to the Z-axis, meaning that the associated rotation matrix for an angle θ is

$$\mathbf{R}_Z(\theta) = \begin{bmatrix} \cos\theta & -\sin\theta & 0 \\ \sin\theta & \cos\theta & 0 \\ 0 & 0 & 1 \end{bmatrix} = \begin{bmatrix} a_{11} & a_{12} & a_{13} \\ a_{21} & a_{22} & a_{23} \\ a_{31} & a_{32} & a_{33} \end{bmatrix} \tag{6.67}$$

Using the first set of ratios in Equation (6.64)

$$x_0 : x_1 : x_2 : x_3 = 1 + a_{11} + a_{22} + a_{33} : a_{32} - a_{23} : a_{13} - a_{31} : a_{21} - a_{12},$$

and the elements of the rotation matrix in Equation (6.67) it is to be seen that

$$x_1 \;=\; a_{32} - a_{23} \;=\; 0 - 0 \;=\; 0$$

and

$$x_2 \;=\; a_{13} - a_{31} \;=\; 0 - 0 \;=\; 0.$$

Using the definitions of the y_i soma in Equation (6.65) it is to be seen that

$$y_0 \;=\; \frac{1}{2}\left(t_1x_1 + t_2x_2 + t_3x_3\right) \;=\; \frac{1}{2}\left(0 + 0 + 0\right) \;=\; 0$$

and

$$y_3 \;=\; \frac{1}{2}\left(-t_3x_0 + t_2x_1 - t_1x_2\right) \;=\; \frac{1}{2}\left(0 + 0 + 0\right) \;=\; 0.$$

Therefore displacements restricted to the plane $Z = z = 0$ leaves us with only the four soma coordinates

$$[x_0 : x_3 : y_1 : y_2]. \tag{6.68}$$

The non-zero condition is now $x_0^2 + x_3^2 \neq 0$, and the fourth row and column of the reduced $\mathbf{T}$ contains only this condition as the last element, with zeros elsewhere, leading to the trivial equation $Z = z = 0$. We can therefore eliminate the fourth row and column and normalise the coordinates with the nonzero condition giving the planar mapping equation

$$\mathbf{T} \;=\; \frac{1}{x_0^2 + x_3^2}\begin{bmatrix} x_0^2 + x_3^2 & 0 & 0 \\ 2(-x_0y_1 + x_3y_2) & x_0^2 - x_3^2 & -2x_0x_3 \\ -2(x_0y_2 + x_3y_1) & 2x_0x_3 & x_0^2 - x_3^2 \end{bmatrix}. \tag{6.69}$$

We can now express a point in Σ in terms of the soma coordinates and the corresponding point coordinates in E as

$$\begin{bmatrix} 1 \\ X \\ Y \end{bmatrix} = \mathbf{T}\begin{bmatrix} 1 \\ x \\ y \end{bmatrix} = \frac{1}{x_0^2+x_3^2}\begin{bmatrix} x_0^2+x_3^2 \\ 2(-x_0y_1+x_3y_2)+(x_0^2-x_3^2)x-(2x_0x_3)y \\ -2(x_0y_2+x_3y_1)+(2x_0x_3)x+(x_0^2-x_3^2)y \end{bmatrix}. \tag{6.70}$$

The novelty of the approach to deriving the algebraic $4R$ IO equation begins with the creation of two Cartesian vector constraint equations containing the nonhomogeneous coordinates in Equations (6.59) and (6.60), but substituting

the values in Equation (6.70) for (X, Y). These two vector equations are $\mathbf{F}_1 = \mathbf{0}$ and $\mathbf{F}_2 = \mathbf{0}$:

$$\mathbf{F}_1 = \frac{1}{x_0^2+x_3^2}\begin{bmatrix} 2(-x_0y_1+x_3y_2)+(x_0^2-x_3^2)x-2x_0x_3y-(a_1\cos\theta_1)(x_0^2+x_3^2) \\ -2(x_0y_2+x_3y_1)+2x_0x_3x+(x_0^2-x_3^2)y-(a_1\sin\theta_1)(x_0^2+x_3^2) \end{bmatrix} = \mathbf{0};$$

$$\mathbf{F}_2 = \frac{1}{x_0^2+x_3^2}\begin{bmatrix} 2(-x_0y_1+x_3y_2)+(x_0^2-x_3^2)x-2x_0x_3y-(a_3\cos\theta_4+a_1)(x_0^2+x_3^2) \\ -2(x_0y_2+x_3y_1)+2x_0x_3x+(x_0^2-x_3^2)y-(a_3\sin\theta_4)(x_0^2+x_3^2) \end{bmatrix} = \mathbf{0}.$$

Now we determine equations for the coupler, a_2. The coordinate system that moves with the coupler has its origin, point E, on the centre of the R-pair, as in Figure 6.15, having coordinates $(x, y) = (0, 0)$, while point F is on the R-pair centre on the other end having coordinates $(x, y) = (a_2, 0)$. One more vector equation, $\mathbf{H}_1$ is obtained by substituting $(x, y) = (0, 0)$ in $\mathbf{F}_1$, and another, $\mathbf{H}_2$ is obtained by substituting $(x, y) = (a_2, 0)$ in $\mathbf{F}_2$. Next $\mathbf{H}_1$ and $\mathbf{H}_2$, two rational expressions, are converted to factored normal form. This is the form where the numerator and denominator are relatively prime polynomials with integer coefficients. The denominators for both $\mathbf{H}_1$ and $\mathbf{H}_2$ are the nonzero condition $x_0^2 + x_3^2$, which can safely be factored out of each equation leaving the following two vector equations with polynomial elements:

$$\mathbf{H}_1 = \begin{bmatrix} -a_1\cos\theta_1(x_0^2+x_3^2)+2(-x_0y_1+x_3y_2) \\ -a_1\sin\theta_1(x_0^2+x_3^2)-2(x_0y_1+x_3y_2) \end{bmatrix} = \mathbf{0}; \tag{6.71}$$

$$\mathbf{H}_2 = \begin{bmatrix} -(a_3\cos\theta_4+a_4)(x_0^2+x_3^2)+a_2(x_0^2-x_3^2)+2(-x_0y_1+x_3y_2) \\ -a_3\sin\theta_4(x_0^2+x_3^2)+2a_2(x_0x_3)-2(x_0y_2+x_3y_1) \end{bmatrix} = \mathbf{0}. \tag{6.72}$$

The system of four displacement constraints on the IO equations are $\mathbf{H}_1 = \mathbf{0}$ and $\mathbf{H}_2 = \mathbf{0}$. However, these are trigonometric equations. We convert them to algebraic ones using the tangent of the half-angle substitutions

$$v_1 = \tan\frac{\theta_1}{2}, \quad v_2 = \tan\frac{\theta_4}{2},$$

and

$$\cos\theta_1 = \frac{1-v_1^2}{1+v_1^2}, \quad \sin\theta_1 = \frac{2v_1}{1+v_1^2},$$
$$\cos\theta_4 = \frac{1-v_2^2}{1+v_2^2}, \quad \sin\theta_4 = \frac{2v_2}{1+v_2^2}.$$

The usual constraint equations in the kinematic mapping image space are obtained by considering $\mathbf{H}_1$ and $\mathbf{H}_2$ with the tangent of the half-angles, giving four new algebraic polynomials when considering the individual elements converted to factored normal form. The denominators are v_1^2+1 and v_2^2+1 which can safely be factored out because they are always non-vanishing. The resulting four algebraic equations are expressed in terms of the elements of $\mathbf{K}_1 = \mathbf{0}$ and $\mathbf{K}_2 = \mathbf{0}$:

$$\mathbf{K}_1 = \begin{bmatrix} (a_1v_1^2-a_1)(x_0^2+x_3^2)+2v_1^2(-x_0y_1+x_3y_2)+2(-x_0y_2+x_3y_1) \\ \\ -2a_1v_1(x_0^2+x_3^2)-2(1+v_1^2)(-x_0y_2+x_3y_1) \end{bmatrix} = \mathbf{0}; \tag{6.73}$$

$$\mathbf{K}_2 = \begin{bmatrix} (v_2^2(a_3-a_4)+a_3-a_4)(x_0^2+x_3^2)+(a_2v_2^2+a_2)(x_0^2-x_3^2)+2(1+v_2^2)(-x_0y_1+x_3y_2) \\ \\ 2a_2v_2^2x_0x_3-2(v_2^2+a_3v+1)(x_0^2+x_3^2)+2a_2x_0x_3 \end{bmatrix} = \mathbf{0}. \tag{6.74}$$

Factoring the resultant of the first and second elements of $\mathbf{K}_1 = \mathbf{0}$ with respect to v_1, as well as the first and second elements of $\mathbf{K}_2 = \mathbf{0}$ with respect to v_2 yields the two displacement constraint equations in the image space:

$$a_1^2(x_0^2+x_3^2) - 4(y_1^2+y_2^2) \quad = \quad 0,$$

$$\begin{aligned}(\,a_3^2-a_2^2-a_4^2)(x_0^2+x_3^2) + 2a_2a_4(x_0^2-x_3^2) + 4a_2(x_0y_1+x_3y_2)+ \\ 4a_4(-x_0y_1+x_3y_2) - 4(y_1^2+y_2^2) \quad = \quad 0.\end{aligned}$$

Inspection of the quadratic forms of these two equations reveals that they are two hyperboloids of one sheet in coordinate space of the soma coordinates x_3, y_1, y_2 projected into the hyperplane $x_0 = 1$, which is exactly what is expected for two RR dyads [42]. For a particular linkage, where values for a_1, a_2, a_3, and a_4 have been specified, the two constraint surfaces will intersect in the displacement curve of the coupler, see for example Figure (6.17).

But these are not the constraints we are looking for. We want to eliminate the image space coordinates using $\mathbf{K}_1 = \mathbf{0}$ and $\mathbf{K}_2 = \mathbf{0}$ to obtain an algebraic polynomial with the tangent half angles v_1 and v_4 as variables and link lengths as coefficients. To obtain this algebraic polynomial we start by setting the homogenising coordinate $x_0 = 1$, which can safely be done since we are only concerned with real finite displacements. Next, observe that the two equations represented by the components of $\mathbf{K}_1 = \mathbf{0}$ (Equation (6.73)) have a simpler form than those of $\mathbf{K}_2 = \mathbf{0}$ (Equation (6.74)), and are linear in y_1 and y_2. Solving

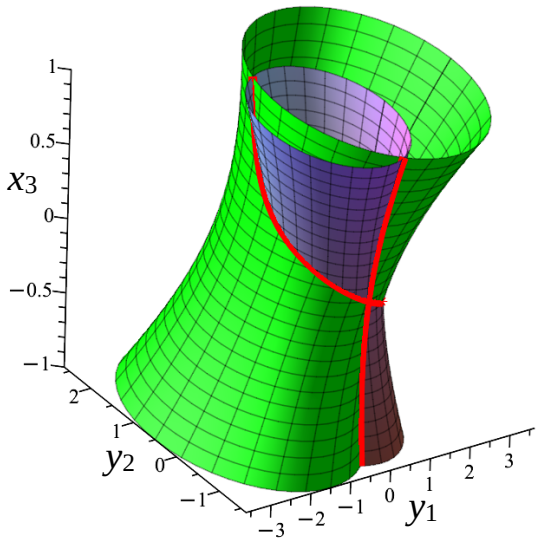

Figure 6.17: Two intersecting constraint hyperboloids of one sheet in the hyperplane $x_0 = 1$.

these two equations for y_1 and y_2 reveals that

$$y_1 = \frac{1}{2}\frac{a_1(v_1^2 - 2v_1x_3 - 1)}{v_1^2 + 1}, \tag{6.75}$$

$$y_2 = \frac{1}{2}\frac{a_1(v_1^2x_3 + 2v_1 - x_3)}{v_1^2 + 1}. \tag{6.76}$$

Equations (6.75) and (6.76) reveal the common denominator of v_1^2+1, which can never be less than 1, and hence may be factored out. Now we back-substitute these expressions for y_1 and y_2 into the array components of Equation (6.74), thereby eliminating these image space coordinates, and factor the resultant with respect to x_3 which yields four factors. The first three are

$$4a_2^2, \;\; (v_1^2 + 1)^3, \;\; (v_4^2 + 1)^3.$$

None of these three factors can ever be zero and at the same time represent a real displacement constraint, hence they are eliminated. The remaining factor is a polynomial with only v_1 and v_4 as variables and link lengths a_1, a_2, a_3, and a_4, as coefficients. This is exactly the constraint equation we desire. It is factored, and the terms collected then distributed over v_1 and v_4 revealing

$$Av_1^2v_4^2 + Bv_1^2 + Cv_4^2 - 8a_1a_3v_1v_4 + D = 0, \tag{6.77}$$

where:

$$\begin{aligned} A &= (a_1 - a_2 - a_3 + a_4)(a_1 + a_2 - a_3 + a_4) = A_1 A_2; \\ B &= (a_1 - a_2 + a_3 + a_4)(a_1 + a_2 + a_3 + a_4) = B_1 B_2; \\ C &= (a_1 - a_2 + a_3 - a_4)(a_1 + a_2 + a_3 - a_4) = C_1 C_2; \\ D &= (a_1 + a_2 - a_3 - a_4)(a_1 - a_2 - a_3 - a_4) = D_1 D_2. \end{aligned}$$

Equation (6.77) is an algebraic polynomial of degree four which represents the v_1-v_4 IO equation for any planar $4R$ mechanism. A plot of the v_1-v_4 IO curve for a mechanism with generic link lengths $a_1 = 2, a_2 = 6, a_3 = 8, a_4 = 5$ is illustrated in Figure 6.18. The Grashof crank-rocker nature of these link lengths is confirmed when the v_1-v_4 IO curve is examined. It is to be seen that the curve asymptotically approaches ∞ in both directions along the v_1-axis. Since $2\tan^{-1}\infty = \pi$ radians (180°) along the v_1-axis, one may conclude that the link a_1 is a crank, in that its joint angle passes through 180° along both the $-v_1$ and the $+v_1$ directions on the axis.

6.5.5 Algebraic Input-output Equation Using Relative Angles

All moveable four-bar linkages generate six distinct functions between the four distinct joint variable parameters taken two at a time, which we abstractly call

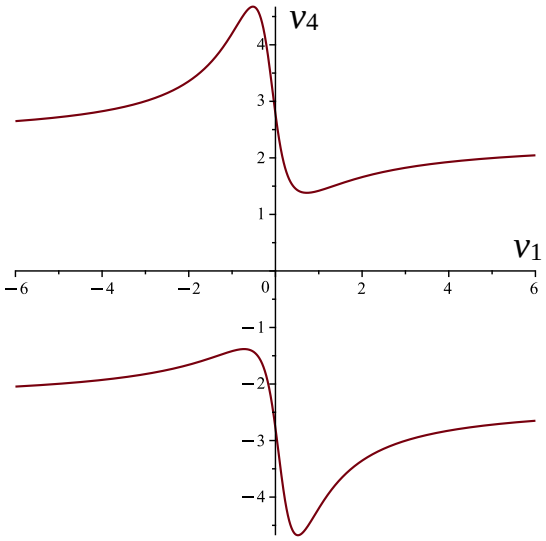

Figure 6.18: v_1-v_4 IO curve of a crank-rocker with $a_1 = 2, a_2 = 6, a_3 = 8, a_4 = 5$.

v_i and v_j. While this is common knowledge in the kinematics community, there do not exist convenient and consistent ways to determine and express these six functions using algebraic means. Moreover, only the v_1-v_4 and v_1-v_3 IO equations can be found in vast body of archival literature, but they are derived using absolute measures of joint angle and expressed as trigonometric implicit equations, see [31, 43] for standard examples. Using absolute angle measures, all referenced to a single reference axis, these are the only two IO equations, and their coefficients are fundamentally different.

Here we will present a novel algorithm, built on tools from algebraic-geometry, that derives the algebraic polynomials which model the relative displacements of all six IO joint displacement pairs in each class of arbitrary planar and spherical single degree of freedom simple closed kinematic chains. First, the class of open kinematic chains is parameterised using the well known notation for lower-pair kinematic chains of arbitrary architecture: Denavit-Hartenberg (DH) notation [44]. The resulting coordinate transformation matrix describing the forward kinematics of the open chain is equated to the identity matrix to conceptually close the chain [44]. Measures of angle elements in the resulting matrix are converted to their respective tangent half-angle parameters. This modified transformation matrix is then mapped to the coordinates of the seven dimensional projective kinematic image space using the well known definitions of the Study soma coordinates [3, 19, 37, 45]. Next, using an appropriate subset of the soma, elimination theory [46] is used to eliminate undesired variable joint displacement parameters leaving only the implicit algebraic IO equation for the desired IO parameter pair. Here we will derive the six different v_i-v_j IO equations for each of the planar 4R, RRRP, PRRP and spherical 4R linkages, and thereby provide a long needed catalogue of these 24 algebraic IO equations.

6.5.5.1 Denavit-Hartenberg (DH) Parametrisation

The literature contains many variations of the original Denavit-Hartenberg (DH) coordinate system and parameter assignment convention. For example, subtly different coordinate frame attachment rules and parameter definitions have been devised for mechanical system calibration, dynamic analysis, accounting for misalignment of joint axis directions, etc., see [24, 47, 48, 49] for several different examples. Therefore, it is important to precisely define the convention used in this work to avoid confusion and misinterpretation since the corresponding coordinate transformations are all different from those of Denavit and Hartenberg.

To visualise the four DH parameters, consider two arbitrary sequential neighbouring links, $i-1$ and i. Two such links are illustrated, together with their DH

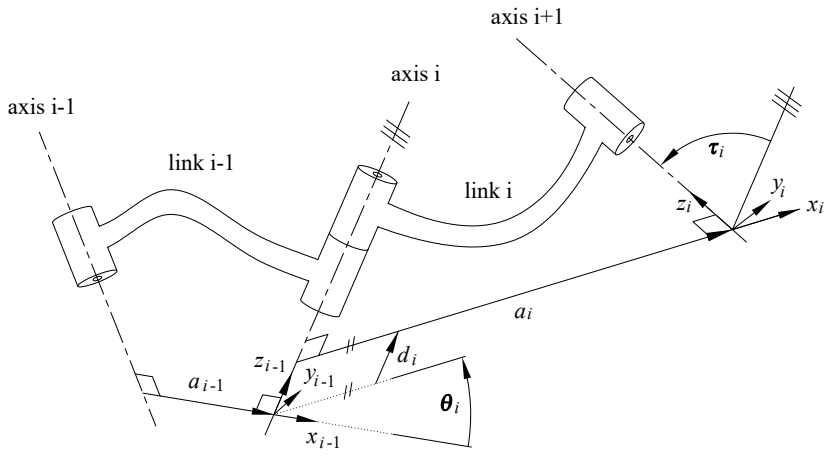

Figure 6.19: DH parameters in a general serial 3R kinematic chain.

coordinate systems and parameters, in Figure 6.19. The procedure for assigning the location of the origin and the basis vectors for the coordinate system for the i^{th} link, in which the DH parameters are defined, is as follows.

1. Identify all joint axes. Consider neighbours $i-1$, i, and $i+1$, illustrated in Figure 6.19.

2. Identify the common perpendicular between the two axes i and $i+1$, or their point of intersection. At the point of intersection, or where the common perpendicular meets the $i+1^{st}$ joint axis, assign the link coordinate system origin, 0_i.

3. For coordinate systems 0 and 1, ensure the coordinate axes are aligned when $\theta_1 = 0$.

4. Assign the z_i axis to point along the joint axis $i+1$.

5. Assign the x_i axis to point along the common perpendicular between the joint axes i and $i+1$. If the axes are parallel, any convenient normal can be selected. If the axes intersect, assign x_i to be perpendicular to the plane containing z_{i-1} and z_i.

6. Assign the y_i axis to complete a right-handed coordinate system.

Now, the four DH parameters [44] are defined for each link in the following way.

θ_i, joint angle: the angle from x_{i-1} to x_i measured about z_{i-1}.

d_i, link offset: the distance from x_{i-1} to x_i measured along z_{i-1}.

τ_i, link twist: the angle from z_{i-1} to z_i measured about x_i.

a_i, link length: the directed distance from z_{i-1} to z_i measured along x_i.

According to this convention the coordinate transformation from the coordinate system for joint i relative to the coordinate system of the previous joint $i-1$ can be divided into two screw displacements, i.e., two pure rotations and two pure translations in terms of the DH parameters

$$\mathbf{T}(d_i) = \left[\begin{array}{ccc|c} 1 & 0 & 0 & 0 \\ 0 & 1 & 0 & 0 \\ 0 & 0 & 1 & d_i \\ \hline 0 & 0 & 0 & 1 \end{array}\right]; \quad \mathbf{T}(\theta_i) = \left[\begin{array}{ccc|c} \cos(\theta_i) & -\sin(\theta_i) & 0 & 0 \\ \sin(\theta_i) & \cos(\theta_i) & 0 & 0 \\ 0 & 0 & 1 & 0 \\ \hline 0 & 0 & 0 & 1 \end{array}\right];$$

$$\mathbf{T}(a_i) = \left[\begin{array}{ccc|c} 1 & 0 & 0 & a_i \\ 0 & 1 & 0 & 0 \\ 0 & 0 & 1 & 0 \\ \hline 0 & 0 & 0 & 1 \end{array}\right]; \quad \mathbf{T}(\tau_i) = \left[\begin{array}{ccc|c} 1 & 0 & 0 & 0 \\ 0 & \cos(\tau_i) & -\sin(\tau_i) & 0 \\ 0 & \sin(\tau_i) & \cos(\tau_i) & 0 \\ \hline 0 & 0 & 0 & 1 \end{array}\right].$$

Multiplying the rotations and translations following

$$\mathbf{T}(\theta_i) \cdot \mathbf{T}(d_i) \cdot \mathbf{T}(a_i) \cdot \mathbf{T}(\tau_i) \tag{6.78}$$

yields the transformation between two coordinate frames which is given by

$${}^{i-1}_{i}\mathbf{T} = \left[\begin{array}{ccc|c} \cos\theta_i & -\sin\theta_i\cos\tau_i & \sin\theta_i\sin\tau_i & a_i\cos\theta_i \\ \sin\theta_i & \cos\theta_i\cos\tau_i & -\cos\theta_i\sin\tau_i & a_i\sin\theta_i \\ 0 & \sin\tau_i & \cos\tau_i & d_i \\ \hline 0 & 0 & 0 & 1 \end{array}\right] = \left[\begin{array}{ccc|c} & \mathbf{A} & & \mathbf{t} \\ \hline 0 & 0 & 0 & 1 \end{array}\right].$$

Hence, to describe the end-effector coordinate frame of a kinematic chain with respect to the base frame, the overall transformation matrix becomes

$${}^{0}_{i}\mathbf{T} = {}^{0}_{1}\mathbf{T}\,{}^{1}_{2}\mathbf{T}\,{}^{2}_{3}\mathbf{T} \ldots {}^{i-1}_{i}\mathbf{T}. \tag{6.79}$$

Applying this algebraic representation to linkages requires that the end-effector coordinate frame coincides with the coordinate frame of the base. Therefore, the overall transformation equates to the identity matrix [50].

6.5.5.2 Planar Four-bar Linkages Revisited

We start with a generic 4R open kinematic chain and assign the standard DH coordinate systems and parameters according to [44], see Table 6.1 and Figure 6.20a. The four link lengths are the a_i, and the four joint angles are the θ_i,

$i \in \{1, 2, 3, 4\}$. While we do not require them for the planar 4R, there are non-zero link twist angles, τ_i, for the RRRP, PRRP, and spherical 4R linkages, as well as link offsets, d_i, for the RRRP and PRRP linkages. All measures of angle are converted to algebraic parameters using the tangent half-angle substitutions:

$$v_i = \tan\frac{\theta_i}{2} \Rightarrow \cos\theta_i = \frac{1-v_i^2}{1+v_i^2}, \quad \sin\theta_i = \frac{2v_i}{1+v_i^2},$$
$$\alpha_i = \tan\frac{\tau_i}{2} \Rightarrow \cos\tau_i = \frac{1-\alpha_i^2}{1+\alpha_i^2}, \quad \sin\tau_i = \frac{2\alpha_i}{1+\alpha_i^2}.$$

The transformation matrix implied by the algebrised parameters is equated to the identity matrix thereby conceptually closing the kinematic chain. Closing the serial 4R chain by grounding link a_4 means that we may have clockwise (CW) or counter clockwise (CCW) joint index circulation. The CW circulation means that the origins of x_4-y_4 and x_0-y_0 are coincident, but the basis vector directions in each coordinate system are out of phase by π radians, see Figure 6.20c. Whereas the CCW circulation means the two coordinate systems are congruent, see Figure 6.20b, and we call them the $x_{0/4}$ - $y_{0/4}$ coordinate system. The equations that follow are expressed in that coordinate system.

Table 6.1: DH parameters for an arbitrary open 4R chain.

axis i	link length a_i	angle θ_i	link offset d_i	twist τ_i
1	a_1	θ_1	0	0
2	a_2	θ_2	0	0
3	a_3	θ_3	0	0
4	a_4	θ_4	0	0

Using the definitions found in [51], the DH transformation matrix of the open 4R chain is mapped to the soma array of eight homogeneous coordinates

$$[x_0 : x_1 : x_2 : x_3 : y_0 : y_1 : y_2 : y_3].$$

Since we are only considering the special Euclidean subgroup of direct planar isometries $SE(2)$ generated by planar 4R, RRRP, and PRRP linkages at the moment, four of the soma coordinates always vanish and what remains are

$$\text{planar 4R and RRRP:} \qquad [x_0 : 0 : 0 : x_3 : 0 : y_1 : y_2 : 0]; \tag{6.80}$$
$$\text{PRRP:} \qquad [x_0 : x_1 : 0 : 0 : 0 : 0 : y_2 : y_3]. \tag{6.81}$$

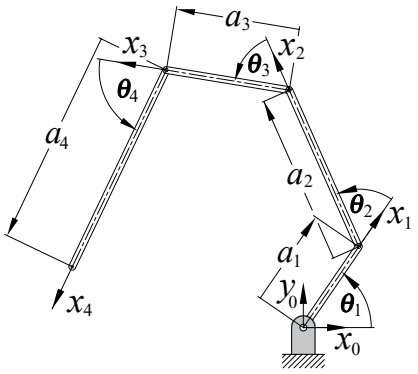

(a) Open 4R kinematic chain.

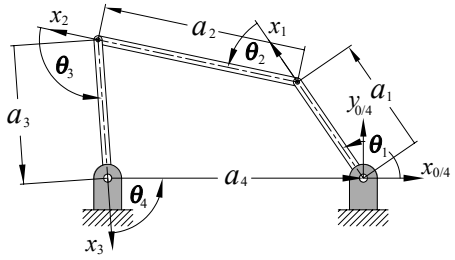

(b) Counter-clockwise closed 4R chain.

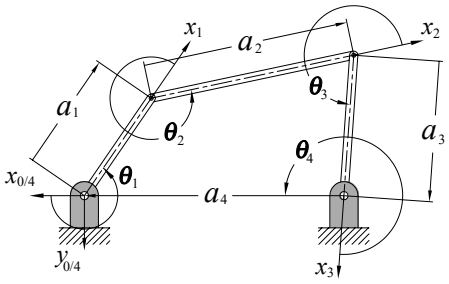

(c) Clockwise closed 4R chain.

Figure 6.20: Counter-clockwise and clockwise joint angle circulation.

Regardless, for a generic representation we use the full Study array here since the 0 elements are also different for spherical linkages [51, 52]. To close the planar serial 4R kinematic chain, the Study array is equated to the identity array thus

$$[x_0 : 0 : 0 : x_3 : 0 : y_1 : y_2 : 0] \quad = \quad [1 : 0 : 0 : 0 : 0 : 0 : 0 : 0]. \qquad (6.82)$$

The Gröbner bases of the ideal generated by the three polynomials $x_3 = 0$, $y_1 = 0$, and $y_2 = 0$ are used to eliminate the two unwanted v_i joint angle parameters leading to the desired v_i-v_j algebraic IO equation. For example, v_2 and v_4 must be eliminated to obtain the v_1-v_3 algebraic IO equation. Because the soma are homogeneous coordinates, and because we are only interested in the kinematic images of real rigid body displacements, we will not use the homogenising coordinate $x_0 = 1$ as a polynomial in our elimination computations.

It is important to note that the IO equations may also be obtained directly on S_6^2. In [53] the DH transformations are expressed as 8×8 matrices and manipulated directly on S_6^2. When equated to the identity array, the IO equation

can be obtained with elimination methods. Similarly, in [54] dual quaternions are used to obtain the closure equation of spatial 6R linkages. These methods could be applied to determine the soma coordinates, but that is not the focus of this paper. What is important is the general unified way to model the kinematic geometry of each of the four classes of four-bar linkage and obtain the six v_i-v_j algebraic IO equations from the associated soma coordinates for each of the planar 4R, RRRP, PRRP, and spherical 4R linkages.

6.5.5.3 Derivation of the Six Planar 4R Linkage v_i-v_j IO Equations

Let the input angle parameter be v_1 and the output angle parameter be v_4. In [51] two elimination steps were applied to the Gröbner bases of the ideal generated by the soma coordinates x_3, y_1 and y_2 to eliminate the angle parameters v_2 and v_3 from the equations yielding the algebraic IO equation relating the v_1 and v_4 angle parameters, which we call the v_1-v_4 IO equation. It has the form

$$Av_1^2v_4^2 + Bv_1^2 + Cv_4^2 - 8a_1a_3v_1v_4 + D = 0, \tag{6.83}$$

where

$$\begin{aligned}
A = A_1A_2 &= (a_1 - a_2 + a_3 - a_4)(a_1 + a_2 + a_3 - a_4),\\
B = B_1B_2 &= (a_1 + a_2 - a_3 - a_4)(a_1 - a_2 - a_3 - a_4),\\
C = C_1C_2 &= (a_1 - a_2 - a_3 + a_4)(a_1 + a_2 - a_3 + a_4),\\
D = D_1D_2 &= (a_1 + a_2 + a_3 + a_4)(a_1 - a_2 + a_3 + a_4),\\
v_1 &= \tan\frac{\theta_1}{2},\\
v_4 &= \tan\frac{\theta_4}{2}.
\end{aligned}$$

This algebraic equation is of degree 4 in the v_1 and v_4 variable parameters, while the coefficients labelled A, B, C, and D are each products of two bilinear factors which can be viewed as eight distinct planes treating the four a_i link lengths as homogeneous coordinates. See Section 6.10.2 for a detailed description of this design parameter space.

In the approach used in [51] to obtain this IO equation from the ideal $\langle x_3, y_1, y_2\rangle$ both v_2 and v_3 are eliminated by first computing the Gröbner bases of the ideal using the Maple 2021 "`tdeg`" monomial ordering with the list sequence (v_3, v_2, v_4, v_1). This is *graded reverse lexicographic order*, also known as *degrevlex* in the literature [55], with indeterminate ordering $v_3 > v_2 > v_4 > v_1$. This monomial ordering sorts the terms by total degree before breaking ties between terms with identical degree by comparing the smallest indeterminate first

and considering a higher degree as smaller in the term ordering. The execution of this step is immediate on a standard computer with an Intel Core i7-7700 CPU @ 3.60 GHz. In this case, 12 bases are computed, all functions of all four v_i. We eliminate v_2 and v_3 by computing the bases of these 12 with the reverse monomial ordering by using "`plex`", which is the *pure lexicographic order*, also known as *lex* [55]. This results in 8 new bases, with one that is a function of only v_1 and v_4 and the four a_i, which represents the IO equation we are looking for.

However, we have since discovered that a single application of the elimination monomial ordering called "`lexdeg`" in Maple 2021 leads directly to the desired planar 4R v_1-v_4 IO equation. When the ideal generated by the system of polynomials contains coefficients that are not too large or complicated, as for the planar 4R linkages, this elimination monomial ordering is very efficient, in the sense that it does not compute an entire "`plex`" basis. For the two disjoint lists of variables, those to be eliminated and those to be retained, the "`lexdeg`" ordering is equivalent to a product order which uses "`tdeg`" on each of the two disjoint lists of variables. All six of the distinct IO equations for each of the planar 4R, RRRP, and PRRP kinematic architectures are easily computed using the "`lexdeg`" elimination monomial ordering. This is how the IO equations for these planar four-bar linkages have been derived. For the planar 4R, the five remaining v_i-v_j IO equations each contain all eight of the bilinear factors of the coefficients labelled $A_1, A_2, B_1, B_2, C_1, C_2, D_1$, and D_2 in Equation (6.83), but in different permutations. This means that the design parameter space, as defined in [56], is the same for all six of these IO equations. The execution of the code is immediate for all six IO equations for each of the three kinematic architectures.

By applying the "`lexdeg`" monomial term orderings to the planar 4R variables in the appropriate disjoint lists, the v_1-v_2, v_1-v_3, v_2-v_3, v_2-v_4, and v_3-v_4 IO equations are obtained and listed as follows.

$$A_1B_2v_1^2v_2^2 + A_2B_1v_1^2 + C_1D_2v_2^2 - 8a_2a_4v_1v_2 + C_2D_1 = 0, \tag{6.84}$$

$$A_1B_1v_1^2v_3^2 + A_2B_2v_1^2 + C_2D_2v_3^2 + C_1D_1 = 0, \tag{6.85}$$

$$A_1D_2v_2^2v_3^2 + B_2C_1v_2^2 + B_1C_2v_3^2 - 8a_1a_3v_2v_3 + A_2D_1 = 0, \tag{6.86}$$

$$A_1C_1v_2^2v_4^2 + B_2D_2v_2^2 + A_2C_2v_4^2 + B_1D_1 = 0, \tag{6.87}$$

$$A_1C_2v_3^2v_4^2 + B_1D_2v_3^2 + A_2C_1v_4^2 + 8a_2a_4v_3v_4 + B_2D_1 = 0. \tag{6.88}$$

Equations (6.83), (6.84), (6.86), and (6.88) all contain a bilinear quadratic term

because they relate adjacent angle pairs, while Equations (6.85) and (6.87) relate opposite angle pairs, and hence do not possess a bilinear quadratic term.

Each of these six IO equations is of degree 4 in the two variable angle parameters, defining quartic curves in the planes spanned by the different v_i-v_j angle parameter pairs. They also all have genus 1 meaning that there is a maximum number of two assembly modes. This is so because of a theorem on algebraic curves proved by Axel Harnack in 1876 [25] which relates the circuits of an algebraic curve to its genus. Each of the v_i-v_j algebraic IO equations are quartic curves of genus 1, therefore, following Harnack, each can have at most two circuits. Each circuit of a particular v_i-v_j IO curve corresponds to one of the mechanisms assembly modes. In essence, Harnack's theorem states that an algebraic curve of genus n can have at most $n + 1$ circuits. One may therefore immediately conclude that a planar 4R mechanism can never have more than two assembly modes.

6.6 Differential Kinematics of the Planar 4R

There are six algebraic IO equations for every four-bar kinematic architecture, planar, spherical, and spatial, that relate the six distinct pairings of variable joint parameters taken two at a time. Because these are algebraic polynomials, it is straightforward to differentiate Equations (6.83)-(6.88) with respect to time, thereby revealing the velocity- and acceleration-level kinematics [57]. In this section, we will discuss a novel approach to determining output angular velocity and acceleration extrema.

The first work investigating extreme output angular velocities is likely that of Kraus from 1939 [58, 59]. In that work, it was proposed that the angular velocity output/input ratio, $\dot{\theta}_4/\dot{\theta}_1$, of a double crank planar linkage reaches an extreme value when the coupler and follower, links a_2 and a_3 in Figure 6.21, become mutually perpendicular. However, in 1944 Rosenauer [60] demonstrated that this is generally not true. Following Kraus, the extreme angular velocities and accelerations of four-bar mechanisms were later investigated in a methodical and more complete way by Ferdinand Freudenstein in 1956 [61]. In that work, Freudenstein used graphical methods to derive the $\dot{\theta}_4/\dot{\theta}_1$ angular velocity ratio based on a directed distance ratio along the Aronhold-Kennedy line of three collinear instantaneous centres of velocity (ICV), P_{13}, P_{14}, and P_{34}, see Figure 6.21. This angular velocity ratio is the reciprocal of the mechanical advantage of the linkage [6], and hence an important index of merit. But, there are in fact six distinct angular velocity ratios that are revealed with the six planar

4R $\dot{v}_i$-$\dot{v}_j$ IO equations [62]. Recall that the collineation axis is the line joining the two secondary ICV, P_{13} and P_{24}. In [61], Freudenstein proposed that an extreme value of the angular velocity ratio $\dot{\theta}_4/\dot{\theta}_1$ occurs when the collineation axis is perpendicular to the coupler, now known as Freudenstein's Theorem 1. In an appendix to that same paper, A.S. Hall rigourously proved the theorem.

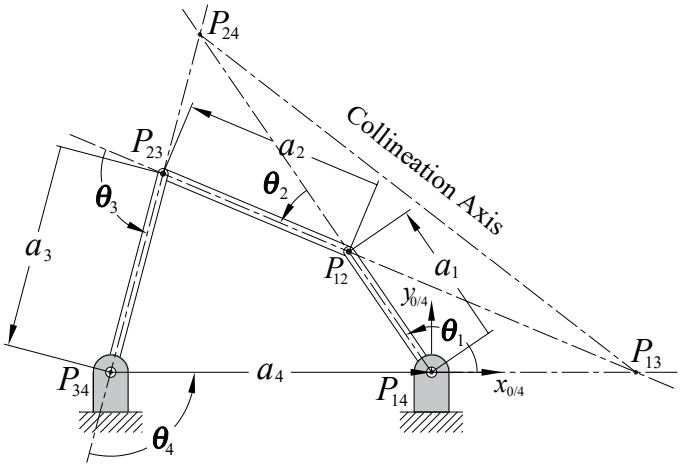

Figure 6.21: The collineation axis and six instantaneous centres of velocity, P_{ij}, in a planar 4R linkage.

Consider the planar 4R linkage illustrated in Figure 6.21. It is well known that as the 4R linkage moves it has four primary ICV, one at the centre of each R-pair, and two secondary ICV. The six ICV are known as *velocity poles* and the curves they move along are described as *polodes*, or *centrodes* as they are often called, see [6, 50, 63, 64] for example. Two of the primary ICV, P_{12} and P_{23}, move on polodes defined by the link lengths, while P_{14} and P_{34} are stationary. The two secondary ICV, P_{13} and P_{24}, also move on polodes. By virtue of the Aronhold-Kennedy theorem, P_{13}, P_{14}, and P_{34} remain collinear as the motion evolves over time meaning that the polode for P_{13} is a segment of the line joining the two ground-fixed R-pairs, the x_0-axis, and is located at the point of intersection of the x_0-axis and the extension of the centreline of the coupler, a_2. Freudenstein's Theorem 1 implies that the value of the ratio of the output angular velocity and the input angular velocity, $\dot{\theta}_4$ and $\dot{\theta}_1$, can be expressed by the ratio of the values of the relative directed distances between

the three ICV located on the x_0-axis in the following way [61, 65]:

$$\frac{\dot{\theta}_4}{\dot{\theta}_1} = \frac{d_{P_{13}P_{14}}}{d_{P_{13}P_{14}} + d_{P_{14}P_{34}}}, \tag{6.89}$$

where the directed distances $d_{P_{14}P_{34}}$ and $d_{P_{13}P_{14}}$ can be positive or negative depending on their relative directions. For example, $d_{P_{13}P_{14}}$ is the distance from P_{13} to P_{14}. The angular velocities are oppositely directed when the ratio is negative.

However, Freudenstein's Theorem 1 also applies to the ICV on each of the three other Aronhold-Kennedy lines of three collinear ICV with respect to a number line coincident with the line of three ICV having its origin on the central ICV. It seems that, to the best of the authors collective knowledge, with the exception of [7, 8], this fact has not been discussed in the literature. Following Freudenstein's derivation logic, the three remaining velocity ratios expressed as ratios of the relative locations of the three ICV on the three other Aronhold-Kennedy lines, see Figure 6.21, have never been stated explicitly as:

$$\frac{\dot{\theta}_1}{\dot{\theta}_2} = \frac{d_{P_{24}P_{12}}}{d_{P_{24}P_{12}} + d_{P_{12}P_{14}}} \tag{6.90}$$

$$\frac{\dot{\theta}_3}{\dot{\theta}_2} = \frac{d_{P_{13}P_{12}}}{d_{P_{13}P_{12}} + d_{P_{12}P_{23}}} \tag{6.91}$$

$$\frac{\dot{\theta}_4}{\dot{\theta}_3} = \frac{d_{P_{24}P_{23}}}{d_{P_{24}P_{23}} + d_{P_{23}P_{34}}}. \tag{6.92}$$

Regardless, the angular velocity ratios of $\dot{\theta}_1/\dot{\theta}_3$ and $\dot{\theta}_2/\dot{\theta}_4$ cannot be derived as ratios of collinear ICV relative directed distances.

6.6.1 Time Derivatives of the Six v_i - v_j Algebraic IO Equations

The first time derivative of the variable angle parameter v_i needs a few words of discussion. Because the angle parameter is $v = \tan(\theta/2)$, the time derivative is configuration dependent in the following way

$$\begin{aligned} \dot{v} &= \frac{d}{dt}\tan(\theta/2) = \frac{\dot{\theta}}{2}\sec^2(\theta/2) = \frac{\dot{\theta}}{2}\left(\frac{\cos^2(\theta/2) + \sin^2(\theta/2)}{\cos^2(\theta/2)}\right) \\ &= \frac{\dot{\theta}}{2}\left(1 + v^2\right). \end{aligned} \tag{6.93}$$

Therefore the six angular velocity parameter IO equations are

$$\begin{aligned}\left(\left(A_1B_2v_2^2+A_2B_1\right)v_1-4a_2a_4v_2\right)\dot{v}_1+\left(\left(A_1B_2v_1^2+C_1D_2\right)v_2-4a_2a_4v_1\right)\dot{v}_2\\ =\ 0\end{aligned}\tag{6.94}$$

$$\left(A_1B_1v_3^2+A_2B_2\right)v_1\dot{v}_1+\left(A_1B_1v_1^2+C_2D_2\right)v_3\dot{v}_3=0,\tag{6.95}$$

$$\begin{aligned}\left(\left(A_1A_2v_4^2+B_1B_2\right)v_1-4a_1a_3v_4\right)\dot{v}_1+\left(\left(A_1A_2v_1^2+C_1C_2\right)v_4-4a_1a_3v_1\right)\dot{v}_4\\ =0,\end{aligned}\tag{6.96}$$

$$\begin{aligned}\left(\left(A_1D_2v_3^2+B_2C_1\right)v_2-4a_1a_3v_3\right)\dot{v}_2+\left(\left(A_1D_2v_2^2+B_1C_2\right)v_3-4a_1a_3v_2\right)\dot{v}_3\\ =0,\end{aligned}\tag{6.97}$$

$$\left(A_1C_1v_4^2+B_2D_2\right)v_2\dot{v}_2+\left(A_1C_1v_2^2+A_2C_2\right)v_4\dot{v}_4=0,\tag{6.98}$$

$$\begin{aligned}\left(\left(A_1C_2v_4^2+B_1D_2\right)v_3+4a_2a_4v_4\right)\dot{v}_3+\left(\left(A_1C_2v_3^2+A_2C_1\right)v_4+4a_2a_4v_3\right)\dot{v}_4\\ =0.\end{aligned}\tag{6.99}$$

Using Equation (6.93), the six angular velocity ratios and measures mechanical advantage are trivially obtained as

$$\frac{\dot{\theta}_2}{\dot{\theta}_1}\ =\ -\frac{\left((A_1B_2v_2^2+A_2B_1)v_1-4a_2a_4v_2\right)\left(1+v_1^2\right)}{\left((A_1B_2v_1^2+C_1D_2)v_2-4a_2a_4v_1\right)\left(1+v_2^2\right)}\ =\ \frac{T_1}{T_2},\tag{6.100}$$

$$\frac{\dot{\theta}_3}{\dot{\theta}_1}\ =\ -\frac{\left(A_1B_1v_3^2+A_2B_2\right)\left(1+v_1^2\right)v_1}{\left(A_1B_1v_1^2+C_2D_2\right)\left(1+v_3^2\right)v_3}\ =\ \frac{T_1}{T_3},\tag{6.101}$$

$$\frac{\dot{\theta}_4}{\dot{\theta}_1}\ =\ -\frac{\left((A_1A_2v_4^2+B_1B_2)v_1-4a_1a_3v_4\right)\left(1+v_1^2\right)}{\left((A_1A_2v_1^2+C_1C_2)v_4-4a_1a_3v_1\right)\left(1+v_4^2\right)}\ =\ \frac{T_1}{T_4},\tag{6.102}$$

$$\frac{\dot{\theta}_3}{\dot{\theta}_2}\ =\ -\frac{\left((A_1D_2v_3^2+B_2C_1)v_2-4a_1a_3v_3\right)\left(1+v_2^2\right)}{\left((A_1D_2v_2^2+B_1C_2)v_3-4a_1a_3v_2\right)\left(1+v_3^2\right)}\frac{T_2}{T_3},\tag{6.103}$$

$$\frac{\dot{\theta}_2}{\dot{\theta}_4}\ =\ -\frac{\left(A_1C_1v_4^2+A_2C_2\right)\left(1+v_4^2\right)v_4}{\left(A_1C_1v_2^2+B_2D_2\right)\left(1+v_2^2\right)v_2}\ =\ \frac{T_4}{T_2},\tag{6.104}$$

$$\frac{\dot{\theta}_4}{\dot{\theta}_3}\ =\ -\frac{\left((A_1C_2v_4^2+B_1D_2)v_3+4a_2a_4v_4\right)\left(1+v_3^2\right)}{\left((A_1C_2v_3^2+A_2C_1)v_4+4a_2a_4v_3\right)\left(1+v_4^2\right)}\ =\ \frac{T_3}{T_4}.\tag{6.105}$$

It is a straightforward exercise to show that Equations (6.89) and (6.102) yield identical results.

The six angular acceleration parameter IO equations are easily obtained as the time derivatives of the angular velocity parameter IO equations. The time derivative of $\dot{v}$ is a somewhat more complicated compound function requiring a combination of the chain and power rules from elementary differential calculus [66] to determine that

$$\ddot{v} = \frac{1}{2}\left(\ddot{\theta} + \dot{\theta}^2\right)\left(1 + v^2\right), \tag{6.106}$$

which reveals that the angular acceleration parameter $\ddot{v}$ depends not only on angular acceleration, but on angular velocity and configuration as well. The six angular acceleration parameter equations are

$$\begin{aligned}\left((A_1B_2v_2^2 + A_2B_1)v_1 - 4a_2a_4v_2\right)\ddot{v}_1 + \left((A_1B_2v_1^2 + C_1D_2)v_2 - 4a_2a_4v_1\right)\ddot{v}_2 \\ +(A_1B_2v_2^2 + A_2B_1)\dot{v}_1^2 + (A_1B_2v_1^2 + C_1D_2)\dot{v}_2^2 \\ +4(A_1B_2v_1v_2 - 2a_2a_4)\dot{v}_1\dot{v}_2 = 0,\end{aligned} \tag{6.107}$$

$$\begin{aligned}(A_1B_1v_3^2 + A_2B_2)v_1\ddot{v}_1 + (A_1B_1v_1^2 + C_2D_2)v_3\ddot{v}_3 \\ +(A_1B_1v_3^2 + A_2B_2)\dot{v}_1^2 + (A_1B_1v_1^2 + C_2D_2)\dot{v}_3^2 + 4A_1B_1v_1v_3\dot{v}_1\dot{v}_3 = 0,\end{aligned} \tag{6.108}$$

$$\begin{aligned}\left((A_1A_2v_4^2 + B_1B_2)v_1 - 4a_1a_3v_4\right)\ddot{v}_1 + \left((A_1A_2v_1^2 + C_1C_2)v_4 - 4a_1a_3v_1\right)\ddot{v}_4 \\ +(A_1A_2v_4^2 + B_1B_2)\dot{v}_1^2 + (A_1A_2v_1^2 + C_1C_2)\dot{v}_4^2 \\ +4(A_1A_2v_1v_4 - 2a_1a_3)\dot{v}_1\dot{v}_4 = 0,\end{aligned} \tag{6.109}$$

$$\begin{aligned}\left((A_1D_2v_3^2 + B_2C_1)v_2 - 4a_1a_3v_3\right)\ddot{v}_2 + \left((A_1D_2v_2^2 + B_1C_2)v_3 - 4a_1a_3v_2\right)\ddot{v}_3 \\ +(A_1D_2v_3^2 + B_2C_1)\dot{v}_2^2 + (A_1D_2v_2^2 + B_1C_2)\dot{v}_3^2 \\ +4(A_1D_2v_2v_3 - 2a_1a_3)\dot{v}_2\dot{v}_3 = 0,\end{aligned} \tag{6.110}$$

$$\begin{aligned}(A_1C_1v_4^2 + B_2D_2)v_2\ddot{v}_2 + (A_1C_1v_2^2 + A_2C_2)v_4\ddot{v}_4 \\ +(A_1C_1v_4^2 + B_2D_2)\dot{v}_2^2 + (A_1C_1v_2^2 + A_2C_2)\dot{v}_4^2 + 4A_1C_1v_2v_4\dot{v}_2\dot{v}_4 = 0,\end{aligned} \tag{6.111}$$

$$\begin{aligned}\left((A_1C_2v_4^2 + B_1D_2)v_3 + 4a_2a_4v_4\right)\ddot{v}_3 + \left((A_1C_2v_3^2 + A_2C_1)v_4 + 4a_2a_4v_3\right)\ddot{v}_4 \\ +(A_1C_2v_4^2 + B_1D_2)\dot{v}_3^2 + (A_1C_2v_3^2 + A_2C_1)\dot{v}_4^2 \\ +4(A_1C_2v_3v_4 + 2a_2a_4)\dot{v}_3\dot{v}_4 = 0.\end{aligned} \tag{6.112}$$

6.6.2 Angular Velocity Extrema

We will determine the extreme output angular velocity given a specified set of link lengths and constant input angular velocity. We can use any of the six v_i-v_j algebraic IO equations. To identify extreme angular velocity and acceleration

outputs for a constant input angular velocity requires that the angle parameters be transformed back into angles. While $\dot{\theta}_i$ may be constant, the corresponding parameter $\dot{v}_i$ is not, since it is configuration dependent. For this example, we will consider the v_2-v_4 and $\dot{v}_2$-$\dot{v}_4$ IO equations, Equations (6.87) and (6.104) respectively, since this angle pairing has never been found in the literature. The extreme angular velocities, along with the configurations in which they occur in both assembly modes, can be easily obtained computationally with the following algorithm.

Extreme planar 4R angular velocity algorithm.

If values for a_1, a_2, a_3, and a_4 are given and the input angular velocity is a constant specified value, we wish to determine the critical values $\theta_{i_{\text{crit}}}$ that result in $\dot{\theta}_{j_{\text{min/max}}}$, so θ_j must be eliminated from both the position and angular velocity IO equations.

1. Convert v_i and v_j in the IO equation to angles as $v = \tan(\theta/2)$ and solve for θ_j. There will be two solutions, one for each assembly mode.

2. Substitute the expression for θ_j from Step 1 into the $\dot{\theta}_i$-$\dot{\theta}_j$ equation and solve for $\dot{\theta}_j$, which gives $\dot{\theta}_j = f(\theta_i)$ since $\dot{\theta}_i$ is a specified constant.

3. Solve $\dfrac{d\dot{\theta}_j}{d\theta_i} = 0$ for $\theta_{i_{\text{crit}}}$ and determine the values of $\dot{\theta}_{j_{\text{min/max}}}$ corresponding to each distinct value of $\theta_{i_{\text{crit}}}$.

For this example we will consider v_4 and v_2 as the input and output angle parameters respectively, and let the constant input angular velocity and the link lengths of a planar 4R four-bar mechanism be $\dot{\theta}_4 = 10$ rad/s, $a_1 = 5$, $a_2 = 6$, $a_3 = 8$, $a_4 = 2$. Following the algorithm, we obtain an implicit equation of $\dot{\theta}_2 = f(\theta_4)$ and plot it, see Figure 6.22. Solving $\dfrac{d\dot{\theta}_2}{d\theta_4} = 0$ for $\theta_{4_{\text{crit}}}$ we determine the values of $\dot{\theta}_{2_{\text{min/max}}}$ corresponding to each distinct value of $\theta_{4_{\text{crit}}}$, which are listed in Table 6.2. It should be noted that determining the points of inflection of a particular $\dot{\theta}_j = f(\theta_i)$ curve requires the second derivative, $\dfrac{d^2\dot{\theta}_j}{d\theta_i^2} = 0$.

6.6.3 Angular Acceleration Extrema

According to Freudenstein in [61], one of the extreme output angular accelerations for a crank-rocker, assuming constant input angular velocity, is given

Table 6.2: $\dot{\theta}_{2_{\min/\max}}$ and $\theta_{4_{\text{crit}}}$ for $\dot{\theta}_4 = 10$ rad/s.

Assembly mode	$\dot{\theta}_{2_{\min/\max}}$ rad/s	$\theta_{4_{\text{crit}}}$ rad
1	5.385202141	-1.481326671
	-5.385202141	1.4813266715
2	-5.385202141	-1.481326671
	5.385202141	1.481326671

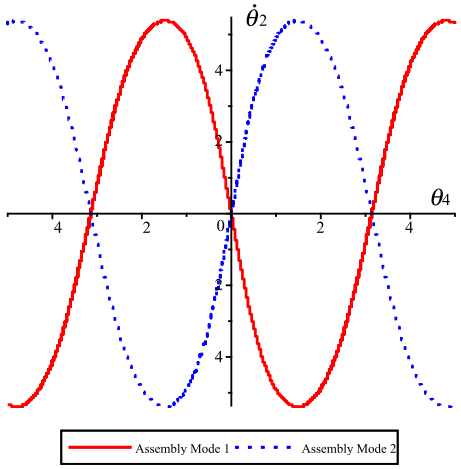

Figure 6.22: The $\dot{\theta}_2 = f(\theta_4)$ angular velocity profile.

by

$$\ddot{\theta}_{4_{\max}} = \frac{\dot{\theta}_1^2 a_1}{a_2 a_3}(a_1 + a_2), \tag{6.113}$$

where the link lengths are subject to the condition

$$(a_1 + a_2)^2 + a_3^2 = a_4^2. \tag{6.114}$$

This extreme output angular acceleration occurs when the angle $\angle BCD = 90°$, see Figure 6.23a. Freudenstein continues in the same paper to state an equation for one extreme output angular acceleration for drag-link mechanisms, which is given by

$$\ddot{\theta}_{4_{\max}} = \frac{\dot{\theta}_1^2 a_4}{a_2 a_3}(a_2 + a_3), \tag{6.115}$$

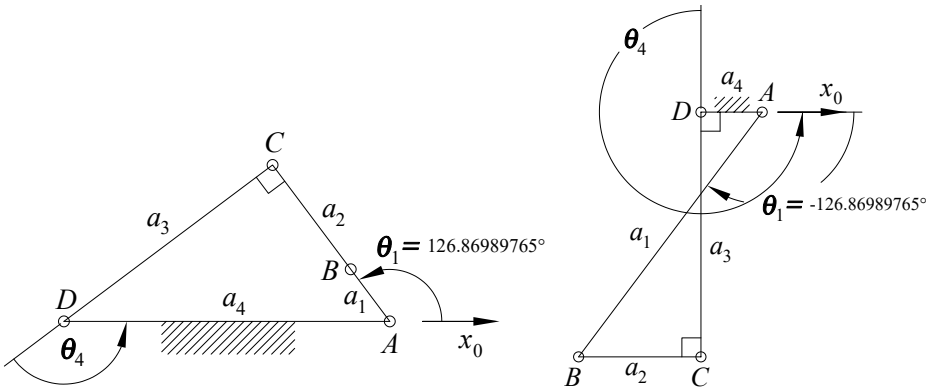

(a) Folding crank-rocker: $a_1 = 1$, $a_2 = 2$, $a_3 = 4$, $a_4 = 5$.

(b) Folding drag-link: $a_1 = 5$, $a_2 = 2$, $a_3 = 4$, $a_4 = 1$.

Figure 6.23: Configurations where $\ddot{\theta}_{4_{\max}}$ occur.

where the link lengths are subject to the condition

$$(a_2 + a_4)^2 + a_3^2 \quad = \quad a_1^2. \tag{6.116}$$

At an extreme output angular acceleration the coupler a_2 and fixed base link a_4 are parallel and the angle $\angle ADC = 90°$, see Figure 6.23b. Together, these two conditions further mean that $\angle DCB = 90°$. We will verify both theorems with examples, but also demonstrate that they are incomplete because of the link length conditions, and only partially correct. In fact, the length conditions can impose a folding singularity on each linkage type for certain integer values of link lengths, thereby meaning that the linkage will pass through a singularity as it folds along the base link a_4. Moreover, it is important to note that Equations (6.113) and (6.115) apply only to these two classes of linkage.

Let a crank-rocker, where a_1 is the crank and a_4 is the rocker, be defined by the link lengths that satisfy Equation (6.114), which are listed in Table 6.3. It turns out that the linkage is a folding drag-link for these lengths. The angular velocity and acceleration profiles for a constant input angular velocity of $\dot{\theta}_1 = 10$ rad/s are illustrated in Figure 6.24, where the folding singularity appears as discontinuities in the profile curves. Substituting the link lengths and constant input angular velocity $\dot{\theta}_1 = 10$ into Equation (6.113) predicts that a maximum output angular acceleration is $\ddot{\theta}_4 = 37.5$ rad/s^2. Freudenstein predicts that this extreme angular acceleration will occur when links a_1 and a_2 are parallel and a_2 is perpendicular to a_3.

Table 6.3: Folding crank-rocker and drag-link mechanism link lengths.

Link	Crank-rocker lengths	Drag-link lengths
a_1	1	5
a_2	2	2
a_3	4	4
a_4	5	1

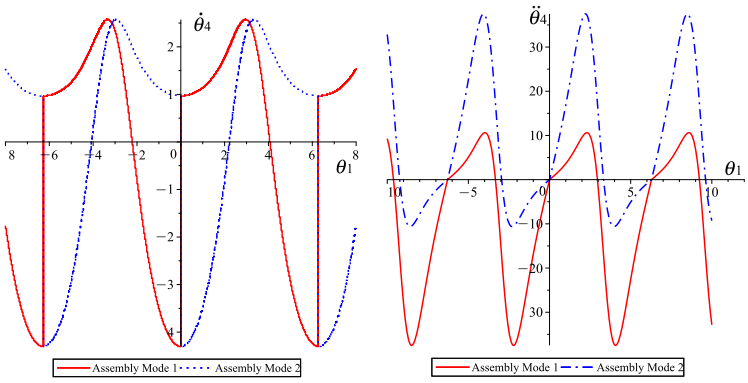

(a) The $\dot{\theta}_4 = f(\theta_1)$ angular velocity profile.

(b) The $\ddot{\theta}_4 = f(\theta_1)$ angular acceleration profile.

Figure 6.24: The angular velocity and acceleration profiles for the Freudenstein crank-rocker.

Furthermore, let a folding drag-link mechanism, where a_1 is the input crank and a_4 is the output crank, be defined by the link lengths that satisfy Equation (6.116), which are also listed in Table 6.3. Substituting the link lengths and constant input angular velocity $\dot{\theta}_1 = 10$ rad/s into Equation (6.115) predicts that a maximum output angular acceleration is $\ddot{\theta}_4 = 75$ rad/s^2. Freudenstein predicts that the extreme angular acceleration for the drag-link will occur when links a_2 and a_4 are parallel and a_3 is perpendicular to a_4. The two linkages were sketched in AutoCAD, and the input angle where an extreme angular acceleration occurs was measured to be precisely $\pm 126.86989765°$ for the crank-rocker/drag-link mechanisms, see Figure 6.23.

In order to confirm the results for both the crank-rocker and drag-link mechanisms, a method to compute the extreme output angular accelerations and

associated configurations is needed. Hence, the following algorithm is proposed.

Extreme planar 4R angular acceleration algorithm.

If values for a_1, a_2, a_3, and a_4 are given and the input angular velocity is a constant specified value, we wish to determine the critical values $\theta_{i_{\text{crit}}}$ that result in $\ddot{\theta}_{j_{\text{min/max}}}$, so both θ_j and $\dot{\theta}_j$ must be eliminated from the position, angular velocity, and acceleration IO equations.

1. Convert v_i and v_j in the IO equation to angles as $v = \tan(\theta/2)$ and solve for θ_j.
2. Substitute the expression for θ_j from Step 1 into the $\dot{\theta}_i$-$\dot{\theta}_j$ equation and solve for $\dot{\theta}_j$, which gives $\dot{\theta}_j = f(\theta_i)$, since $\dot{\theta}_i$ is a specified constant.
3. Substitute the expressions for θ_j and $\dot{\theta}_j$ into the $\ddot{\theta}_i$-$\ddot{\theta}_j$ equation.
4. Solve the resulting equation for $\ddot{\theta}_j$, which gives $\ddot{\theta}_j = f(\theta_i)$, since $\ddot{\theta}_i = 0$.
5. Solve $\dfrac{d\ddot{\theta}_j}{d\theta_i} = 0$ for $\theta_{i_{\text{crit}}}$ and determine the values of $\ddot{\theta}_{j_{\text{min/max}}}$ corresponding to each distinct value of $\theta_{i_{\text{crit}}}$.

If the associated points of inflection are required, then the second derivative, $\dfrac{d^2\ddot{\theta}_j}{d\theta_i^2} = 0$, must be solved for the critical input angles.

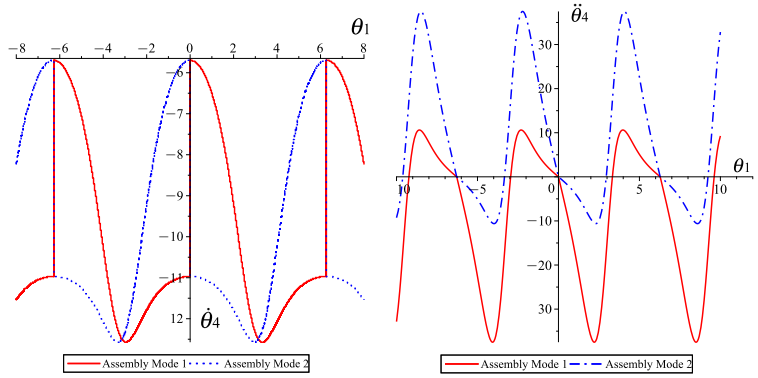

(a) The $\dot{\theta}_4 = f(\theta_1)$ angular velocity profile.

(b) The $\ddot{\theta}_4 = f(\theta_1)$ angular acceleration profile.

Figure 6.25: The angular velocity and acceleration profiles for the Freudenstein drag-link.

Table 6.4: Folding crank-rocker and drag-link mechanism angular velocity and acceleration extrema.

Mechanism	Assembly mode	$\dot{\theta}_{4_{\min/\max}}$ rad/s	$\theta_{1_{\text{crit}}}$ rad (deg)	$\ddot{\theta}_{4_{\min/\max}}$ rad/s^2	$\theta_{1_{\text{crit}}}$ rad (deg)
Crank-rocker	1	2.5736	2.9520 (169.1349°)	-37.5	-2.2143 (-126.8699°)
		-4.3019	0 (0°)	10.6139	2.3047 (132.0490°)
	2	2.5736	-2.9520 (-169.1349°)	37.5	2.2141 (126.86990°)
		1.1375	0 (0°)	-10.6139	-2.3047 (-132.0490°)
Drag-link	1	-12.5736	-2.9520 (-169.1349°)	-37.5	2.2143 (126.8698977°)
		-5.6981	0 (0°)	10.6139	-2.3047 (-132.0490°)
	2	-12.5736	2.9520 (169.1349°)	37.5	-2.2143 (-126.8699°)
		-5.6981	0 (0°)	-10.6139	2.3047 (132.0490°)

Following the extreme angular velocity and acceleration algorithms for a constant input angular velocity of $\dot{\theta}_1 = 10$ rad/s, and crank-rocker as well as drag-link link lengths listed in Table 6.3, we obtain the angular velocity and acceleration profiles for $\dot{\theta}_4 = f(\theta_1)$ and $\ddot{\theta}_4 = g(\theta_1)$ that are illustrated in Figures 6.24 and 6.25. Moreover, the computed values for $\dot{\theta}_{4_{\min/\max}}$, $\ddot{\theta}_{4_{\min/\max}}$, and the associated $\theta_{1_{crit}}$ for the crank-rocker and drag-link mechanisms are listed in Table 6.4. It is to be seen that for the crank-rocker, the value for $\ddot{\theta}_{4_{\max}}$ computed with Freudenstein's Equation (6.113) is indeed correct, as well as the configuration in which it occurs. See the value for $\theta_{1_{crit}}$ in Assembly Mode 2 in Table 6.4, which is identical to the empirically measured value in Figure 6.23.

However, the remaining extreme value for the output angular acceleration is not accounted for. Additionally, it is to be seen for the drag-link that the configuration in which an extreme value for $\ddot{\theta}_{4_{\max}}$ is correct, see the value for $\theta_{1_{crit}}$ in Assembly Mode 2 in Table 6.4, which is the same as the empirically measured value in Figure 6.23. However, the value for the maximum angular acceleration is not correct, it is twice the computed value, see the results listed in Table 6.4. The values computed with the angular velocity and acceleration extrema algorithms yield results that agree with the plotted angular velocity and acceleration profiles illustrated in Figures. 6.24 and 6.25.

6.7 Six Planar RRRP Linkage v_i-v_j IO Equations

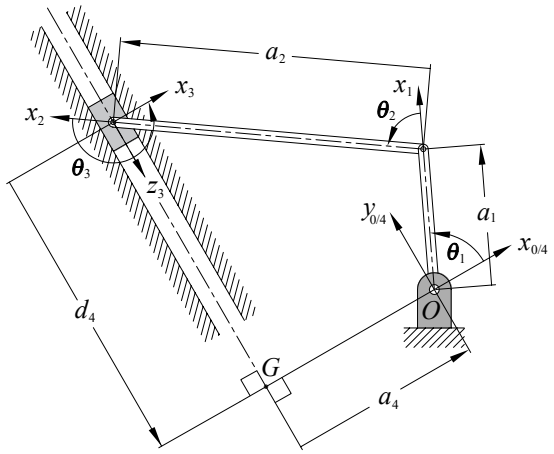

Figure 6.26: Planar RRRP linkage with Denavit-Hartenberg coordinate system and parameter assignments.

Next we shall list the six algebraic IO equations for planar RRRP mechanisms obtained using our technique employing the "`lexdeg`" elimination monomial ordering. An arbitrary RRRP linkage is illustrated in Figure 6.26. The P-pair z_3-axis induces the two link twist angles and a link offset listed in Table 6.5.

Applying the methods in [51] to the DH parameters by algebraising the angle parameters with tangent half-angle equivalents, projecting the DH closure equation into Study's kinematic mapping image space as soma coordinates, then

Table 6.5: DH parameters for the RRRP.

i	θ_i	d_i	a_i	τ_i	α_i
1	θ_1	0	a_1	0	0
2	θ_2	0	a_2	0	0
3	θ_3	0	0	$\pi/2$	1
4	0	d_4	a_4	-$\pi/2$	-1

eliminating the intermediate joint variable parameters v_2 and v_3 using "`lexdeg`" leads to the RRRP v_1-d_4 algebraic IO equation:

$$v_1^2 d_4^2 + R v_1^2 + d_4^2 - 4 a_1 v_1 d_4 + S = 0, \tag{6.117}$$

where

$$R = R_1 R_2 = (a_1 + a_2 - a_4)(a_1 - a_2 - a_4),$$
$$S = S_1 S_2 = (a_1 + a_2 + a_4)(a_1 - a_2 + a_4),$$
$$v_1 = \tan \frac{\theta_1}{2}.$$

The four bilinear factors R_1, R_2, S_1, and S_2 can be regarded as four planes intersecting in the faces of a four-sided pyramid in the design parameter space orthogonally spanned by the three lengths a_1, a_2, and a_4, see [67] for a detailed description.

Using the same approach, the five remaining joint variable parameter pairings lead to the following five additional RRRP algebraic IO equations:

$$R_2 v_1^2 v_2^2 + R_1 v_1^2 - S_2 v_2^2 + 4 a_2 v_1 v_2 - S_1 = 0; \tag{6.118}$$

$$R_1 v_1^2 v_3^2 + R_2 v_1^2 - S_2 v_3^2 - S_1 = 0; \tag{6.119}$$

$$S_2 v_2^2 v_3^2 - R_2 v_2^2 - R_1 v_3^2 - 4 a_1 v_2 v_3 + S_1 = 0; \tag{6.120}$$

$$v_2^2 d_4^2 - R_2 S_2 v_2^2 + d_4^2 - R_1 S_1 = 0; \tag{6.121}$$

$$v_3^2 d_4^2 - R_1 S_2 v_3^2 + d_4^2 + 4 a_2 v_3 d_4 - R_2 S_1 = 0. \tag{6.122}$$

All six of the RRRP algebraic IO equations are of degree 4, representing quartic curves in the respective joint variable parameter planes. These six IO equations

also all possess genus 1 meaning again that there is a maximum number of two assembly modes.

For the RRRP linkages that are rocker-sliders, each distinct circuit of the IO curve also contains two branches, one for each working mode. When the input angle reaches minimum or maximum values the mechanism instantaneously stops moving as the coupler becomes perpendicular to the direction of travel of the P-pair. In this singular configuration, unless mechanical constraints are imposed, the slider may move in one of two directions as the rocker input link begins to move again in the opposite sense. These are defined as the working modes of the particular assembly mode. Each working mode traces a distinct branch in the particular circuit of the IO curve. Together, both branches cover the entire circuit.

6.8 Six Planar PRRP Linkage v_i-v_j IO Equations

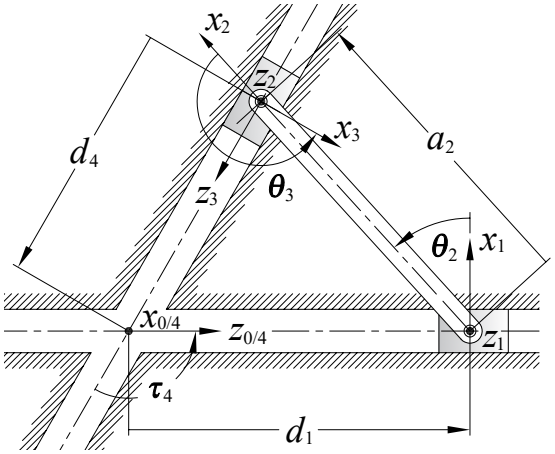

Figure 6.27: Planar PRRP linkage with Denavit-Hartenberg coordinate systems and parameter assignments.

An identical approach is used for the planar PRRP linkages. Referring to Figure 6.27, it is to be seen that general PRRP elliptical trammel linkages have but two design parameters, namely a_2 and τ_4, the coupler length, and the twist angle between the two P-pairs. The twist angle is typically $\tau_4 = \pi/2$, though it can be any other value. The DH parameters for an arbitrary PRRP are listed in Table 6.6. Again we apply the methods in [51] and the "`lexdeg`" monomial ordering to the DH parameters of the PRRP by algebraising the

Table 6.6: DH parameters for the PRRP.

i	θ_i	v_i	d_i	a_i	τ_i	α_i
1	$-\pi/2$	-1	d_1	0	$-\pi/2$	-1
2	θ_2	v_2	0	a_2	0	0
3	θ_3	v_2	0	0	$\pi/2$	1
4	$\pi/2$	1	d_4	0	τ_4	α_4

angle parameters with tangent half-angle equivalents, projecting the DH closure equation into Study's kinematic mapping image space as soma coordinates, then eliminating the intermediate joint variable parameters leading to the PRRP algebraic IO equations. The symmetry of the six algebraic IO equations is better revealed when we define the following three coefficients:

$$\begin{aligned} T &= a_2^2(\alpha_4^2+1); \\ U &= a_2(\alpha_4^2-1); \\ V &= a_2(\alpha_4^2+1). \end{aligned}$$

Using these coefficients the six algebraic IO equations are:

$$(\alpha_4^2+1)(d_1^2+d_4^2) - 2(\alpha_4^2-1)d_1d_4 - T = 0; \tag{6.123}$$

$$2\alpha_4 d_1 v_2^2 + U v_2^2 + 2\alpha_4 d_1 - 4a_2\alpha_4 v_2 - U = 0; \tag{6.124}$$

$$2\alpha_4 d_1 v_3^2 - V v_3^2 + 2\alpha_4 d_1 + V = 0; \tag{6.125}$$

$$\alpha_4 v_2 v_3 - v_2 - v_3 - \alpha_4 = 0; \tag{6.126}$$

$$2\alpha_4 v_2^2 d_4 + V v_2^2 + 2\alpha_4 d_4 - V = 0; \tag{6.127}$$

$$2\alpha_4 v_3^2 d_4 - U v_3^2 + 4a_2\alpha_4 v_3 + 2\alpha_4 d_4 + U = 0. \tag{6.128}$$

It is to be seen that Equations (6.124), (6.125), (6.127), and (6.128) are of degree 3, representing cubic curves in their respective joint variable parameter planes, while Equations (6.123) and (6.126) are of degree 2, and are different conics. When the respective quadratic forms are diagonalised it is easy to show that Equation (6.123) is an ellipse, while Equation (6.126) is an hyperbola which depends only on the link twist α_4. Figure 6.28 illustrates one ellipse generating and one hyperbola generating PRRP mechanism.

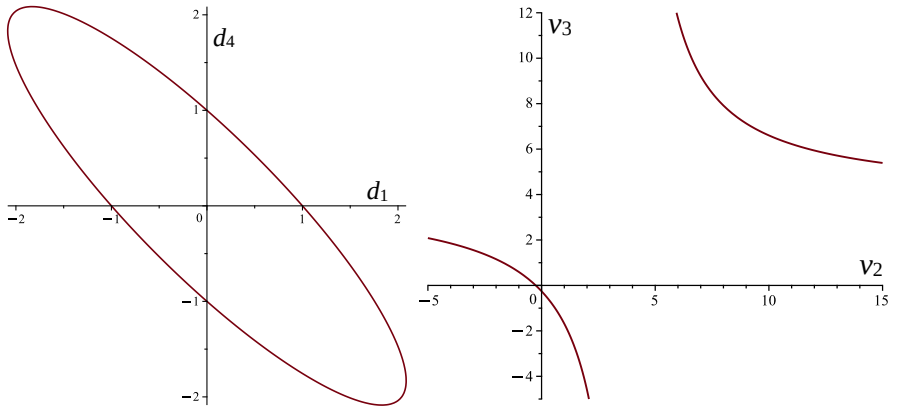

(a) d_1-d_4 IO with $a_2 = 1$, $\alpha_4 = \tan \pi/4$. (b) v_2-v_3 IO with$\alpha_4 = \tan \pi/4$.

Figure 6.28: Ellipse and hyperbola generating PRRP mechanisms..

Moreover, each of the six PRRP algebraic IO equations, Equations (6.123-6.128) possess genus 0, unlike the planar 4R and RRRP IO equations. According to Harnak's theorem we conclude that the PRRP linkage has at most one assembly mode since each IO equation has a single circuit.

6.9 Spherical 4R Linkages

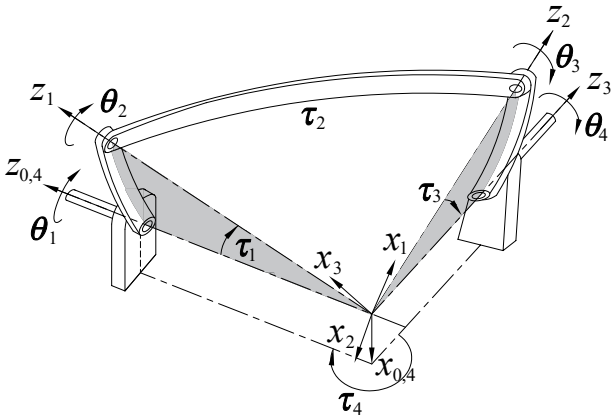

Figure 6.29: Spherical 4R DH reference frames and parameters.

Consider the arbitrary spherical 4R linkage illustrated in Figure 6.29. The general IO equation expresses the implicit functional relationship between the

input and output angles, θ_i and θ_j, in terms of the constant twist angles between the four R-pair centres, τ_i. For a unit sphere, the twist angles are equivalent to the corresponding arc lengths. The derivation of the algebraic form of the spherical IO equation [51] also makes use of the original Denavit-Hartenberg (DH) parametrisation of the kinematic geometry [50].

The forward kinematics of an arbitrary serial 4R spherical kinematic chain is obtained as a linear transformation matrix in terms of the DH parameters. This linear transformation can then be mapped to the corresponding eight Study soma coordinates [51]. For spherical kinematic chains there are also only four homogeneous soma coordinates since the displacement group contains only rotations about a fixed point. The corresponding Study array is:

$$[x_0 : x_1 : x_2 : x_3 : 0 : 0 : 0 : 0]. \tag{6.129}$$

The ideal generated by the three non-trivial soma that equate to zero, namely x_1, x_2, and x_3 are used to derive the algebraic IO equations relating the six distinct edges of an arbitrary spherical quadrangle.

Algebrising the joint angles and link twists with the tangent half-angle parameters $v_i = \tan(\theta_i/2)$ and $\alpha_i = \tan(\tau_i/2)$ leads to the algebraic form of each v_i-v_j IO equation. The v_1-v_4 algebraic IO equation is

$$Av_1^2v_4^2 + Bv_1^2 + Cv_4^2 + 8\alpha_1\alpha_3\left(\alpha_4^2+1\right)\left(\alpha_2^2+1\right)v_1v_4 + D = 0, \tag{6.130}$$

where

$$\begin{aligned}
A = A_1A_2 &= (\alpha_1\alpha_2\alpha_3 - \alpha_1\alpha_2\alpha_4 + \alpha_1\alpha_3\alpha_4 - \alpha_2\alpha_3\alpha_4 + \alpha_1 - \alpha_2 + \alpha_3 - \alpha_4)\\
&\quad (\alpha_1\alpha_2\alpha_3 - \alpha_1\alpha_2\alpha_4 - \alpha_1\alpha_3\alpha_4 - \alpha_2\alpha_3\alpha_4 - \alpha_1 - \alpha_2 - \alpha_3 + \alpha_4),\\
B = B_1B_2 &= (\alpha_1\alpha_2\alpha_3 + \alpha_1\alpha_2\alpha_4 - \alpha_1\alpha_3\alpha_4 - \alpha_2\alpha_3\alpha_4 + \alpha_1 + \alpha_2 - \alpha_3 - \alpha_4)\\
&\quad (\alpha_1\alpha_2\alpha_3 + \alpha_1\alpha_2\alpha_4 + \alpha_1\alpha_3\alpha_4 - \alpha_2\alpha_3\alpha_4 - \alpha_1 + \alpha_2 + \alpha_3 + \alpha_4),\\
C = C_1C_2 &= (\alpha_1\alpha_2\alpha_3 - \alpha_1\alpha_2\alpha_4 - \alpha_1\alpha_3\alpha_4 + \alpha_2\alpha_3\alpha_4 - \alpha_1 + \alpha_2 + \alpha_3 - \alpha_4)\\
&\quad (\alpha_1\alpha_2\alpha_3 - \alpha_1\alpha_2\alpha_4 + \alpha_1\alpha_3\alpha_4 + \alpha_2\alpha_3\alpha_4 + \alpha_1 + \alpha_2 - \alpha_3 + \alpha_4),\\
D = D_1D_2 &= (\alpha_1\alpha_2\alpha_3 + \alpha_1\alpha_2\alpha_4 + \alpha_1\alpha_3\alpha_4 + \alpha_2\alpha_3\alpha_4 - \alpha_1 - \alpha_2 - \alpha_3 - \alpha_4)\\
&\quad (\alpha_1\alpha_2\alpha_3 + \alpha_1\alpha_2\alpha_4 - \alpha_1\alpha_3\alpha_4 + \alpha_2\alpha_3\alpha_4 + \alpha_1 - \alpha_2 + \alpha_3 + \alpha_4).
\end{aligned}$$

The coefficients A, B, C, and D all have two bicubic factors. It can be shown that when the radius of the sphere is infinite then Equations (6.130) and (6.83) are functionally identical [51], hence the same coefficient names A, B, C, and D are used. While the derivation of this algebraised v_1-v_4 IO equation is novel and far from intuitive, the algebraic form of this fourth degree polynomial in

the v_1-v_4 IO angle parameters is not. The earliest derivations of similar equations representing manipulatable octahedra, identical in form, are due to Raoul Bricard in 1897 [68]. This fascinating similarity between movable octahedral and spherical linkage algebraic IO equations is not at all a coincidence, as will be illustrated in Section 6.10.2.

6.9.1 Derivation of the Six Spherical v_i-v_j IO Equations

Using the eight bicubic coefficient definitions from Equation (6.130), the remaining five v_i-v_j equations contain all eight of the bicubic coefficients, but in different permutations:

$$A_1B_2v_1^2v_2^2+A_2B_1v_1^2+C_1D_2v_2^2+8\alpha_2\alpha_4\big(\alpha_1^2+1\big)\big(\alpha_3^2+1\big)v_1v_2+C_2D_1=0; \quad (6.131)$$

$$A_1B_1v_1^2v_3^2 + A_2B_2v_1^2 + C_2D_2v_3^2 + C_1D_1 = 0; \quad (6.132)$$

$$A_1D_2v_2^2v_3^2+B_2C_1v_2^2+B_1C_2v_3^2-8\alpha_1\alpha_3\big(\alpha_2^2+1\big)\big(\alpha_4^2+1\big)\,v_2v_3+A_2D_1=0; \quad (6.133)$$

$$A_1C_1v_2^2v_4^2 + B_2D_2v_2^2 + A_2C_2v_4^2 + B_1D_1 = 0; \quad (6.134)$$

$$A_1C_2v_3^2v_4^2+B_1D_2v_3^2+A_2C_1v_4^2+8\alpha_2\alpha_4\big(\alpha_1^2+1\big)\big(\alpha_3^2+1\big)\,v_3v_4+B_2D_1=0. \quad (6.135)$$

As for the planar 4R and RRRP linkage algebraic IO equations, we see that Equations (6.132) and (6.134) do not contain a bilinear quadratic term because they relate angle parings between the spherical quadrangle edges that intersect in opposite vertices. Each of Equations (6.130)-(6.135) has genus 1.

The v_1-v_4 IO Equation. The soma coordinates representing the forward kinematics of the spherical 4R are polynomials containing coefficients are already to complicated to efficiently use the "`lexdeg`" elimination monomial ordering. To obtain this IO equation from the ideal generated by the three soma coordinates that equate to zero, both v_2 and v_3 are eliminated by first computing the Gröbner bases using the Maple 2021 "`tdeg`" monomial ordering with the list sequence (v_3, v_2, v_4, v_1), meaning that the indeterminate ordering is $v_3 > v_2 > v_4 > v_1$. In this case, 12 bases are computed, all functions of all four v_i. We eliminate v_2 and v_3 by computing the bases of these 12 with the reverse monomial ordering by using "`plex`". This results in 10 new bases, with one that is a function of only v_1 and v_4 and the four α_i, which represents the IO equation we are looking for. This polynomial splits into three factors. The first two are $(1 + v_1^2)(1 + v_4^2)$, a product that is always greater than zero, and can be safely factored out, leaving us with Equation (6.130). This, and some of the other spherical 4R IO equations are computable in one application of the "`lexdeg`" elimination monomial ordering, but the computation time is

more than an order of magnitude greater, about 3500 s, than the 120 s for the sequential application of "`tdeg`" and "`plex`" on an Intel Core i7-7700 CPU @ 3.60 GHz.

It is important to note that we are using the standard Denavit-Hartenberg [50] relative joint angle parameters, which are each a measure of the relative angle a link makes with the previous link in the kinematic chain. This fact enables us to derive the remaining five IO equations such that the same eight bicubic coefficient factors characterise all six IO equations. This is generally not the case when vector loop methods are used together with trigonometry, see [62] for a detailed example.

The v_1-v_2 IO Equation. The derivation steps are precisely the same as for the v_1-v_4 IO equation. Eliminating v_3 and v_4 from the same three soma coordinates, the resulting v_1-v_2 IO equation splits into three similar factors. The first two, $(1+v_1^2)(1+v_2^2)$, can be safely factored out, leaving us with Equation (6.131).

The v_1-v_3 IO Equation. The derivation steps are precisely the same as for the previous two IO equations. But, after the elimination of v_2 and v_4 from the same three soma coordinates, the resulting v_1-v_3 IO equation splits into five factors. The first two are $(1+v_1^2)(1+v_3^2)$, and can be safely factored out. The next two are

$$(\alpha_2^2\alpha_3^2 + 2\alpha_2\alpha_3 + 1)v_3^2 + \alpha_2^2\alpha_3^2 - 2\alpha_2\alpha_3 + 1, \tag{6.136}$$

$$(\alpha_2^2 - 2\alpha_2\alpha_3 + \alpha_3^2)v_3^2 + \alpha_2^2 + 2\alpha_2\alpha_3 + \alpha_3^2. \tag{6.137}$$

In order for either, or both, of Equations (6.136) or (6.137) to be identically zero the arc length parameters α_2 and α_3 must be complex. This means these two factors may also eliminated since we are only interested in real linkages, leaving us with Equation (6.132).

The v_2-v_3 IO Equation. To derive this IO equation using elimination methods on the three soma coordinates we have been using requires a very different approach. We were successful by first applying the graded reverse lexicographical order "`tdeg`" to the three soma coordinates using the list sequence (v_1, v_4, v_2, v_3), then applying *graded lexicographic order* using "`grlex`" to the bases identified with "`tdeg`". After each computation we obtain 12 bases, all in terms of the four α_i and the four v_i, with the exception of one in the graded lexicographic order set of bases, which is in terms of the four α_i, but only v_1, v_2, and v_3, and is used in the elimination steps. Next, resultants are used to eliminate v_4 first, then v_1. We obtain a v_2-v_3 IO equation that splits into nine factors.

The first five of these factors are simple to divide out since they are trivially non-zero: the first is -1; the other four are the squares of a single α_i added to a positive integer. The next three factors are functions of v_2 and v_3, but only α_1, α_2, and α_3:

$$(\alpha_1\alpha_2 - \alpha_1\alpha_3 + \alpha_2\alpha_3 + 1)^2 v_2^2 v_3^2 + (\alpha_1\alpha_2 + \alpha_1\alpha_3 - \alpha_2\alpha_3 + 1)^2 v_2^2 + 8\alpha_1\alpha_3(\alpha_2^2+1)v_2v_3 + (\alpha_1\alpha_2 - \alpha_1\alpha_3 - \alpha_2\alpha_3 - 1)^2 v_3^2 + (\alpha_1\alpha_2 + \alpha_1\alpha_3 + \alpha_2\alpha_3 - 1)^2; \quad (6.138)$$

$$(\alpha_1\alpha_2\alpha_3 + \alpha_1 - \alpha_2 + \alpha_3)^2 v_2^2 v_3^2 + (\alpha_1\alpha_2\alpha_3 - \alpha_1 + \alpha_2 + \alpha_3)^2 v_2^2 - 8\alpha_1\alpha_3(\alpha_2^2+1)v_2v_3 + (\alpha_1\alpha_2\alpha_3 + \alpha_1 + \alpha_2 - \alpha_3)^2 v_3^2 + (\alpha_1\alpha_2\alpha_3 - \alpha_1 - \alpha_2 - \alpha_3)^2; \quad (6.139)$$

$$\alpha_3(\alpha_1\alpha_2+1)(\alpha_1-\alpha_2)v_2^2 + 2\alpha_1\alpha_3(\alpha_2^2+1)v_2v_3 - \alpha_1(\alpha_2\alpha_3+1)(\alpha_2-\alpha_3)v_3^2 + \alpha_2(\alpha_1+\alpha_3)(\alpha_1\alpha_3-1). \quad (6.140)$$

In order for Equations (6.138), (6.139), and/or (6.140) to be identically zero the arc length parameters α_1, α_2, and/or α_3 must be complex numbers, so we may safely divide these three factors out, leaving only Equation (6.133) as the desired IO equation.

The v_2-v_4 IO Equation. The derivation steps for the v_2-v_4 IO equation are the same as those for the v_1-v_4, v_1-v_2, and v_1-v_3 IO equations. The the second set of Gröbner bases computed using the pure lexicographic order with list sequence (v_3, v_1, v_2, v_4) lead to an IO equation that splits into five factors, the first two are trivial. The next two are

$$(\alpha_1^2\alpha_2^2 + 2\alpha_1\alpha_2 + 1)v_2^2 + \alpha_1^2\alpha_2^2 - 2\alpha_1\alpha_2 + 1, \quad (6.141)$$

$$(\alpha_1^2 - 2\alpha_1\alpha_2 + \alpha_2^2)v_2^2 + \alpha_1^2 + 2\alpha_1\alpha_2 + \alpha_2^2. \quad (6.142)$$

For either, or both of Equations (6.141) and (6.142) to equate to zero, it requires both α_1 and α_2 to be complex. We can therefore factor both of these out, leaving only the desired v_2-v_4 IO, Equation (6.134).

The v_3-v_4 IO Equation. Finally, the derivation steps for the v_3-v_4 IO equation are precisely the same as for the v_2-v_4 IO equation. After the elimination of v_1 and v_2 from the same three soma coordinates, the resulting v_3-v_4 IO equation splits into three factors. The first two are safely divided out, leaving us with Equation (6.135).

6.10 Applications

6.10.1 Mobility Classification

Treating each pair of v_i-v_j to be coordinate axes in the plane spanned by the two, then each IO equation for a pair of joint angle parameters contains two double points at infinity, one on each of the v_i and v_j axes. The double points at infinity belonging to each of the four distinct v_i coordinate axes together with the type of points at $v_i = 0$ completely define the mobility limits, if they exist, between each v_i-v_j angle parameter pair. For a planar algebraic curve to possess a double point, it's degree must be $n > 3$. Hence, this analysis does not apply to PRRP linkages, but it does apply to the R-pairs in an RRRP linkage. The double point at infinity on the d_4 axis is always an acnode independent of the lengths of the links and offsets, which is reassuring as this means the travel of the prismatic slider is always finite. But, for R-pairs, the nature of the double points determine if extreme orientations exist that are implied by the v_i where the two corresponding links can align. Hence, the examination of these two points is sufficient to determine whether a particular joint enables a crank, a rocker, a π-rocker, or a 0-rocker relative link motion [56, 69].

For example, let us determine the double points for the v_1-v_4 IO curve for a planar 4R. First homogenise Equation (6.83) using the homogenising coordinate v_0, then redefine the IO equation as

$$IO_h := \; Av_1^2v_4^2 + Bv_0^2v_1^2 + Cv_0^2v_4^2 - 8abv_0^2v_1v_4 + Dv_0^4 \;=\; 0. \quad (6.143)$$

Then compute the partial derivatives of IO_h with respect to the three homogeneous coordinates, giving

$$\frac{\partial IO_h}{\partial v_0} := 2Bv_0v_1^2 + 2Cv_0v_4^2 - 16a_1a_3v_0v_1v_4 + 4Dv_0^3 = 0, \quad (6.144)$$

$$\frac{\partial IO_h}{\partial v_1} := 2Av_1v_4^2 + 2Bv_0^2v_1 - 8a_1a_3v_0^2v_4 = 0, \quad (6.145)$$

$$\frac{\partial IO_h}{\partial v_4} := 2Av_1^2v_4 + 2Cv_0^2v_4 - 8a_1a_3v_0^2v_1 = 0. \quad (6.146)$$

Finally solve the system of four equations (6.143)-(6.146) for v_0, v_1, and v_4. In this case, similar for all the IO equations, there are two solutions which are independent of the design parameters a_1, a_2, a_3, and a_4. These two solutions are double points at infinity on the v_1 and v_4 axes, named DP_1 and DP_2:

$$DP_1 = \{v_0 = 0, v_1 = v_1, v_4 = 0\}; \quad (6.147)$$

$$DP_2 = \{v_0 = 0, v_1 = 0, v_4 = v_4\}. \quad (6.148)$$

One possibility to determine the type of double point, i.e., whether it is a crunode (regular double point), acnode (isolated double point), or cusp, is to evaluate whether the double point has a pair of real, or complex conjugate tangents. If the double point has two real distinct tangents, it is a crunode; if it has two real coincident tangents, it is a cusp; and if the tangents are both complex conjugates, the double point is an acnode [45, 70]. Thus, after homogenising each v_i-v_j angle pair IO equation using the homogenising coordinate v_0, leading to IO_h, recall that the discriminant yields information on the double point at infinity on the v_j axis:

It is the nature of the tangents at the double points that determine the mobility of the input and output links. Both double points can have real, or complex tangents, depending on the values of the four link lengths. The possible combinations of these cases have different meanings for the corresponding linkages. The following three cases are demonstrated and proved in [27].

1. When the tangents of both points are real then both input and output links can fully rotate, and the mechanism is a double-crank.

2. One pair of double point tangents is real and the other complex conjugate means that one on the input or output links is a crank while the other is a rocker. The double point corresponding to the complex conjugate tangents is always an *acnode*, or *hermit point*, and the link that is the rocker depends on which double point is the acnode.

3. When both pairs of tangents are complex conjugates then both double points are acnodes and the mechanism is a double rocker.

The *discriminant* of an algebraic equation, evaluated at a double point, reveals whether that double point has a pair of real or complex conjugate tangents [45, 71] in turn yielding information about the topology of the mechanism [27, 71]. If the tangents are complex conjugates the double point is an acnode: a *hermit* point that satisfies the equation of the curve but is isolated from all other points on the curve. For an arbitrary v_i-v_j homogeneous IO_h equation, the discriminant for the double point at infinity on the v_j-axis, and the meaning of its value are [45, 71]

$$\Delta_{v_j} = \left(\frac{\partial^2 IO_h}{\partial v_0 \partial v_i}\right)^2 - \frac{\partial^2 IO_h}{\partial v_0^2}\frac{\partial^2 IO_h}{\partial v_i^2} \begin{cases} > 0 \Rightarrow & \text{two real distinct tangents : the double point is a crunode;} \\ = 0 \Rightarrow & \text{two real coincident tangents : the double point is a cusp;} \\ < 0 \Rightarrow & \text{two complex conjugate tangents : the double point is an acnode.} \end{cases} \tag{6.149}$$

Proceeding with the double point analysis of all six v_i-v_j equations, the points at infinity on each axis result in 12 discriminants. However, as the v_i-v_j equations are all dependent on each other, only four are distinct. Each one describes the nature of the double point at infinity of each v_i for $i \in \{1...4\}$:

$$\begin{aligned}
\Delta_{v_1} &= -4(a_1 + a_2 - a_3 - a_4)(a_1 + a_2 + a_3 - a_4) \\
&\quad (a_1 - a_2 + a_3 - a_4)(a_1 - a_2 - a_3 - a_4);
\end{aligned}$$

$$\begin{aligned}
\Delta_{v_2} &= -4(a_1 - a_2 - a_3 + a_4)(a_1 - a_2 + a_3 + a_4) \\
&\quad (a_1 - a_2 + a_3 - a_4)(a_1 - a_2 - a_3 - a_4);
\end{aligned}$$

$$\begin{aligned}
\Delta_{v_3} &= -4(a_1 - a_2 + a_3 + a_4)(a_1 + a_2 - a_3 + a_4) \\
&\quad (a_1 + a_2 - a_3 - a_4)(a_1 - a_2 + a_3 - a_4);
\end{aligned}$$

$$\begin{aligned}
\Delta_{v_4} &= -4(a_1 + a_2 - a_3 + a_4)(a_1 - a_2 - a_3 + a_4) \\
&\quad (a_1 - a_2 + a_3 - a_4)(a_1 + a_2 + a_3 - a_4).
\end{aligned}$$

Using the bilinear factors defined by Equation (6.83) these discriminants can be rewritten compactly as

$$\Delta_{v_1} = -4\ A_1A_2B_1B_2, \tag{6.150}$$

$$\Delta_{v_2} = -4\ A_1B_2C_1D_2, \tag{6.151}$$

$$\Delta_{v_3} = -4\ A_1B_1C_2D_2, \tag{6.152}$$

$$\Delta_{v_4} = -4\ A_1A_2C_1C_2. \tag{6.153}$$

From these conditions we can extract the following information. If $\Delta_{v_1} \geq 0$, then the double point at infinity on the v_1 axis is either a crunode or a cusp. Knowing that $v_1 = \infty$ corresponds to $\theta_1 = 180°$, which implies that the link a_1 can physically reach the extreme position where a_1 aligns with and overlays the previous link a_4. Similarly, if $\Delta_{v_1} < 0$, then the double point at $v_1 = \infty$ is an acnode which in turn indicates that a_1 can not physically reach the extreme position where a_1 aligns with and overlays a_4. Analogous conclusions can be drawn from Equations (6.151), (6.152), and (6.153).

As previously mentioned, to fully understand the mobility of every link, it equally requires the analysis of whether the other extremes where the link under investigation aligns with, but does not overlay, the previous link. We need to investigate whether the linkage is assemblable at $v_i = 0$. Clearly, one possibility

to obtain a condition with this information can be derived using the six v_i-v_j equations by substituting $v_i = 0$ and solving for v_j. Again, due to the equations' dependencies, we obtain four distinct conditions, one for each v_i:

$$\begin{aligned}
\Omega_{v_1} &= [-(a_1 - a_2 - a_3 + a_4)(a_1 - a_2 + a_3 + a_4) \\
&\quad (a_1 + a_2 - a_3 + a_4)(a_1 + a_2 + a_3 + a_4)]^{\frac{1}{2}}; \\
\Omega_{v_2} &= [-(a_1 + a_2 - a_3 - a_4)(a_1 + a_2 + a_3 - a_4) \\
&\quad (a_1 + a_2 - a_3 + a_4)(a_1 + a_2 + a_3 + a_4)]^{\frac{1}{2}}; \\
\Omega_{v_3} &= [-(a_1 + a_2 + a_3 - a_4)(a_1 - a_2 - a_3 - a_4) \\
&\quad (a_1 - a_2 - a_3 + a_4)(a_1 + a_2 + a_3 + a_4)]^{\frac{1}{2}}; \\
\Omega_{v_4} &= [-(a_1 - a_2 - a_3 - a_4)(a_1 + a_2 - a_3 - a_4) \\
&\quad (a_1 - a_2 + a_3 + a_4)(a_1 + a_2 + a_3 + a_4)]^{\frac{1}{2}}.
\end{aligned}$$

Using the bilinear factors from Equation 6.83 these expressions can be rewritten compactly as:

$$\Omega_{v_1} = \sqrt{-C_1C_2D_1D_2}; \tag{6.154}$$

$$\Omega_{v_2} = \sqrt{-A_2B_1C_2D_1}; \tag{6.155}$$

$$\Omega_{v_3} = \sqrt{-A_2B_2C_1D_1}; \tag{6.156}$$

$$\Omega_{v_4} = \sqrt{-B_1B_2D_1D_2}. \tag{6.157}$$

With this information we can establish a completely generic classification scheme to determine the relative mobilities of every link in the simple closed kinematic chain. Using the bilinear factors the classification can be constructed according to Tables 6.7-6.10. The beauty of this classification scheme lies in its completely generic nature, covering both positive and negative values for the a_i. This result requires the a_i to be considered as directed line segments. For example $a_1 > 0$ means that it is directed from the join with a_4 to a_2, $a_1 < 0$ means a_1 points in the opposite direction. Moreover, the classification scheme is directly linked to the algebraic IO equations. We are now able to explain the different spatial sections that are spanned by the linear factors in the design parameter space reported in [56].

It is straightforward to use this same analysis applied to the spherical 4R as well as the planar RRRP linkages to determine the relative mobility conditions for each link in the chain. However, in the interest if brevity, we will not include these results in this paper.

Table 6.7: Mobility of a_1 relative to a_4.

$A_1A_2B_1B_2$	$C_1C_2D_1D_2$	mobility of a_1
≤ 0	≤ 0	crank
≤ 0	> 0	π-rocker
> 0	≤ 0	0-rocker
> 0	> 0	rocker

Table 6.8: Mobility of a_2 relative to a_1.

$A_1B_2C_1D_2$	$A_2B_1C_2D_1$	mobility of a_2
≤ 0	≤ 0	crank
≤ 0	> 0	π-rocker
> 0	≤ 0	0-rocker
> 0	> 0	rocker

Table 6.9: Mobility of a_3 relative to a_2.

$A_1B_1C_2D_2$	$A_2B_2C_1D_1$	mobility of a_3
≤ 0	≤ 0	crank
≤ 0	> 0	π-rocker
> 0	≤ 0	0-rocker
> 0	> 0	rocker

Table 6.10: Mobility of a_4 relative to a_3.

$A_1A_2C_1C_2$	$B_1B_2D_1D_2$	mobility of a_4
≤ 0	≤ 0	crank
≤ 0	> 0	π-rocker
> 0	≤ 0	0-rocker
> 0	> 0	rocker

6.10.2 Design Parameter Spaces

The first graphical representation of the design parameter space of planar and spherical 4R linkages can be found in [72, 73, 74]. In the case of the planar 4R it reveals plane bound regions in a three-space having the Freudenstein parameters as mutually orthogonal basis vectors. However, the full symmetry of the group of planar 4R linkages is obscured by the trigonometric description of the IO equation. The symmetries of the algebraic IO equations for the spherical and

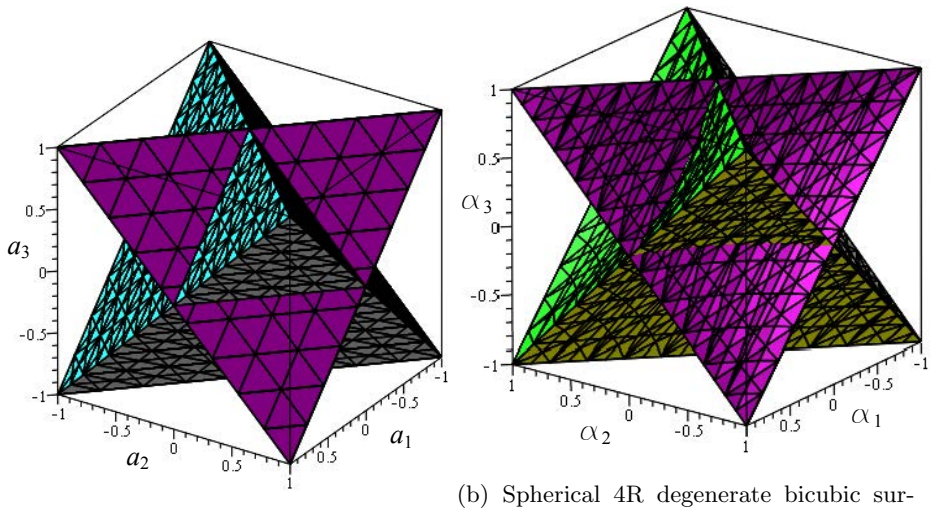

(a) Planar 4R stellated octahedron.

(b) Spherical 4R degenerate bicubic surfaces.

Figure 6.30: Planar and spherical 4R design parameter spaces.

planar 4R and the planar RRRP and PRRP linkages are fully revealed graphically when one considers the link lengths a_i, link offsets d_i, and link twist angle parameters α_i as design parameters, see [52, 56, 67]. For planar and spherical 4R function generators the scale of the linkage is irrelevant. We can consider these four a_i and four α_i design parameters as homogeneous coordinates, and assign a_4 and α_4 to normalise the four coordinates, thereby setting $a_4 = 1$ for the planar and $\alpha_4 = 1$ as the spherical design space parameter coordinates and treat the remaining three lengths or twist angles as mutually orthogonal basis vectors.

In the planar 4R design parameter three-space, each of the distinct eight bilinear factors in Equations (6.83)-(6.88) represent eight distinct planes. These eight planes intersect in 12 lines which are the edges of a setllated octahedron having order 48 octahedral symmetry [75], which Johannes Kepler named "stella octangula", which is Latin for "eight-pointed star", referring to the eight vertices, see Figure 6.30a. In the entire universe of polytopes, it is the only regular compound of two tetrahedra [75]: two tetrahedra which intersect in an octahedron! Each distinct point in the design parameter space represents a distinct planar 4R linkage. The eight planes segment the design parameter space into regions that represent the mobility of the linkages contained in that region [56, 76].

For the spherical 4R, the eight bicubic factors in the four coefficients A, B,

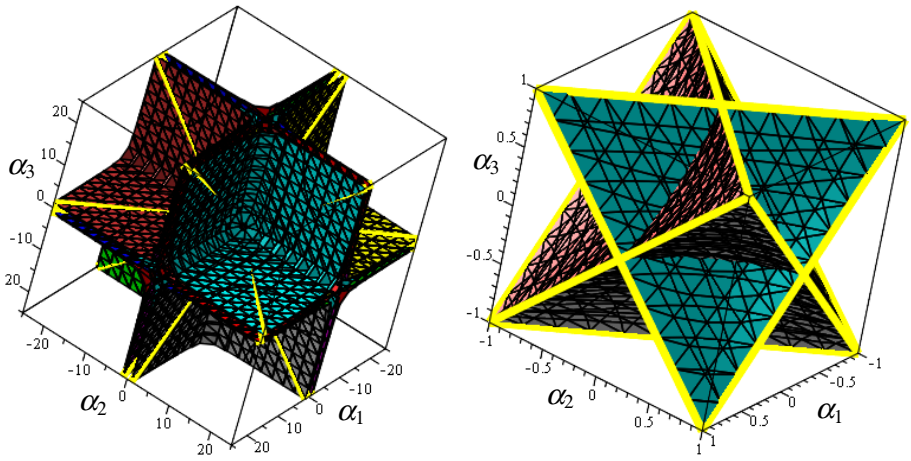

(a) In the range $-25 \leq \alpha_i \leq 25$.

(b) In the range $-1 \leq \alpha_i \leq 1$.

Figure 6.31: Eight cubic surfaces in the spherical 4R design parameter space.

C, and D in Equation (6.130) are symmetric singular cubic surfaces, see Figure 6.30b, which each possess three distinct finite lines and three common lines at infinity [52]. Note that a cubic surface can contain as many as 27 lines [77]; those that contain less than 27 are called *singular*, while those that contain exactly 27 are *non-singular*. Each of these cubic surfaces possess three ordinary double points [52]. It is also shown in [77] that a cubic surface possessing three ordinary double points can have, at most, 12 lines, which is the case for these eight cubic surfaces. Of these 12 lines on each surface, six are complex and six are real. Of the six real lines three are at infinity. The remaining three lines on each surface intersect each other in an equilateral triangle.

Different pairs of the eight cubic surfaces have one finite line in common, meaning there are 12 distinct finite lines among the eight surfaces. The finite lines contain the twelve edges of another stellated octahedron. The faces of the same stellated octahedron are also found in the design parameter space of planar 4R linkages. The edges of this regular double tetrahedron can be regarded as the intersection of the bilinear factors of the coefficients of the planar 4R and the singular cubic surfaces formed by the coefficients of the spherical 4R IO equations in the design parameter spaces. This is as remarkable as it is fascinating! Figure 6.31 illustrates the eight cubic surfaces and the three finite lines on each. This illustrates the connection between Bricard's movable octahedra mentioned at the end of Section 6.9 and the intersection of the spherical 4R and planar 4R design parameter spaces.

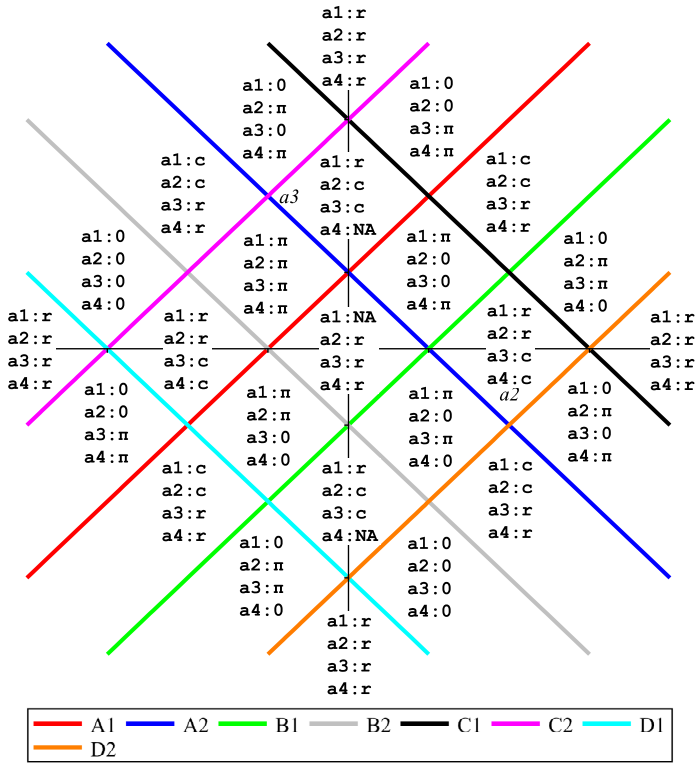

Figure 6.32: Intersection of the planar 4R stellated octahedron in the design parameter space with the plane $a_1 = 0.5$.

With the six algebraic v_i-v_j equations, and the previously identified mobility classification using double points and discriminants, it becomes evident that the planes containing the faces of the stellated octahedron contain even more mobility information than stated in [56], namely, information on the relative mobility of every link in the chain! In fact, the stellated octahedron face planes segment the design parameter space into distinct regions which each describes the relative mobility of a_1, a_2, a_3 and a_4. Since a complete analysis of the design parameter space would go well beyond the scope of this paper, we will limit the discussion herein to one short example as follows.

Consider the intersection traces of the bilinear factors in the parameter plane $a_1 = 0.5$ spanned by a_2 and a_3 in the design parameter space where a_2 and a_3 are the horizontal and vertical axes, respectively. Here the bilinear factors are parallel and orthogonal plane trace lines. Together with Tabs. 6.7-6.10, the mobility of all a_2 and a_3 of any length can now be identified, resulting

in Figure 6.32 where **r** indicates that the corresponding link is a rocker, **c** a crank, π a π-rocker, and **0** a 0-rocker, while NA indicates the linkage is not assemblable. This analysis can be conducted for every area separated by the bilinear factors in the design parameter space, resulting in a complete geometric mobility classification of planar four bar linkages which is directly linked to the six algebraic v_i-v_j IO equations.

6.11 Some Spatial Four-bar Mechanisms

In this section the analysis of two spatial four-bar mechanisms will be considered: the Bennett spatial 4R mechanism; and the RSSR spatial mechanism.

6.11.1 Bennett Mechanism

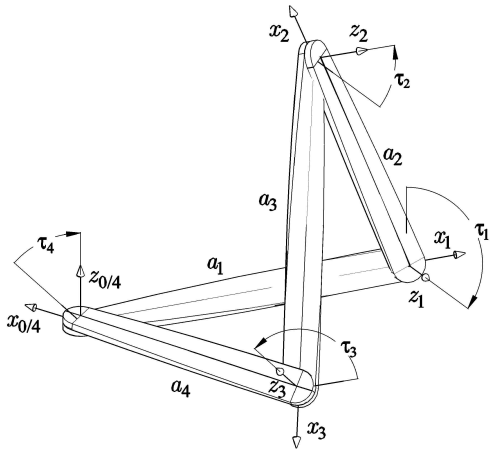

Figure 6.33: Spatial 4R function generator: the Bennett linkage.

The Bennett linkage is, as the planar 4R, composed of four rigid links that are connected by four R joints. According to the Chebychev–Grübler–Kutzbach criterion the Bennett linkage has a mobility of -2, which in theory prevents it from moving. However, its actual mobility is 1, and thereby, it is the only known mobile spatial 4R linkage. The linkage is able to move if, and only if, it satisfies the following conditions which were discovered by Bennett and for that reason

known as the Bennett conditions [78]

$$\left.\begin{array}{ll} a_1 = a_3 & a_2 = a_4 \\ \tau_1 = \tau_3 & \tau_2 = \tau_4 \\ \dfrac{\sin(\tau_1)}{a_1} = \dfrac{\sin(\tau_2)}{a_2}. & \end{array}\right\} \tag{6.158}$$

The IO equation is well known, for example [12, 78, 79, 80, 81] show different derivations. While the former authors favoured a geometric approach, Denavit used Cayley-Klein parameters, and Pfurner et al. used an algebraic method to first derive the Bennett conditions and second, obtain an IO equation in terms of the tangent half input and output angles.

The IO equation for the Bennett mechanism is derived following the same procedure as that of the planar 4R using relative angles, recall Section 6.5.5. First, as illustrated in Figure (6.33) the coordinate frames are attached to the linkage according to the DH convention. The DH coordinate frame assignment allows to define the DH parameters for the linkage. It turns out that the Bennett linkage does not contain any link offsets d_i. However, it contains the four variable joint angles θ_i of the R joints and the design parameters a_i and τ_i. The DH parameters for the Bennett linkage are given in Table 6.2. To evaluate

Table 6.2: DH parameters for the Bennett linkage.

joint axis i	link angle θ_i	link offset d_i	link length a_i	link twist τ_i
1	θ_1	0	a_1	τ_1
2	θ_2	0	a_2	τ_2
3	θ_3	0	a_3	τ_3
4	θ_4	0	a_4	τ_4

the overall transformation of the position and orientation of the last joint with respect to the base coordinate system, the DH parameters from Table 6.2 are substituted into Equation (6.5.5.1), and multiplied according to Equation (6.79).

Recall that the Bennett linkage is subjected to special conditions. The Bennett conditions from Equation (6.158) can be reformulated with the tangent

half-angle substitution and expressed algebraically as

$$\begin{aligned} a_2 &= \frac{a_1\alpha_2(\alpha_1^2+1)}{\alpha_1(\alpha_2^2+1)}; \\ a_4 &= \frac{a_1\alpha_2(\alpha_1^2+1)}{\alpha_1(\alpha_2^2+1)}; \\ a_3 &= a_1; \\ \alpha_3 &= \alpha_1; \\ \alpha_4 &= \alpha_2; \end{aligned} \tag{6.159}$$

where $\alpha_i = \tan(\tau_i/2)$.

Equation (6.159) is substituted into the overall transformation matrix which reduces the number of unknown parameters. After mapping the transformation matrix into Study's parameters, the vector yields

$$\begin{aligned} x_0 &= \alpha_1^3\alpha_2^4v_1v_2v_3v_4 + \alpha_1^3\alpha_2^4v_1v_2 - \alpha_1^3\alpha_2^4v_1v_3 + \alpha_1^3\alpha_2^4v_1v_4 + \alpha_1^3\alpha_2^4v_2v_3 \\ &\quad -\alpha_1^3\alpha_2^4v_2v_4 + \alpha_1^3\alpha_2^4v_3v_4 + 4\alpha_1^2\alpha_2^3v_1v_2v_3v_4 - \alpha_1\alpha_2^4v_1v_2v_3v_4 + \alpha_1^3\alpha_2^4 \\ &\quad -2\alpha_1^3\alpha_2^2v_1v_3 + 2\alpha_1^3\alpha_2^2v_1v_4 + 2\alpha_1^3\alpha_2^2v_2v_3 - 2\alpha_1^3\alpha_2^2v_2v_4 - \alpha_1^3v_1v_2v_3v_4 \\ &\quad +4\alpha_1^2\alpha_2v_1v_2v_3v_4 + \alpha_1\alpha_2^4v_1v_2 - \alpha_1\alpha_2^4v_1v_3 - \alpha_1\alpha_2^4v_1v_4 - \alpha_1\alpha_2^4v_2v_3 - \alpha_1\alpha_2^4v_2v_4 \\ &\quad +\alpha_1\alpha_2^4v_3v_4 - \alpha_1^3v_1v_2 - \alpha_1^3v_1v_3 + \alpha_1^3v_1v_4 + \alpha_1^3v_2v_3 - \alpha_1^3v_2v_4 - \alpha_1^3v_3v_4 \\ &\quad -4\alpha_1^2\alpha_2^3 - \alpha_1\alpha_2^4 - 2\alpha_1\alpha_2^2v_1v_3 - 2\alpha_1\alpha_2^2v_1v_4 - 2\alpha_1\alpha_2^2v_2v_3 - 2\alpha_1\alpha_2^2v_2v_4 + \alpha_1v_1v_2v_3v_4 \\ &\quad -\alpha_1^3 - 4\alpha_1^2\alpha_2 - \alpha_1v_1v_2 - \alpha_1v_1v_3 - \alpha_1v_1v_4 - \alpha_1v_2v_3 - \alpha_1v_2v_4 - \alpha_1v_3v_4 + \alpha_1, \\ x_1 &= -2\alpha_1^3\alpha_2^3v_1v_2v_3v_4 + 2\alpha_1^2\alpha_2^4v_1v_2v_3v_4 - 2\alpha_1^3\alpha_2^3v_1v_2 - 2\alpha_1^3\alpha_2^3v_3v_4 - 2\alpha_1^3\alpha_2v_1v_2v_3v_4 \\ &\quad +2\alpha_1^2\alpha_2^4v_1v_4 - 2\alpha_1^2\alpha_2^4v_2v_3 + 2\alpha_1\alpha_2^3v_1v_2v_3v_4 - 2\alpha_1^3\alpha_2^3 - 2\alpha_1^3\alpha_2v_1v_2 - 2\alpha_1^3\alpha_2v_3v_4 \\ &\quad -2\alpha_1^2\alpha_2^4 + 4\alpha_1^2\alpha_2^2v_1v_4 - 4\alpha_1^2\alpha_2^2v_2v_3 - 2\alpha_1^2v_1v_2v_3v_4 - 2\alpha_1\alpha_2^3v_1v_2 - 2\alpha_1\alpha_2^3v_3v_4 \\ &\quad +2\alpha_1\alpha_2v_1v_2v_3v_4 - 2\alpha_1^3\alpha_2 + 2\alpha_1^2v_1v_4 - 2\alpha_1^2v_2v_3 + 2\alpha_1\alpha_2^3 - 2\alpha_1\alpha_2v_1v_2 - 2\alpha_1\alpha_2v_3v_4 \\ &\quad +2\alpha_1^2 + 2\alpha_1\alpha_2, \\ x_2 &= -2\alpha_1^3\alpha_2^3v_1v_3v_4 + 2\alpha_1^3\alpha_2^3v_2v_3v_4 - 2\alpha_1^2\alpha_2^4v_1v_2v_3 - 2\alpha_1^2\alpha_2^4v_2v_3v_4 - 2\alpha_1^3\alpha_2^3v_1 + 2\alpha_1^3\alpha_2^3v_2 \\ &\quad -2\alpha_1^3\alpha_2v_1v_3v_4 + 2\alpha_1^3\alpha_2v_2v_3v_4 - 2\alpha_1^2\alpha_2^4v_1 - 2\alpha_1^2\alpha_2^4v_4 - 4\alpha_1^2\alpha_2^2v_1v_2v_3 - 2\alpha_1\alpha_2^3v_1v_3v_4 \\ &\quad -2\alpha_1\alpha_2^3v_2v_3v_4 - 2\alpha_1^3\alpha_2v_1 + 2\alpha_1^3\alpha_2v_2 - 4\alpha_1^2\alpha_2^2v_4 - 2\alpha_1^2v_1v_2v_3 + 2\alpha_1^2v_2v_3v_4 + 2\alpha_1\alpha_2^3v_1 \\ &\quad +2\alpha_1\alpha_2^3v_2 - 2\alpha_1\alpha_2v_1v_3v_4 - 2\alpha_1\alpha_2v_2v_3v_4 + 2\alpha_1^2v_1 - 2\alpha_1^2v_4 + 2\alpha_1\alpha_2v_1 + 2\alpha_1\alpha_2v_2, \\ x_3 &= \alpha_1^3\alpha_2^4v_1v_2v_3 - \alpha_1^3\alpha_2^4v_1v_2v_4 + \alpha_1^3\alpha_2^4v_1v_3v_4 - \alpha_1^3\alpha_2^4v_2v_3v_4 + \alpha_1^3\alpha_2^4v_1 - \alpha_1^3\alpha_2^4v_2 + \alpha_1^3\alpha_2^4v_3 \\ &\quad -\alpha_1^3\alpha_2^4v_4 + 2\alpha_1^3\alpha_2^2v_1v_2v_3 - 2\alpha_1^3\alpha_2^2v_1v_2v_4 - 4\alpha_1^2\alpha_2^3v_2v_3v_4 - \alpha_1\alpha_2^4v_1v_2v_3 - \alpha_1\alpha_2^4v_1v_2v_4 \\ &\quad +\alpha_1\alpha_2^4v_1v_3v_4 + \alpha_1\alpha_2^4v_2v_3v_4 + 2\alpha_1^3\alpha_2^2v_3 - 2\alpha_1^3\alpha_2^2v_4 + \alpha_1^3v_1v_2v_3 - \alpha_1^3v_1v_2v_4 - \alpha_1^3v_1v_3v_4 \\ &\quad +\alpha_1^3v_2v_3v_4 - 4\alpha_1^2\alpha_2^3v_1 - 4\alpha_1^2\alpha_2v_2v_3v_4 - \alpha_1\alpha_2^4v_1 - \alpha_1\alpha_2^4v_2 + \alpha_1\alpha_2^4v_3 + \alpha_1\alpha_2^4v_4 \\ &\quad -2\alpha_1\alpha_2^2v_1v_2v_3 - 2\alpha_1\alpha_2^2v_1v_2v_4 - \alpha_1^3v_1 + \alpha_1^3v_2 + \alpha_1^3v_3 - \alpha_1^3v_4 - 4\alpha_1^2\alpha_2v_1 + 2\alpha_1\alpha_2^2v_3 \end{aligned}$$

$$
\begin{aligned}
& +2\alpha_1\alpha_2^2 v_4 - \alpha_1 v_1 v_2 v_3 - \alpha_1 v_1 v_2 v_4 - \alpha_1 v_1 v_3 v_4 - \alpha_1 v_2 v_3 v_4 + \alpha_1 v_1 + \alpha_1 v_2 + \alpha_1 v_3 + \alpha_1 v_4, \\
y_0 \;=\; & -2a_1\alpha_1^4\alpha_2^2 v_1 v_2 v_3 v_4 + 4a_1\alpha_1^3\alpha_2^3 v_1 v_2 v_3 v_4 - 2a_1\alpha_1^2\alpha_2^4 v_1 v_2 v_3 v_4 - 2a_1\alpha_1^4\alpha_2^2 v_1 v_2 \\
& -2a_1\alpha_1^4\alpha_2^2 v_3 v_4 - 2a_1\alpha_1^2\alpha_2^4 v_1 v_4 - 2a_1\alpha_1^2\alpha_2^4 v_2 v_3 - 2a_1\alpha_1^4\alpha_2^2 - 4a_1\alpha_1^3\alpha_2^3 - 2a_1\alpha_1^2\alpha_2^4 \\
& -4a_1\alpha_1^2\alpha_2^2 v_1 v_2 - 4a_1\alpha_1^2\alpha_2^2 v_1 v_4 - 4a_1\alpha_1^2\alpha_2^2 v_2 v_3 - 4a_1\alpha_1^2\alpha_2^2 v_3 v_4 + 2a_1\alpha_1^2 v_1 v_2 v_3 v_4 \\
& -4a_1\alpha_1\alpha_2 v_1 v_2 v_3 v_4 + 2a_1\alpha_2^2 v_1 v_2 v_3 v_4 - 2a_1\alpha_1^2 v_1 v_4 - 2a_1\alpha_1^2 v_2 v_3 - 2a_1\alpha_2^2 v_1 v_2 - 2a_1\alpha_2^2 v_3 v_4 \\
& +2a_1\alpha_1^2 + 4a_1\alpha_1\alpha_2 + 2a_1\alpha_2^2, \\
y_1 \;=\; & -a_1\alpha_1^4\alpha_2^3 v_1 v_2 v_3 v_4 + a_1\alpha_1^3\alpha_2^4 v_1 v_2 v_3 v_4 - a_1\alpha_1^4\alpha_2^3 v_1 v_2 - a_1\alpha_1^4\alpha_2^3 v_3 v_4 + a_1\alpha_1^4\alpha_2 v_1 v_2 v_3 v_4 \\
& +a_1\alpha_1^3\alpha_2^4 v_1 v_4 - a_1\alpha_1^3\alpha_2^4 v_2 v_3 - 4a_1\alpha_1^3\alpha_2^2 v_1 v_2 v_3 v_4 + 4a_1\alpha_1^2\alpha_2^3 v_1 v_2 v_3 v_4 - a_1\alpha_1\alpha_2^4 v_1 v_2 v_3 v_4 \\
& -a_1\alpha_1^4\alpha_2^3 + a_1\alpha_1^4\alpha_2 v_1 v_2 + a_1\alpha_1^4\alpha_2 v_3 v_4 - a_1\alpha_1^3\alpha_2^4 + 2a_1\alpha_1^3\alpha_2^2 v_1 v_4 - 2a_1\alpha_1^3\alpha_2^2 v_2 v_3 \\
& -a_1\alpha_1^3 v_1 v_2 v_3 v_4 - 2a_1\alpha_1^2\alpha_2^3 v_1 v_2 - 2a_1\alpha_1^2\alpha_2^3 v_3 v_4 + 4a_1\alpha_1^2\alpha_2 v_1 v_2 v_3 v_4 - a_1\alpha_1\alpha_2^4 v_1 v_4 \\
& +a_1\alpha_1\alpha_2^4 v_2 v_3 - 4a_1\alpha_1\alpha_2^2 v_1 v_2 v_3 v_4 + a_1\alpha_2^3 v_1 v_2 v_3 v_4 + a_1\alpha_1^4\alpha_2 + 4a_1\alpha_1^3\alpha_2^2 + a_1\alpha_1^3 v_1 v_4 \\
& -a_1\alpha_1^3 v_2 v_3 + 4a_1\alpha_1^2\alpha_2^3 + 2a_1\alpha_1^2\alpha_2 v_1 v_2 + 2a_1\alpha_1^2\alpha_2 v_3 v_4 + a_1\alpha_1\alpha_2^4 - 2a_1\alpha_1\alpha_2^2 v_1 v_4 \\
& +2a_1\alpha_1\alpha_2^2 v_2 v_3 + a_1\alpha_1 v_1 v_2 v_3 v_4 - a_1\alpha_2^3 v_1 v_2 - a_1\alpha_2^3 v_3 v_4 - a_1\alpha_2 v_1 v_2 v_3 v_4 + a_1\alpha_1^3 + 4a_1\alpha_1^2\alpha_2 \\
& +4a_1\alpha_1\alpha_2^2 - a_1\alpha_1 v_1 v_4 + a_1\alpha_1 v_2 v_3 + a_1\alpha_2^3 + a_1\alpha_2 v_1 v_2 + a_1\alpha_2 v_3 v_4 - a_1\alpha_1 - a_1\alpha_2, \\
y_2 \;=\; & -a_1\alpha_1^4\alpha_2^3 v_1 v_3 v_4 + a_1\alpha_1^4\alpha_2^3 v_2 v_3 v_4 - a_1\alpha_1^3\alpha_2^4 v_1 v_2 v_3 - a_1\alpha_1^3\alpha_2^4 v_2 v_3 v_4 \\
& -a_1\alpha_1^4\alpha_2^3 v_1 + a_1\alpha_1^4\alpha_2^3 v_2 + a_1\alpha_1^4\alpha_2 v_1 v_3 v_4 - a_1\alpha_1^4\alpha_2 v_2 v_3 v_4 - a_1\alpha_1^3\alpha_2^4 v_1 \\
& -a_1\alpha_1^3\alpha_2^4 v_4 - 2a_1\alpha_1^3\alpha_2^2 v_1 v_2 v_3 + 4a_1\alpha_1^3\alpha_2^2 v_2 v_3 v_4 - 2a_1\alpha_1^2\alpha_2^3 v_1 v_3 v_4 \\
& -4a_1\alpha_1^2\alpha_2^3 v_2 v_3 v_4 + a_1\alpha_1\alpha_2^4 v_1 v_2 v_3 + a_1\alpha_1\alpha_2^4 v_2 v_3 v_4 + a_1\alpha_1^4\alpha_2 v_1 - a_1\alpha_1^4\alpha_2 v_2 \\
& +4a_1\alpha_1^3\alpha_2^2 v_1 - 2a_1\alpha_1^3\alpha_2^2 v_4 - a_1\alpha_1^3 v_1 v_2 v_3 + a_1\alpha_1^3 v_2 v_3 v_4 + 4a_1\alpha_1^2\alpha_2^3 v_1 \\
& +2a_1\alpha_1^2\alpha_2^3 v_2 + 2a_1\alpha_1^2\alpha_2 v_1 v_3 v_4 - 4a_1\alpha_1^2\alpha_2 v_2 v_3 v_4 + a_1\alpha_1\alpha_2^4 v_1 + a_1\alpha_1\alpha_2^4 v_4 \\
& +2a_1\alpha_1\alpha_2^2 v_1 v_2 v_3 + 4a_1\alpha_1\alpha_2^2 v_2 v_3 v_4 - a_1\alpha_2^3 v_1 v_3 v_4 - a_1\alpha_2^3 v_2 v_3 v_4 + a_1\alpha_1^3 v_1 \\
& -a_1\alpha_1^3 v_4 + 4a_1\alpha_1^2\alpha_2 v_1 - 2a_1\alpha_1^2\alpha_2 v_2 + 4a_1\alpha_1\alpha_2^2 v_1 + 2a_1\alpha_1\alpha_2^2 v_4 \\
& +a_1\alpha_1 v_1 v_2 v_3 - a_1\alpha_1 v_2 v_3 v_4 + a_1\alpha_2^3 v_1 + a_1\alpha_2^3 v_2 + a_1\alpha_2 v_1 v_3 v_4 \\
& +a_1\alpha_2 v_2 v_3 v_4 - a_1\alpha_1 v_1 + a_1\alpha_1 v_4 - a_1\alpha_2 v_1 - a_1\alpha_2 v_2, \\
y_3 \;=\; & -2a_1\alpha_1^4\alpha_2^2 v_1 v_3 v_4 + 2a_1\alpha_1^4\alpha_2^2 v_2 v_3 v_4 - 4a_1\alpha_1^3\alpha_2^3 v_2 v_3 v_4 - 2a_1\alpha_1^2\alpha_2^4 v_1 v_2 v_3 \\
& +2a_1\alpha_1^2\alpha_2^4 v_2 v_3 v_4 - 2a_1\alpha_1^4\alpha_2^2 v_1 + 2a_1\alpha_1^4\alpha_2^2 v_2 - 4a_1\alpha_1^3\alpha_2^3 v_1 - 2a_1\alpha_1^2\alpha_2^4 v_1 \\
& +2a_1\alpha_1^2\alpha_2^4 v_4 - 4a_1\alpha_1^2\alpha_2^2 v_1 v_2 v_3 - 4a_1\alpha_1^2\alpha_2^2 v_1 v_3 v_4 + 4a_1\alpha_1^2\alpha_2^2 v_2 + 4a_1\alpha_1^2\alpha_2^2 v_4 \\
& -2a_1\alpha_1^2 v_1 v_2 v_3 - 2a_1\alpha_1^2 v_2 v_3 v_4 + 4a_1\alpha_1\alpha_2 v_2 v_3 v_4 - 2a_1\alpha_2^2 v_1 v_3 v_4 \\
& -2a_1\alpha_2^2 v_2 v_3 v_4 + 2a_1\alpha_1^2 v_1 + 2a_1\alpha_1^2 v_4 + 4a_1\alpha_1\alpha_2 v_1 + 2a_1\alpha_2^2 v_1 + 2a_1\alpha_2^2 v_2.
\end{aligned}
$$

Again, to form a closed-loop chain it requires that the base and the fourth coordinate frames align. Hence, the Study array is equated to the identity array. As the Study coordinates are homogeneous, i.e., a point represented by these

coordinates remains unchanged if every entry is multiplied by the same factor, the system of equations which has to be solved consists of seven equations.

One method to eliminate the intermediate link angles is using Gröbner basis. A pure lexicographic ordering of $(x_1 > ... > x_n) \rightarrow (v_2 > v_3 > v_4 > v_1)$ reveals one polynomial that no longer contains v_2 and v_3

$$(v_4^2 + 1)(v_1^2 + 1)((\alpha_1 - \alpha_2)v_1v_4 - \alpha_1 - \alpha_2) = 0. \tag{6.160}$$

Since the expressions $(v_4^2 + 1)$ and $(v_1^2 + 1)$ can never be zero, we can safely divide Equation (6.160) by these two terms. This yields the IO equation for the Bennett linkage

$$(\alpha_1 - \alpha_2)v_1v_4 - \alpha_1 - \alpha_2 = 0, \tag{6.161}$$

where $\alpha_i = \tan(\tau_i/2)$ and $v_i = \tan(\theta_i/2)$. Equation (6.161) is identical to the IO relation of the Bennett linkage obtained in [79] after algebraisation with tangent half-angle substitutions.

6.11.2 The RSSR Spatial Mechanism

The RSSR mechanism has been investigated since 1955 [82], if not earlier. It has been broadly used in modern applications ranging from hinging to landing gear deployment systems so there has long been a need for design tools for synthesis and analysis. The earliest works considering mobility limits date from as early as 1969, see [83, 84, 85, 86]. Displacement and dynamic analysis of the RSSR dates from 1972, if not earlier [87, 88]. Optimal synthesis of RSSR linkages for various objectives can be traced to the early 1980s [89], but there is also modern interest, see [90] for example. Rigid body motion synthesis using Study's kinematic mapping [37] was elegantly developed for planar four-bar linkages in [91]. Motivated by this, a derivation algorithm that describes the linkage using Denavit Hartenberg (DH) parameters, projects the displacement transformation matrix into Study's kinematic image space, and manipulates the resulting equations via Gröbner bases to obtain the algebraic input-output (IO) equation for planar, spherical, and Bennett linkages has been investigated with results reported in the literature by the authors of this paper. A natural extension of this algorithm to general motion in three dimensional space is to apply it to another well-investigated spatial linkage, the RSSR, which will be the main focus of this paper. In addition, the results obtained using the polynomial elimination method [92] are supported by a numerical method [93] leading to an identical algebraic IO equation, as well as a verification of the equation using an animated example linkage that was created in the GeoGebra software.

It is important to note that we make no claims regarding the relative ease or difficulty of the method presented in this paper for deriving the RSSR algebraic IO equation compared to any existing method, we simply claim that it is different. However, to underscore the utility of this form of the algebraic RSSR IO equation as the cornerstone for development of powerful novel mechanical design tools for synthesis and analysis, three detailed example applications are presented: continuous approximate synthesis for function generation minimising the design and structural errors; mobility limits; and extreme values of angular velocity and acceleration.

The RSSR linkage consists of two revolute (R) and two spherical (S) joints and following the Kutzbach criterion, possesses 2 degrees of freedom (dof). However, one dof that does not influence the IO equation corresponds to the rotation of the coupler link between the two spherical joints about its own longitudinal axis. This so-called idle dof can have a positive effect on the durability of the linkage in engineering applications, as it helps to evenly wear the S joints. Generally, the IO equation of the RSSR is much more involved compared to the planar, and spherical ones, as in addition to the link lengths between the four joints, the linkage further possesses three additional design parameters between the revolute joints, i.e., two link offsets and a link twist. Previous trigonometric derivations of the RSSR IO equation are available, for example, in [50, 82, 94]. Hartenberg and Denavit's derivation of the IO equation [50] uses their well-known parameters and trigonometric relations, while the derivation in [94] leads to an equation that resembles a more complex version of the Freudenstein equation [31]. This is not entirely surprising given that the planar four-bar is a special case of the RSSR linkage.

6.11.2.1 Denavit-Hartenberg (DH) Parametrisation

Each of the two S joints of the RSSR can be modelled as three R joints whose rotation axes are mutually orthogonal and intersect at the sphere centre. Hence, eight coordinate frames are attached to the linkage. The chosen coordinate systems are illustrated in Figure 6.34 and the corresponding DH parameters are to be found in Table 6.1. Note that the only link twist that is a design parameter is τ_8. The twists between the three mutually orthogonal R joint axes comprising the S joints are $\pm\pi$. We arbitrarily use the positive value, as the sign has no impact on the resulting algebraic IO equation.

In the remainder of this paper, the tangent half angle substitutions for the angle parameters $v_i = \tan(\theta_i/2)$ and $\alpha_i = \tan(\tau_i/2)$ will be used in order to

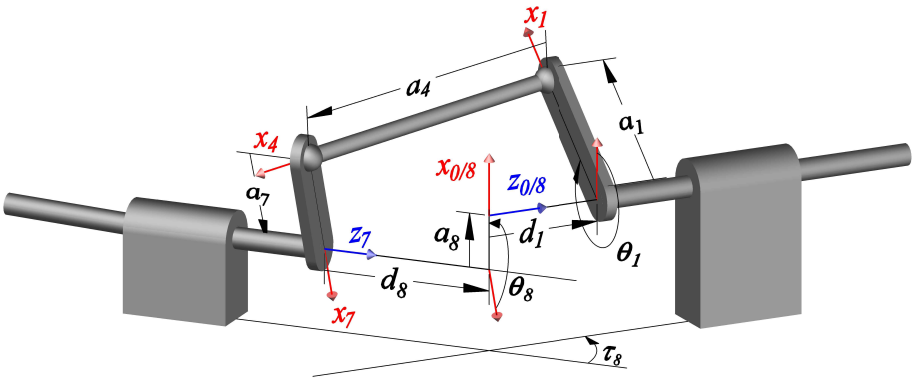

Figure 6.34: An arbitrary RSSR mechanism.

algebraise the transformations. This implies that

$$\cos\theta_i = \frac{1-v_i^2}{1+v_i^2}, \quad \sin\theta_i = \frac{2v_i}{1+v_i^2}, \tag{6.162}$$

$$\cos\tau_i = \frac{1-\alpha_i^2}{1+\alpha_i^2}, \quad \sin\tau_i = \frac{2\alpha_i}{1+\alpha_i^2}. \tag{6.163}$$

We begin with a serial RSSR kinematic chain and determine the forward kinematics following [44]. The required multiplication of the individual DH transformation matrices from one coordinate frame to another yields the overall homogeneous transformation matrix that describes the relationship between the first and last coordinate frames. To close the kinematic chain, we want the first and last coordinate systems to align in both their orientation and origin. Algebraically, this is specified using the kinematic closure equation, where the overall transformation equates to the identity [44]

$$\prod_{i=1}^{8} {}_i^{i-1}\mathbf{T} = \mathbf{I}. \tag{6.164}$$

The elements of this algebraic DH transformation matrix are then directly mapped into Study's kinematic image space where the constraint manifold could be analysed as it has already been successfully demonstrated for the planar 4R, spherical 4R, and Bennett linkage by the authors. However, applying Gröbner bases or other elimination methods to the eight Study soma coordinates to symbolically obtain the IO equation for the RSSR linkage is computationally too demanding for an algebraic geometry approach. While very computationally

Table 6.1: DH parameters for the RSSR mechanism.

joint axis i	joint angle θ_i	link offset d_i	link length a_i	link twist τ_i
1	θ_1	d_1	a_1	0
2	θ_2	0	0	$\pi/2$
3	θ_3	0	0	$\pi/2$
4	θ_4	0	a_4	0
5	θ_5	0	0	$\pi/2$
6	θ_6	0	0	$\pi/2$
7	θ_7	0	a_7	0
8	θ_8	d_8	a_8	τ_8

demanding, a numerical approach that uses the forward kinematics of the serial RSSR chain mapped to the eight soma coordinates, described in Section 6.11.2.3, using pseudowitness sets leads directly to the desired IO equation. Still, there are algebraic approaches.

A well known algebraic geometry approach to obtain an expression for the forward and inverse kinematics of a serial kinematic chain is to split it into two subchains, thereby conceptually splitting the closure equation in two by multiplying both sides by the inverses of half of the DH transformations. In the case of the RSSR, the closure equation becomes

$$ {}^{0}_{1}\mathbf{T}\ {}^{1}_{2}\mathbf{T}\ {}^{2}_{3}\mathbf{T}\ {}^{3}_{4}\mathbf{T} = \mathbf{I}\ {}^{7}_{8}\mathbf{T}^{-1}\ {}^{6}_{7}\mathbf{T}^{-1}\ {}^{5}_{6}\mathbf{T}^{-1}\ {}^{4}_{5}\mathbf{T}^{-1}. \tag{6.165} $$

This step essentially divides the linkage into two serial chains joined at the 4th coordinate frame located in the second S joint, i.e., one serial chain between the coordinate frames 0 and 4, and one serial chain between the coordinate frames 4 and 8, which correspond to the expressions on the left and right sides of Equation (6.165), respectively, which we call the left RS and right RS dyads. Equation (6.165) will be used in Section 6.11.2.2 to obtain the algebraic IO equation by projecting it to the image space.

The image of the overall DH transformation matrix $\mathbf{T}$ of the RSSR linkage, Equation (6.164), in terms of Study parameters yields

$$
\begin{aligned}
x_0 &= 2v_1v_2v_3v_4v_5v_6v_7v_8 - 2v_1v_2v_3v_4v_5v_6 + ... + 2\alpha_8v_6v_8 + 2v_7v_8 - 2,\\
x_1 &= 2\alpha_8v_1v_2v_3v_4v_5v_6v_7v_8 - 2\alpha_8v_1v_2v_3v_4v_5v_6 + ... + 2\alpha_8v_7v_8 - 2\alpha_8,\\
x_2 &= -2\alpha_8v_1v_2v_3v_4v_5v_6v_7 - 2\alpha_8v_1v_2v_3v_4v_5v_6v_8 + ... - 2\alpha_8v_7 - 2\alpha_8v_8,
\end{aligned}
$$

$$
\begin{aligned}
x_3 =& -2v_1v_2v_3v_4v_5v_6v_7 - 2v_1v_2v_3v_4v_5v_6v_8 + ... + 2\alpha_8v_6 - 2v_7 - 2v_8, \quad (6.166)\\
y_0 =& -a_1\alpha_8v_1v_2v_3v_4v_5v_6v_7v_8 + a_4\alpha_8v_1v_2v_3v_4v_5v_6v_7v_8 + ... - \alpha_8a_8,\\
y_1 =& \, a_1v_1v_2v_3v_4v_5v_6v_7v_8 - a_4v_1v_2v_3v_4v_5v_6v_7v_8 + ... + a_1 + a_4 + a_7 + a_8,\\
y_2 =& -\alpha_8d_1v_1v_2v_3v_4v_5v_6v_7v_8 - \alpha_8d_8v_1v_2v_3v_4v_5v_6v_7v_8 + ... + \alpha_8d_8,\\
y_3 =& -d_1\alpha_8v_1v_2v_3v_4v_5v_6v_7v_8 - d_8v_1v_2v_3v_4v_5v_6v_7v_8 + ... + d_1 + d_8.
\end{aligned}
$$

As these polynomials are extremely large, each containing 128 very large terms, only the beginning and end of the expressions sorted using graded lexicographic ordering with $v_1 > v_2 > \ldots > v_8$ are displayed here. These polynomials will be solved numerically in Section 6.11.2.3, but are otherwise too cumbersome to deal with using algebraic geometry and computer algebra software, such as Maple 2021. For this we require a different approach.

As mentioned earlier, one well known different approach involves conceptually splitting the RSSR into two serial RS chains. In this way, mapping the left hand side of Equation (6.165), the left RS chain, into Study's kinematic image space yields eight significantly smaller polynomials

$$
\begin{aligned}
x_0 =& \, 4v_1v_2v_3v_4 - 4v_1v_3 - 4v_2v_3 - 4v_3v_4,\\
x_1 =& -4v_1v_2 + 4v_1v_4 + 4v_2v_4 + 4,\\
x_2 =& \, 4v_1v_2v_4 + 4v_1 + 4v_2 - 4v_4,\\
x_3 =& -4v_1v_2v_3 - 4v_1v_3v_4 - 4v_2v_3v_4 + 4v_3, \quad (6.167)\\
y_0 =& -2d_1v_1v_2v_3 - 2d_1v_1v_3v_4 - 2d_1v_2v_3v_4 + 2a_1v_1v_2 - 2a_4v_1v_2 - 2a_1v_1v_4\\
&+ 2a_4v_1v_4 + 2a_1v_2v_4 + 2a_4v_2v_4 + 2d_1v_3 + 2a_1 + 2a_4,\\
y_1 =& \, 2a_1v_1v_2v_3v_4 - 2a_4v_1v_2v_3v_4 + 2d_1v_1v_2v_4 - 2a_1v_1v_3 + 2a_4v_1v_3 + 2a_1v_2v_3\\
&+ 2a_4v_2v_3 + 2a_1v_3v_4 + 2a_4v_3v_4 + 2d_1v_1 + 2d_1v_2 - 2d_1v_4,\\
y_2 =& \, 2a_1v_1v_2v_3 + 2a_4v_1v_2v_3 + 2a_1v_1v_3v_4 + 2a_4v_1v_3v_4 - 2a_1v_2v_3v_4 + 2a_4v_2v_3v_4\\
&+ 2d_1v_1v_2 - 2d_1v_1v_4 - 2d_1v_2v_4 + 2a_1v_3 - 2a_4v_3 - 2d_1,\\
y_3 =& -2d_1v_1v_2v_3v_4 + 2a_1v_1v_2v_4 + 2a_4v_1v_2v_4 + 2d_1v_1v_3 + 2d_1v_2v_3 + 2d_1v_3v_4\\
&+ 2a_1v_1 + 2a_4v_1 - 2a_1v_2 + 2a_4v_2 + 2a_1v_4 - 2a_4v_4.
\end{aligned}
$$

And finally, mapping the right hand side of Equation (6.165), the right RS chain, into Study's kinematic image space yields eight additional smaller polynomials

$$
\begin{aligned}
x_0 =& \, 4v_5v_6v_7v_8 - 4v_5v_6 - 4\alpha_8v_5v_7 - 4\alpha_8v_5v_8 - 4v_6v_7 - 4v_6v_8 + 4\alpha_8v_7v_8 - 4\alpha_8,\\
x_1 =& -4\alpha_8v_5v_6v_7v_8 + 4\alpha_8v_5v_6 - 4v_5v_7 - 4v_5v_8 + 4\alpha_8v_6v_7 + 4\alpha_8v_6v_8 + 4v_7v_8 - 4,\\
x_2 =& \, 4\alpha_8v_5v_6v_7 + 4\alpha_8v_5v_6v_8 + 4v_5v_7v_8 + 4\alpha_8v_6v_7v_8 - 4v_5 - 4\alpha_8v_6 + 4v_7 + 4v_8,
\end{aligned}
$$

$$
\begin{aligned}
x_3 =& 4v_5v_6v_7 + 4v_5v_6v_8 - 4\alpha_8v_5v_7v_8 + 4v_6v_7v_8 + 4\alpha_8v_5 - 4v_6 - 4\alpha_8v_7 - 4\alpha_8v_8,\\
y_0 =& -2a_7\alpha_8v_5v_6v_7v_8 + 2a_8\alpha_8v_5v_6v_7v_8 - 2d_8v_5v_6v_7 - 2d_8v_5v_6v_8 - 2\alpha_8d_8v_5v_7v_8\\
&- 2d_8v_6v_7v_8 - 2a_7\alpha_8v_5v_6 - 2a_8\alpha_8v_5v_6 + 2a_7v_5v_7 + 2a_8v_5v_7 - 2a_7v_5v_8\\
&+ 2a_8v_5v_8 - 2a_7\alpha_8v_6v_7 - 2a_8\alpha_8v_6v_7 + 2a_7\alpha_8v_6v_8 - 2a_8\alpha_8v_6v_8 + 2a_7v_7v_8\\
&- 2a_8v_7v_8 + 2\alpha_8d_8v_5 + 2d_8v_6 - 2\alpha_8d_8v_7 - 2\alpha_8d_8v_8 + 2a_7 + 2a_8, \quad (6.168)\\
y_1 =& -2a_7v_5v_6v_7v_8 + 2a_8v_5v_6v_7v_8 + 2\alpha_8d_8v_5v_6v_7 + 2\alpha_8d_8v_5v_6v_8 - 2d_8v_5v_7v_8\\
&+ 2\alpha_8d_8v_6v_7v_8 - 2a_7v_5v_6 - 2a_8v_5v_6 - 2a_7\alpha_8v_5v_7 - 2a_8\alpha_8v_5v_7 + 2a_7\alpha_8v_5v_8\\
&- 2a_8\alpha_8v_5v_8 - 2a_7v_6v_7 - 2a_8v_6v_7 + 2a_7v_6v_8 - 2a_8v_6v_8 - 2a_7\alpha_8v_7v_8\\
&+ 2a_8\alpha_8v_7v_8 + 2d_8v_5 - 2\alpha_8d_8v_6 - 2d_8v_7 - 2d_8v_8 - 2a_7\alpha_8 - 2a_8\alpha_8,\\
y_2 =& 2\alpha_8d_8v_5v_6v_7v_8 - 2a_7v_5v_6v_7 - 2a_8v_5v_6v_7 + 2a_7v_5v_6v_8 - 2a_8v_5v_6v_8\\
&- 2a_7\alpha_8v_5v_7v_8 + 2a_8\alpha_8v_5v_7v_8 + 2a_7v_6v_7v_8 - 2a_8v_6v_7v_8 - 2\alpha_8d_8v_5v_6\\
&- 2d_8v_5v_7 - 2d_8v_5v_8 - 2\alpha_8d_8v_6v_7 - 2\alpha_8d_8v_6v_8 + 2d_8v_7v_8 - 2a_7\alpha_8v_5\\
&- 2a_8\alpha_8v_5 + 2a_7v_6 + 2a_8v_6 + 2a_7\alpha_8v_7 + 2a_8\alpha_8v_7 - 2a_7\alpha_8v_8 + 2a_8\alpha_8v_8 - 2d_8,\\
y_3 =& 2d_8v_5v_6v_7v_8 + 2a_7\alpha_8v_5v_6v_7 + 2a_8\alpha_8v_5v_6v_7 - 2a_7\alpha_8v_5v_6v_8 + 2a_8\alpha_8v_5v_6v_8\\
&- 2a_7v_5v_7v_8 + 2a_8v_5v_7v_8 - 2a_7\alpha_8v_6v_7v_8 + 2a_8\alpha_8v_6v_7v_8 - 2d_8v_5v_6\\
&+ 2\alpha_8d_8v_5v_7 + 2\alpha_8d_8v_5v_8 - 2d_8v_6v_7 - 2d_8v_6v_8 - 2\alpha_8d_8v_7v_8 - 2a_7v_5 - 2a_8v_5\\
&- 2a_7\alpha_8v_6 - 2a_8\alpha_8v_6 + 2a_7v_7 + 2a_8v_7 - 2a_7v_8 + 2a_8v_8 + 2\alpha_8d_8.
\end{aligned}
$$

The polynomials of Equations (6.167) and (6.168) will be manipulated in Section 6.11.2.2 using the linear implicitisation algorithm [92] to reveal the algebraic RSSR IO equation.

6.11.2.2 Algebraic Geometry Approach

To obtain the RSSR algebraic IO equation, the parametric equations of the Study coordinates of Equations (6.167) and (6.168) need to be expressed implicitly as a single polynomial equation in the desired motion parameters v_1 and v_8 in the seven-dimensional kinematic mapping image space. This requires an algorithm that eliminates the unwanted motion parameters v_i where $i \in \{2, \ldots, 7\}$. One implicitisation algorithm that allows for the transformation from the explicit parametric Study representation into a set of implicit polynomial equations is known as the linear implicitisation algorithm. The resulting constraint equations are implicit polynomials that form an algebraic variety in $\mathbb{P}^7$ and can be manipulated with different tools to obtain the IO equation. A detailed description of the linear implicitisation algorithm, together with illustrative examples is to be found in [92, 95].

The two serial RS chains of the RSSR linkage consist of one revolute and one spherical joint each. Clearly, the S joint spherical displacements, $SO(3)$, are completely contained on sub-spaces of the Study quadric as there is no translation involved and thus, all four y_i Study coordinates are identically zero. In other words, the displacements constrained by the S joints form special A-planes on the Study quadric. Further, the R joint in the serial RS chain rotates the S joint in a planar displacement thereby moving this special A-plane on S_6^2. It is well known that a 3-space can be represented by the intersection of four hyperplanes in the kinematic image space. To determine the RSSR algebraic IO equation we must identify these hyperplanes, one set for each serial RS chain. To obtain their implicit equations the linear implicitisation algorithm will be employed. The main goal of the linear implicitisation algorithm is to find the minimal number of implicit equations that describe the mechanical constraints in the image space. It allows for the elimination of motion parameters which, in the case of the RSSR, correspond to the variables $v_2, v_3, \ldots, v_7$. On the other hand, the design parameters a_i, d_i and α_i are fixed values that depend on the chosen linkage. However, to obtain the implicit polynomials for the spherical special 3-spaces v_1 and v_8 are temporarily also considered as design parameter constants.

To begin, we assume that the resulting variety is defined by linear constraint equations, and hence a general linear ansatz polynomial can be written, using the graded reverse lexicographic monomial ordering [96], as

$$C_1 y_3 + C_2 y_2 + C_3 y_1 + C_4 y_0 + C_5 x_3 + C_6 x_2 + C_7 x_1 + C_8 x_0 = 0. \qquad (6.169)$$

This linear ansatz polynomial has eight unknown coefficients C_i, $i \in \{1, \cdots, 8\}$. In the case of the left hand side of the RSSR chain, Equation (6.167) is substituted into Equation (6.169) and after reorganising such that the variable angle parameters of the spherical displacement are collected, yields

$$
\begin{aligned}
&(-2C_1d_1v_1 + 2C_3a_1v_1 - 2C_3a_4v_1 + 4C_8v_1 - 2C_4d_1 - 2C_2a_1 + 2C_2a_4 - 4C_5)v_2v_3v_4 \\
&+ (2C_2a_1v_1 + 2C_2a_4v_1 - 2C_4d_1v_1 - 4C_5v_1 + 2C_1d_1 + 2C_3a_1 + 2C_3a_4 - 4C_8)v_2v_3 \\
&+ (2C_1a_1v_1 + 2C_1a_4v_1 + 2C_3d_1v_1 + 4C_6v_1 - 2C_2d_1 + 2C_4a_1 + 2C_4a_4 + 4C_7)v_2v_4 \\
&+ (2C_2d_1v_1 + 2C_4a_1v_1 - 2C_4a_4v_1 - 4C_7v_1 - 2C_1a_1 + 2C_1a_4 + 2C_3d_1 + 4C_6)v_2 \\
&+ (2C_2a_1v_1 + 2C_2a_4v_1 - 2C_4d_1v_1 - 4C_5v_1 + 2C_1d_1 + 2C_3a_1 + 2C_3a_4 - 4C_8)v_3v_4 \\
&+ (2C_1d_1v_1 - 2C_3a_1v_1 + 2C_3a_4v_1 - 4C_8v_1 + 2C_2a_1 - 2C_2a_4 + 2C_4d_1 + 4C_5)v_3 \\
&+ (-2C_2d_1v_1 - 2C_4a_1v_1 + 2C_4a_4v_1 + 4C_7v_1 + 2C_1a_1 - 2C_1a_4 - 2C_3d_1 - 4C_6)v_4 \\
&+ (2C_1a_1v_1 + 2C_1a_4v_1 + 2C_3d_1v_1 + 4C_6v_1 - 2C_2d_1 + 2C_4a_1 + 2C_4a_4 + 4C_7) = 0.
\end{aligned} \tag{6.170}
$$

To fulfil this equation, the coefficients of the variables in Equation (6.170) must vanish since the v_2, v_3, and v_4 orientation angle parameters are, in general non-zero. In matrix form, this can be expressed as

$$
\begin{bmatrix}
2a_1v_1 + 2a_4v_1 & -2d_1 & 2d_1v_1 & 2a_1 + 2a_4 & 0 & 4v_1 & 4 & 0 \\
-2d_1v_1 & -2a_1 + 2a_4 & 2a_1v_1 - 2a_4v_1 & -2d_1 & -4 & 0 & 0 & 4v_1 \\
-2a_1 + 2a_4 & 2d_1v_1 & 2d_1 & 2a_1v_1 - 2a_4v_1 & 0 & 4 & -4v_1 & 0 \\
2a_1v_1 + 2a_4v_1 & -2d_1 & 2d_1v_1 & 2a_1 + 2a_4 & 0 & 4v_1 & 4 & 0 \\
2d_1 & 2a_1v_1 + 2a_4v_1 & 2a_1 + 2a_4 & -2d_1v_1 & -4v_1 & 0 & 0 & -4 \\
2d_1 & 2a_1v_1 + 2a_4v_1 & 2a_1 + 2a_4 & -2d_1v_1 & -4v_1 & 0 & 0 & -4 \\
2d_1v_1 & 2a_1 - 2a_4 & -2a_1v_1 + 2a_4v_1 & 2d_1 & 4 & 0 & 0 & -4v_1 \\
2a_1 - 2a_4 & -2d_1v_1 & -2d_1 & -2a_1v_1 + 2a_4v_1 & 0 & -4 & 4v_1 & 0
\end{bmatrix}
\begin{bmatrix} C_1 \\ C_2 \\ C_3 \\ C_4 \\ C_5 \\ C_6 \\ C_7 \\ C_8 \end{bmatrix}
=
\begin{bmatrix} 0 \\ 0 \\ 0 \\ 0 \\ 0 \\ 0 \\ 0 \\ 0 \end{bmatrix}.
$$

Solving for the unknown C_i and back-substituting their solutions into the general linear ansatz polynomial Equation (6.169) reveals all four hyperplanes that satisfy the variety in $\mathbb{P}^7$. The solution shows that C_1, C_3, C_4, and C_8 are all free parameters with arbitrary values while C_2, C_5, C_6, and C_7 are expressions containing only v_1 and the design parameters and, after simplifying, are each linear in four of the Study parameters, and therefore hyperplanes. These four hyperplanes collected in terms of the Study parameters are

$$
\begin{aligned}
0 &= (a_1^2v_1^2 - a_4^2v_1^2 + d_1^2v_1^2 + a_1^2 - a_4^2 + d_1^2)x_3 + (-2d_1v_1^2 - 2d_1)y_0 \\
&\quad + 4a_1v_1y_1 + (2a_1v_1^2 - 2a_4v_1^2 - 2a_1 - 2a_4)y_2, && (6.171) \\
0 &= (a_1^2v_1^2 - a_4^2v_1^2 + d_1^2v_1^2 + a_1^2 - a_4^2 + d_1^2)x_2 - 4a_1v_1y_0 + (-2d_1v_1^2 - 2d_1)y_1 \\
&\quad + (-2a_1v_1^2 + 2a_4v_1^2 + 2a_1 + 2a_4)y_3, && (6.172) \\
0 &= (a_1^2v_1^2 - a_4^2v_1^2 + d_1^2v_1^2 + a_1^2 - a_4^2 + d_1^2)x_1 + (2a_1v_1^2 + 2a_4v_1^2 - 2a_1 + 2a_4)y_0 \\
&\quad + (2d_1v_1^2 + 2d_1)y_2 - 4a_1v_1y_3, && (6.173) \\
0 &= (a_1^2v_1^2 - a_4^2v_1^2 + d_1^2v_1^2 + a_1^2 - a_4^2 + d_1^2)x_0 + (-2a_1v_1^2 - 2a_4v_1^2 + 2a_1 - 2a_4)y_1
\end{aligned}
$$

$$+ 4a_1v_1y_2 + (2d_1v_1^2 + 2d_1)y_3. \tag{6.174}$$

The same procedure can be done with the right hand side of the RSSR by substituting Equation (6.168) in the general linear ansatz polynomial, Equation (6.169). In this case, the motion parameters to be eliminated are v_5, v_6 and v_7. Solving the resulting homogeneous matrix equation for the new unknown C_i yields the following four hyperplanes in a similar way. They are

$$\begin{aligned}0 = {} & (a_7^2\alpha_8^2v_8^2 - 2a_7a_8\alpha_8^2v_8^2 + a_8^2\alpha_8^2v_8^2 + \alpha_8^2d_8^2v_8^2 + a_7^2v_8^2 - 2a_8a_7v_8^2 \\ & + a_8^2v_8^2 + d_8^2v_8^2 + \alpha_8^2a_7^2 + 2a_7a_8\alpha_8^2 + a_8^2\alpha_8^2 + \alpha_8^2d_8^2 + a_7^2 + 2a_7a_8 + a_8^2 + d_8^2)x_3 \\ & + (-2\alpha_8^2d_8v_8^2 + 2d_8v_8^2 + 8a_7\alpha_8v_8 - 2\alpha_8^2d_8 + 2d_8)y_0 \\ & + (-4d_8\alpha_8v_8^2 - 4\alpha_8^2a_7v_8 + 4a_7v_8 - 4d_8\alpha_8)y_1 \\ & + (-2a_7\alpha_8^2v_8^2 + 2\alpha_8^2a_8v_8^2 - 2a_7v_8^2 + 2a_8v_8^2 + 2a_7\alpha_8^2 + 2\alpha_8^2a_8 + 2a_7 + 2a_8)y_2,\end{aligned} \tag{6.175}$$

$$\begin{aligned}0 = {} & (a_7^2\alpha_8^2v_8^2 - 2a_7a_8\alpha_8^2v_8^2 + a_8^2\alpha_8^2v_8^2 + \alpha_8^2d_8^2v_8^2 + a_7^2v_8^2 - 2a_8a_7v_8^2 \\ & + a_8^2v_8^2 + d_8^2v_8^2 + \alpha_8^2a_7^2 + 2a_7a_8\alpha_8^2 + a_8^2\alpha_8^2 + \alpha_8^2d_8^2 + a_7^2 + 2a_7a_8 + a_8^2 + d_8^2)x_2 \\ & + (4d_8\alpha_8v_8^2 + 4\alpha_8^2a_7v_8 - 4a_7v_8 + 4d_8\alpha_8)y_0 \\ & + (-2\alpha_8^2d_8v_8^2 + 2d_8v_8^2 + 8a_7\alpha_8v_8 - 2\alpha_8^2d_8 + 2d_8)y_1 \\ & + (2a_7\alpha_8^2v_8^2 - 2\alpha_8^2a_8v_8^2 + 2a_7v_8^2 - 2a_8v_8^2 - 2a_7\alpha_8^2 - 2\alpha_8^2a_8 - 2a_7 - 2a_8)y_3,\end{aligned} \tag{6.176}$$

$$\begin{aligned}0 = {} & (a_7^2\alpha_8^2v_8^2 - 2a_7a_8\alpha_8^2v_8^2 + a_8^2\alpha_8^2v_8^2 + \alpha_8^2d_8^2v_8^2 + a_7^2v_8^2 - 2a_8a_7v_8^2 \\ & + a_8^2v_8^2 + d_8^2v_8^2 + \alpha_8^2a_7^2 + 2a_7a_8\alpha_8^2 + a_8^2\alpha_8^2 + \alpha_8^2d_8^2 + a_7^2 + 2a_7a_8 + a_8^2 + d_8^2)x_1 \\ & + (-2a_7\alpha_8^2v_8^2 + 2\alpha_8^2a_8v_8^2 - 2a_7v_8^2 + 2a_8v_8^2 + 2a_7\alpha_8^2 + 2\alpha_8^2a_8 + 2a_7 + 2a_8)y_0 \\ & + (2\alpha_8^2d_8v_8^2 - 2d_8v_8^2 - 8a_7\alpha_8v_8 + 2\alpha_8^2d_8 - 2d_8)y_2 \\ & + (4d_8\alpha_8v_8^2 + 4\alpha_8^2a_7v_8 - 4a_7v_8 + 4d_8\alpha_8)y_3,\end{aligned} \tag{6.177}$$

$$\begin{aligned}0 = {} & (a_7^2\alpha_8^2v_8^2 - 2a_7a_8\alpha_8^2v_8^2 + a_8^2\alpha_8^2v_8^2 + \alpha_8^2d_8^2v_8^2 + a_7^2v_8^2 - 2a_8a_7v_8^2 \\ & + a_8^2v_8^2 + d_8^2v_8^2 + \alpha_8^2a_7^2 + 2a_7a_8\alpha_8^2 + a_8^2\alpha_8^2 + \alpha_8^2d_8^2 + a_7^2 + 2a_7a_8 + a_8^2 + d_8^2)x_0 \\ & + (2a_7\alpha_8^2v_8^2 - 2\alpha_8^2a_8v_8^2 + 2a_7v_8^2 - 2a_8v_8^2 - 2a_7\alpha_8^2 - 2\alpha_8^2a_8 - 2a_7 - 2a_8)y_1 \\ & + (-4d_8\alpha_8v_8^2 - 4\alpha_8^2a_7v_8 + 4a_7v_8 - 4d_8\alpha_8)y_2 \\ & + (2\alpha_8^2d_8v_8^2 - 2d_8v_8^2 - 8a_7\alpha_8v_8 + 2\alpha_8^2d_8 - 2d_8)y_3.\end{aligned} \tag{6.178}$$

Solving Equations (6.171), ..., (6.174) for the four y_i and substituting these expressions into Equations (6.175), ..., (6.178) leaves four equations in the four unknown Study parameters x_i. This suggests solving the system of four equations for the four unknown x_i. However, doing so leads only to the trivial

solution $x_i = y_i = 0$, $i \in \{0, 1, 2, 3\}$, which we call the null point. This result can be explained geometrically in $\mathbb{P}^7$ as follows: the two special 3-spaces representing the displacements of the S joints are two $SO(3)$ A-planes that are moved around on S_6^2 under the action of the two R joints, and only ever intersect in the null point.

But, there is a solution. Further inspection of the four equations shows that the equations form a homogeneous system of linear equations. Expressing this linear homogeneous system in matrix-vector form $\mathbf{Cx} = \mathbf{0}$, we know that this system only has a nontrivial solution when the determinant of the 4×4 coefficient matrix $\mathbf{C}$ with respect to the x_i vanishes [97]. Thus, after computing the determinant and omitting the factors that can never vanish, the general algebraic IO equation of the RSSR linkage arises directly from the determinant as

$$\begin{aligned} &Av_1^2v_8^2 + 8d_1\alpha_8a_7v_1^2v_8 + 8d_8\alpha_8a_1v_1v_8^2 + Bv_1^2 \\ &+8a_1a_7(\alpha_8 - 1)(\alpha_8 + 1)v_1v_8 + Cv_8^2 + 8d_8\alpha_8a_1v_1 + 8d_1\alpha_8a_7v_8 + D = 0, \end{aligned} \tag{6.179}$$

where

$$\begin{aligned} A &= (\alpha_8^2 + 1)A_1A_2 + R, \\ B &= (\alpha_8^2 + 1)B_1B_2 + R, \\ C &= (\alpha_8^2 + 1)C_1C_2 + R, \\ D &= (\alpha_8^2 + 1)D_1D_2 + R, \end{aligned}$$

and

$$\begin{aligned} A_1 &= (a_1 - a_4 + a_7 - a_8), & A_2 &= (a_1 + a_4 + a_7 - a_8), \\ B_1 &= (a_1 + a_4 - a_7 - a_8), & B_2 &= (a_1 - a_4 - a_7 - a_8), \\ C_1 &= (a_1 - a_4 - a_7 + a_8), & C_2 &= (a_1 + a_4 - a_7 + a_8), \\ D_1 &= (a_1 + a_4 + a_7 + a_8), & D_2 &= (a_1 - a_4 + a_7 + a_8), \end{aligned}$$

with

$$R = (d_1 - d_8)^2\alpha_8^2 + (d_1 + d_8)^2.$$

Equation (6.179) is an implicit biquadratic algebraic curve of degree 4 in the joint angle parameters v_1 and v_8, as one would expect.

6.11.2.3 Numerical Approach

The degree four algebraic IO equation for the RSSR expressed as Equation (6.179) will be compared to the result from a concomitant numerical method. The aim

for the numerical method is to compute an eliminant with the general approach of numerical elimination theory [98, Ch. 16]. This involves performing computations using the given polynomial system from Equation (6.166) and geometrically projecting points via pseudowitness sets [99]. For this problem, the pseudowitness set provided that the degree of the eliminant is 8 in 9 variables $(v_1, v_8, \alpha_8, a_1, a_4, a_7, a_8, d_1, d_8)$. Since there are a total of $\binom{9+8}{8} = 24310$ monomials of degree at most 8 in 9 variables, the approach is to use the pseudowitness set to generate at least 24310 sample points and then to use interpolation to recover the eliminant [100, Ch. 6]. To gather these sample points, one randomly fixes values of the parameters $\alpha_8, a_1, a_4, a_7, a_8, d_1, d_8$, and solves for the angle parameter values, v_1 and v_8 using any of a variety of sampling methods within numerical algebraic geometry [101, Sec. 2.3]. This yields precisely the same IO equation as the linear implicitisation approach, Equation (6.179).

6.11.2.4 Geometric Verification

To verify both the algebraic and numerical results, the IO equation of an arbitrary linkage was animated in GeoGebra. The model enabled measurement of the output angle for any given input angle. Tracing the locus of each input-output pair results in a curve which is compared with the herein derived IO equation, Equation (6.179). The chosen design parameters for the example linkage are $a_1 = 3$, $a_4 = 5$, $a_7 = 9$, $a_8 = 11$, $d_1 = 1$, $d_8 = 3$, and $\tau_8 = 60°$. While the

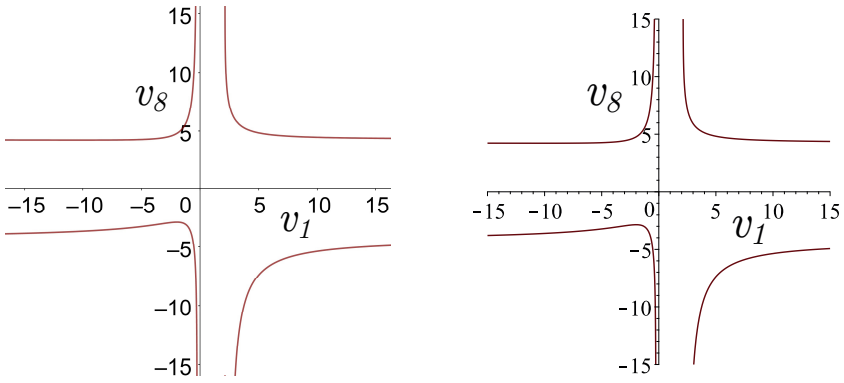

(a) IO equation generated in GeoGebra. (b) Derived according to Equation (6.179).

Figure 6.35: Example RSSR function generator with $a_1 = 3$, $a_4 = 5$, $a_7 = 9$, $a_8 = 11$, $d_1 = 1$, $d_8 = 3$, and $\tau_8 = 60°$.

result of the GeoGebra file is displayed in Figure 6.35a, substituting the same design parameters into Equation (6.179) yields the curve in Figure 6.35b. As can

be seen, the curves are congruent which further suggests that Equation (6.179) is indeed correct.

6.11.3 Applications

To demonstrate how the form of the algebraic IO equation for the RSSR linkage that has been obtained by the methods outlined in this paper is particularly useful for mechanical design by way of synthesis and analysis of RSSR mechanisms, several applications will be summarised and illustrated with examples. While it must be acknowledged that the IO equation itself is not new, see the 1955 book by J.S. Beggs for example [82], the algebraic form leads to computationally efficient and mathematically elegant tools for synthesis and analysis of RSSR linkages that are entirely new, and will be reported for the first time in what follows.

6.11.3.1 Mobility Limits

With the algebraic IO equation, it is a very simple matter to determine general conditions for the relative mobility of the two ground fixed links. Treating the v_1-v_8 IO pair to be coordinate axes in the plane spanned by the two, then the IO equation contains two double points at infinity on the v_1 and v_8 axes. The double points at infinity belonging to each of the coordinate axes together with the ability of links a_1 and a_7 to reach $v_1 = 0$ and $v_8 = 0$ completely define the mobility limits, if they exist, between the v_1-v_8 angle parameter pair. The examination of this is sufficient to determine whether a particular joint enables a crank, a rocker, a π-rocker, or a 0-rocker link motion. See [85] from 1971 for the first double point analysis of the RSSR, but only for a simplified special case, where mobility criteria, though incomplete, are reported.

We proceed by evaluating whether each double point has a pair of real, or complex conjugate tangents. If the double point has two real distinct tangents, it is a crunode; if it has two real coincident tangents, it is a cusp; and if the tangents are both complex conjugates, the double point is an acnode. Thus, after homogenising the v_1-v_8 IO equation using the homogenising coordinate v_0, leading to IO_h, the discriminant in Equation (6.149) yields information on the double point at infinity on each of the v_1 and v_8 axes.

The values for Δ_{v_1} and Δ_{v_8} are obtained by substituting values for the seven variable link DH design parameters into the following two discriminants:

$$\Delta_{v_1} = 32a_7^2\alpha_8^2d_1^2 - AB; \tag{6.180}$$

Table 6.2: Mobility of a_1 and a_7.

Δ_{v_1}	Ω_{v_1}	mobility of a_1	Δ_{v_8}	Ω_{v_8}	mobility of a_7
≥ 0	≥ 0	crank	≥ 0	≥ 0	crank
≥ 0	< 0	π-rocker	≥ 0	< 0	π-rocker
< 0	≥ 0	0-rocker	< 0	≥ 0	0-rocker
< 0	< 0	rocker	< 0	< 0	rocker

and

$$\Delta_{v_8} \quad = \quad 32a_1^2\alpha_8^2d_8^2 - AC, \tag{6.181}$$

where A, B, and C are all defined in Equation (6.179).

From these conditions we can extract information on the ability of the input and output links to rotate through π. For example, if $\Delta_{v_1} \geq 0$, then the double point at $v_1 = \infty$ is either a crunode or a cusp. Knowing that $v_1 = \infty$ corresponds to $\theta_1 = 180°$, this implies that the link a_1 can rotate through π. Similarly, if $\Delta_{v_1} < 0$, then the double point at $v_1 = \infty$ is an acnode which in turn indicates that a_1 has a rotation limit less than π.

It is equally required to investigate whether the linkage is assemblable at $v_i = 0$. Clearly, one possibility to obtain a condition with this information can be derived using the v_1-v_8 equation by substituting $v_i = 0$ and solving for v_j. For each of v_1 and v_8 we obtain a radicand Ω_v whose value must be $\Omega_v \geq 0$ if the link can rotate through 0:

$$\begin{aligned}\Omega_{v_1} \quad = \quad & -\alpha_8^2\left(d_1-d_8\right)^2\left(\alpha_8^2\left(d_1-d_8\right)^2+2\left(d_1+d_8\right)^2\right)-\left(d_1+d_8\right)^4+\\ & 2\left(a_1^2+2a_1a_8-a_4^2+a_7^2+a_8^2\right)\left[4d_8\left(\alpha_8^4d_1-\alpha_8^2d_8-d_1\right)-\left(d_1^2+d_8^2\right)\left(\alpha_8^4+1\right)\right]+\\ & 4\left(a_1^2+2a_1a_8-a_4^2-3a_7^2+a_8^2\right)\alpha_8^2d_1^2-C_1C_2D_1D_2\left(\alpha_8^2+1\right)^2; \end{aligned} \tag{6.182}$$

$$\begin{aligned}\Omega_{v_8} \quad = \quad & -\alpha_8^2\left(d_1-d_8\right)^2\left(\alpha_8^2\left(d_1-d_8\right)^2+2\left(d_1+d_8\right)^2\right)-\left(d_1+d_8\right)^4+\\ & 2\left(a_1^2-a_4^2+a_7^2+2a_7a_8+a_8^2\right)\left[4d_1\left(d_8\alpha_8^4-\alpha_8^2d_1-d_8\right)-\left(d_1^2+d_8^2\right)\left(\alpha_8^4+1\right)\right]+\\ & 4\left(3a_1^2+a_4^2-a_7^2-2a_7a_8-a_8^2\right)\alpha_8^2d_8^2-B_1B_2D_1D_2\left(\alpha_8^2+1\right)^2; \end{aligned} \tag{6.183}$$

where B_1, B_2, C_1, C_2, D_1, and D_2 are all defined in Equation (6.179). With this information we have a completely general classification scheme to determine the relative mobilities of the RSSR, see Table 6.2.

We will verify the mobility classification with an example. Let the DH parameters be $a_1 = 1/8$, $a_4 = 4$, $a_7 = 1$, $a_8 = 1/8$, $\alpha_8 = \tan((60\pi/180)/2)$, $d_1 = 2$, $d_8 = 2$. Evaluating the discriminants with these DH link design parameters reveals that $\Delta_{v_1} = 10.6667$ and $\Omega_{v_1} = 6.437500000$, indicating that a_1 has no mobility limits while $\Delta_{v_8} = -36$ and $\Omega_{v_8} = -12.6667$, indicating that a_7 is a rocker in each assembly mode. It is a simple matter to determine the configuration and the extreme values of v_8 by evaluating the appropriate derivatives of Equation (6.179) for each assembly mode. The corresponding IO curves in both the v_1-v_8 and θ_1-θ_8 planes are illustrated in Figure 6.36 which validates the classification.

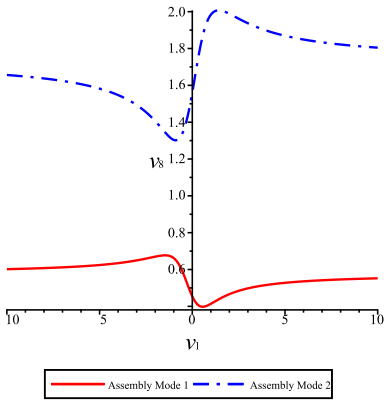

(a) IO curve in v_1-v_8 plane.

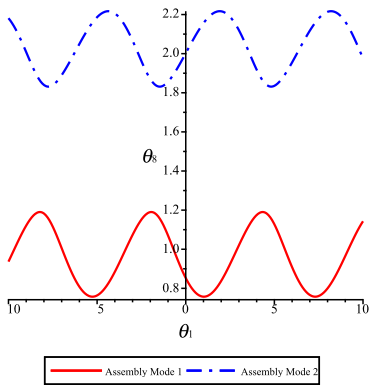

(b) IO curve in θ_1-θ_8 plane.

Figure 6.36: RSSR mobility for $a_1 = 1/8$, $a_4 = 4$, $a_7 = 1$, $a_8 = 1/8$, $\alpha_8 = \tan((60\pi/180)/2)$, $d_1 = 2$, $d_8 = 2$.

Bibliography

[1] Euclid. *The Thirteen Books of the Elements,* second edition, translation by Sir T. L. Heath, vol's 1,2,3. Dover Publications, Inc., New York, N.Y., U.S.A., 1956.

[2] T.Q. Sibley. *Thinking Geometrically: A Survey of Geometries.* The Mathematical Association of America, Washington, DC, U.S.A., 2015.

[3] F. Klein. *Elementary Mathematics from an Advanced Standpoint: Geometry.* Dover Publications, Inc., New York, N.Y., U.S.A., 1939.

[4] J. Angeles. *Spatial Kinematic Chains: Analysis, Synthesis, Optimization.* Springer-Verlag, New York, N.Y., U.S.A., 1982.

[5] F. Grashof. *Theoretische Maschinenlehre,* vol. 2*: Theorie der Getriebe und der Mechanischen Messinstrumente.* Voss, Leipzig, Germany, 1883.

[6] J.M. McCarthy and G.S. Soh. *Geometric Design of Linkages, 2nd Edition* Interdiciplinaty Applied Mathematics. Springer, New York, N.Y., 2011.

[7] J.E. Shigley and J.J. Uicker. *Mechanism and Machine Theory, 2nd ed.* McGraw-Hill, New York, N.Y., U.S.A., 1995.

[8] J.J. Uicker, G.R. Pennock, and J.E. Shigley. *Theory of Machines and Mechanisms,* 5^{th} edition. Oxford University Press, New York, N.Y., 2017.

[9] M. Ceccarelli. *Distinguished Figures in Mechanism and Machine Science, Their Contributions and Legacies Part 1.* Springer, New York, U.S.A., 2007.

[10] J. Watt. Patent No. 1432, April 28, 1784, 1784.

[11] S. Roberts. "On Three-bar Motion in Plane Space". *Proceedings of the London Mathematical Society*, vol. 1: pages 14–23, 1875.

[12] K.H. Hunt. *Kinematic Geometry of Mechanisms.* Clarendon Press, Oxford, England, 1978.

[13] H. Anton. *Elementary Linear Algebra, 5th Ed.* Wiley, New York, N.Y., U.S.A., 1987.

[14] G. Salmon. *A Treatise on the Higher Plane Curves,* third edition. Hodges, Foster, and Figgis, Dublin, Rep. of Ireland, 1879.

[15] E.J.F. Primrose. *Plane Algebraic Curves.* Macmillan & Co. LTD., London, England, 1955.

[16] A.B. Kempe. "On a General Method of Describing Plane Curves of the n^{th} Degree by Linework". *Proceedings of the London Mathematical Society*, vol. 7: pages 213–216, 1876.

[17] E. Bézout. *Théorie Générale des Équations Algébriques.* Kessinger Publishing, Whitefish, MT., U.S.A., 1779.

[18] I. Newton. *The Principia: Mathematical Principles of Natural Philosophy,* English translation by I.B. Cohen, A. Whitman, J. Budenz. University of California Press (Feb. 5 2016), U.S.A., 1687.

[19] O. Bottema and B. Roth. *Theoretical Kinematics.* Dover Publications, Inc., New York, N.Y., U.S.A., 1990.

[20] H.S.M. Coxeter. *Projective Geometry,* 2^{nd} edition. University of Toronto Press, Toronto, On., Canada, 1974.

[21] D.M.Y. Sommerville. *Analytical Geometry of Three Dimensions.* Cambridge University Press, London, England, 1934.

[22] G. Salmon. *Lessons Introductory to the Modern Higher Algebra,* 4^{th} edition. Hodges, Foster, and Figgis, Dublin, Rep. of Ireland, 1885.

[23] J. Plücker. *Theorie der algebraischen Curven.* Adolph Marcus, Bonn, Germany, 1839.

[24] J.J. Craig. *Introduction to Robotics, Mechanics and Control,* 4^{th} edition. Pearson, London, England, 2017.

[25] A. Harnack. Über die Vieltheiligkeit der ebenen algebraischen Curven. *Mathematische Annalen*, 10:189–198, 1876.

[26] M.J.D. Hayes, M.L. Husty, and M. Pfurner. "Input-output Equation for Planar Four-bar Linkages". *Advances in Robot Kinematics 2018,* eds. J. Lenarčič and V. Parenti-Castelli*, Springer, New York*, pages 12–19, 2018.

[27] M.L. Husty and M. Pfurner. An Algebraic Version of the Input-output Equation of Planar Four-bar Mechanisms. International Conference on Geometry and Graphics*, Milan, Italy*, pages 746–757, 2018.

[28] M. Rotzoll. *Algebraic Input-output Equations of Four-bar Kinematic Chains: Planar; Spherical; Spatial.* PhD thesis, Carleton University, Ottawa, ON, Canada, 2023.

[29] F. Freudenstein. "An Analytical Approach to the Design of Four-link Mechanisms.". *Trans. ASME*, vol 77: pages 483–492, 1954.

[30] F. Freudenstein. "Approximate Synthesis of Four-Bar Linkages". *Trans. ASME 77,* pages 853-861, 1955.

[31] F. Freudenstein. *Design of Four-link Mechanisms.* PhD thesis, Columbia University, New York, N.Y., USA, 1954.

[32] S.O. Tinubu and K.C. Gupta. "Optimal Synthesis of Function Generators Without the Branch Defect". *ASME, J. of Mech., Trans., and Autom. in Design*, vol. 106: pages 348–354, 1984.

[33] M.J.D. Hayes, K. Parsa, and J. Angeles. "The Effect of Data-Set Cardinality on the Design and Structural Errors of Four-Bar Function-Generators". *Proceedings of the Tenth World Congress on the Theory of Machines and Mechanisms,* Oulu, Finland, pages 437–442, 1999.

[34] A. Guigue and M.J.D. Hayes. "Continuous Approximate Synthesis of Planar Function-generators Minimising the Design Error". *Mechanism and Machine Theory*, vol. 101: pages 158–167, DOI: 10.1016/j.mechmachtheory.2016.03.012, 2016.

[35] D.J. Wilde. "Error Synthesis in the Least-Squares Design of Function Generating Mechanisms". *ASME, J. of Mechhanical Design*, 104:881–884, 1982.

[36] G. Dahlquist and Å. Björck. *Numerical Methods,* translated from Swedish by N. Anderson. Prentice-Hall, Inc., U.S.A., 1969.

[37] E. Study. *Geometrie der Dynamen.* Teubner Verlag, Leipzig, Germany, 1903.

[38] J.M. Selig. *Geometric Fundamentals of Robotics*. Springer Science + Business Media Inc, New York, NY, U.S.A., 2. edition, 2005.

[39] J.M. Selig. On the Geometry of the Homogeneous Representation for the Group of Proper Rigid-body Displacements. *Rom. J. Techn. Sci.-Appl. Mechanics*, 58(1-2):153–176, 2013.

[40] M. Pfurner. The Family of Two Generator 3-Space Rulings of the Study Quadric. Private Communication, August 25, 2022.

[41] M.L. Husty and H-P. Schröcker. Kinematics and Algebraic Geometry. In J. M. McCarthy, editor, *21st Century Kinematics*, pages 85–123, London, 2013. Springer-Verlag.

[42] M.J.D. Hayes and M.L. Husty. "On the Kinematic Constraint Surfaces of General Three-Legged Planar Robot Platforms". *Mechanism and Machine Theory*, vol. 38, no. 5: pages 379–394, 2003.

[43] S.S. Balli and S. Chand. Transmission Angle in Mechanisms (Triangle in Mech). *Mechanism and Machine Theory*, 37(2):175–195, 2002.

[44] J. Denavit and R.S. Hartenberg. A Kinematic Notation for Lower-pair Mechanisms Based on Matrices. *Trans ASME J. Appl. Mech.*, 22(2):215–221, 1955.

[45] M.L. Husty, A. Karger, H. Sachs, and W. Steinhilper. *Kinematik und Robotik*. Springer-Verlag Berlin, Heidelberg, New York, 1997.

[46] DA.. Cox, J. Little, and D. O'Shea. *Ideals, Varieties, and Algorithms: an Introduction to Computational Algebraic Geometry and Commutative Algebra,* second edition. Springer-Verlag, Berlin, Germany, 1997.

[47] B.W. Mooring, Z.S. Roth, and M.R. Driels. *Fundamentals of Manipulator Calibration*. John Wiley and Sons, Inc., New York, N.Y., U.S.A., 1991.

[48] C.H. An, C.G. Atkeson, and J.M. Hollerbach. *Model-Based Control of a Robot Manipulator*. The MIT Press, Cambridge, Massachusetts, U.S.A., 1988.

[49] S.A. Hayati. "Robot Arm Geometric Link Parameter Estimation". *Proc. 22nd IEEE Conf. on Decision and Control,* San Antonio, TX, pages 1477–1483, 1983.

[50] R.S. Hartenberg and J. Denavit. *Kinematic Synthesis of Linkages*. McGraw-Hill, Book Co., New York, N.Y., U.S.A., 1964.

[51] M. Rotzoll, M.J.D. Hayes, M.L. Husty, and M. Pfurner. A General Method for Determining Algebraic Input-Output Equations for Planar and Spherical 4R Linkages. In Jadran Lenarčič and Bruno Siciliano, editors, *Advances in Robotic Kinematics 2020*, pages 90–97, Cham, Switzerland, 2021. Springer International Publishing.

[52] M.J.D. Hayes, M. Rotzoll, C. Ingalls, and M. Pfurner. Design Parameter Space of Spherical Four-bar Linkages. In Corves B. Pisla, D. and C. Vaida, editors, *New Trends in Mechanism and Machine Science, EuCoMeS*. Springer Nature Switzerland AG.

[53] M. Pfurner. *Analysis of Spatial Serial Manipulators Using Kinematic Mapping*. PhD thesis, University of Innsbruck, Innsbruck, Austria, 2006.

[54] A. Shabani, J.M. Porta, and F. Thomas. A Branch-and-prune Method to Solve Closure Equations in Dual Quaternions. *Mechanism and Machine Theory*, 164, 2021.

[55] W. Adams and P. Loustaunau. *An Introduction to Gröbner Bases*, volume 3. American Mathematical Society, Graduate Studies in Mathematics, 1994.

[56] M.J.D. Hayes, M. Rotzoll, and M.L. Husty. "Design Parameter Space of Planar Four-bar Linkages". Proceedings of the 15^{th} IFToMM World Congress, June 30-July 4, 2019.

[57] M.J.D. Hayes and M. Rotzoll. Dimensional Kinematic Synthesis of Angular Velocity Function Generators. 12th CCToMM Symposium on Mechanisms, Machines, and Mechatronics, ed. C. Gosselin, Université Laval, Québec, QC, Canada, June 19-20, 2023.

[58] R. Kraus. Die Doppelkurbel und ihre Geschwindigkeitsgrenzen. *Maschinenbau/Getriebetechnik*, 18:37–41, 1939.

[59] R. Kraus. Zur Synthese der Doppelkurbel. *Maschinenbau/Getriebetechnik*, 18:93–94, 1939.

[60] N. Rosenauer. Gelenkvierecke mit Vorgeschriebenen Groesst und Kleinstwerten der Abtriebswinkelgeschwindigkeit. *Maschinenbau/Getriebetechnik*, 38:25–27, 1944.

[61] F. Freudenstein. On the Maximum and Minimum Velocities and Accelerations in Four-link Mechanisms. *Transactions of ASME*, 78:779–787, 1956.

[62] M.J.D. Hayes, M. Rotzoll, A. Iraei, A. Nichol, and Q. Bucciol. Algebraic Differential Kinematics of Planar 4R Linkages. 20th International Conference on Advanced Robotics, ICAR 2021, Ljubljana, Slovenia, 2021.

[63] F. Reuleaux. *The Kinematics of Machinery: Outlines of a Theory of Machines,* translated and edited by A.B.W. Kennedy. MacMillan and Co., London, England, 1876.

[64] A.S. Hall. *Kinematics and Linkage Design*. Prentice-Hall, Inc., Englewood Cliffs, N.J., U.S.A., 1961.

[65] L.I. Wu and S. H. Wu. A Note on Freudenstein's Theorem. *Mechanism and Machine Theory*, vol 33(1/2):139–149, 1998.

[66] E.W. Swokowski. *Calculus, a First Course*. PWS-Kent, Nelson, Toronto, Canada, 1988.

[67] A. Nichol, M. Rotzoll, and M.J.D. Hayes. Planar RRRP Mechanism Design Parameter Space. 11th CCToMM Symposium on Mechanisms, Machines, and Mechatronics, eds. S. Nokleby, and P. Cardou, Ontario Tech University, Oshawa, ON, Canada, June 3-4, 2021.

[68] R. Bricard. Mémoire sur la théorie de l'octaèdre articulé. *J. Math. Pures Appl.*, 3:113–148, 1897.

[69] A.P. Murray and P.M. Larochelle. "A Classification Scheme for Planar $4R$, Spherical $4R$, and Spatial $RCCR$ Linkages to Facilitate Computer Animation". Proceedings of 1998 ASME Design Engineering Technical Conferences (DETC'98)*, Atlanta, Georgia, U.S.A.*, September 13-16, 1998.

[70] R. Cipolla and P. Giblin. *Visual Motion of Curves and Surfaces*. Cambridge University Press, Cambridge, U.K., 2000.

[71] H. Hilton. *Plane Algebraic Curves*. Clarendon Press, Oxford, England, 1920.

[72] C.M. Gosselin and J. Angeles. Representation graphique de la region de mobilite des mecanismes plans et spheriques a barres articulees. *Mechanism and Machine Theory*, 22(6):557–562, 1987.

[73] C.M. Gosselin and J. Angeles. Mobility Analysis of Planar and Spherical Linkages. *Computers in Mechanical Engineering*, July/August 1988.

[74] C.M. Gosselin and J. Angeles. Optimization of Planar and Spherical Function Generators as Minimum-defect Linkages. *Mechanism and Machine Theory*, 24(4):293–307, 1989.

[75] H.S.M. Coxeter. *Regular Polytopes, 3^{rd} Edition*. Dover Publications, Inc., New York, NY, U.S.A., 1973.

[76] M. Rotzoll, Q. Bucciol, and M.J.D. Hayes. Algebraic Input-output Angle Equation Derivation Algorithm for the Six Distinct Angle Pairings in Arbitrary Planar 4R Linkages. In *20th International Conference on Advanced Robotics, ICAR 2021,* Ljubljana, Slovenia, 2021.

[77] B. Segre. *The Non-singular Cubic Surfaces; a New Method of Investigation with Special Reference to Questions of Reality*. Oxford, The Clarendon Press, 1942.

[78] G.T. Bennett. A new mechanism. *Engineering*, 76:777, 1903.

[79] J.E. Baker. Kinematic investigation of the deployable bennett loop. *Journal of Mechanical Design*, 129(6):602–610, 2006.

[80] J. Denavit. *Description and Displacement Analysis of Mechanisms Based on (2x2) Dual Matrices*. PhD thesis, Northwestern University, 1956.

[81] M. Pfurner, T. Stigger, and M.L. Husty. Algebraic analysis of overconstrained single loop four link mechanisms with revolute and prismatic joints. *Mechanism and Machine Theory*, 114:11–19, 2017.

[82] J.S. Beggs. *Mechanism*. McGraw-Hill, New York, NY, U.S.A., 1955.

[83] H. Nolle. Ranges of Motion Transfer by the R-G-G-R Linkage. *Journal of Mechanisms*, 4(1):145–157, 1969.

[84] F.C.O. Sticher. Mobility Limit Analysis of R-S-S-R Mechanisms by "Ellipse Diagram". *Journal of Mechanisms*, 5(1):393–414, 1970.

[85] O. Bottema. The Motion of the Skew Four-bar. *Journal of Mechanisms*, 6(1):69–79, 1971.

[86] F. Freudenstein and E.J.F. Primrose. On the Criteria for the Rotability of the Cranks of a Skew Four-bar Linkage. *ASME Journal of Engineering for Industry*, 98(4):1285–1288, 1976.

[87] S. Molian. Kinematics and Dynamics of the RSSR Mechanism. *Journal of Mechanisms*, 6(1):69–79, 1971.

[88] J. Duffy and M.J. Gilmartin. Displacement Analysis of the Generalised RSSR Mechanism. *Mechanism and Machine Theory*, 13(5):533–541, 1978.

[89] A.J. Wilhelm and R. Sodhi. Design of RSSR Function Generator by Curve Matching. In *Unknown Host Publication Title*, pages 118–123. Japan Soc of Precision Engineers, 1984.

[90] C. Mazzotti, M. Troncossi, and V. Parenti-Castelli. Dimensional Synthesis of the Optimal RSSR Mechanism for a Set of Variable Design Parameters. *Meccanica*, 52(1):2439–2447, 2017.

[91] B. Ravani and B. Roth. Motion Synthesis Using Kinematic Mappings. *ASME J. Mech., Trans., and Automation*, 105(3):460–467, 1983.

[92] D.R. Walter and M.L. Husty. On Implicitization of Kinematic Constraint Equations. *Machine Design & Research (CCMMS 2010)*, 26:218–226, 2010.

[93] A.J. Sommese and C.W. Wampler. *The Numerical Solution Of Systems Of Polynomials Arising In Engineering And Science*. World Scientific Publishing Co. Pte. Ldt., Hackensack, NJ, U.S.A., 2005.

[94] A.V.M. Rao, G.N. Sandor, D. Kohli, and A.H. Soni. Closed Form Synthesis of Spatial Function Generating Mechanism for the Maximum Number of Precision Points. *ASME J. Eng. Ind.*, 95(3):725–736, 1973.

[95] M.L. Husty and D.R. Walter. *Mechanism Constraints and Singularities - the Algebraic Formulation*, pages 101–180. CISM International Centre for Mechanical Sciences 589. Springer International Publishing, Cham, Switzerland, 2019.

[96] D.A. Cox, J. Little, and D. O'Shea. *Using Algebraic Geometry*. Springer Science + Business Media Inc., New York, NY, U.S.A., 2. edition, 2004.

[97] A. Dresden. *Solid Analytic Geometry and Determinants*. John Wiley & Sons, Inc., New York, NY, U.S.A., 1930.

[98] D.J. Bates, A.J. Sommese, J.D. Hauenstein, and C.W. Wampler. *Numerically Solving Polynomial Systems with Bertini*. SIAM, Philadelphia, PA, U.S.A., 2013.

[99] J.D. Hauenstein and A.J. Sommese. Witness Sets of Projections. *Applied Mathematics and Computation*, 217(7):3349–3354, 2010.

[100] D. Kincaid and W. Cheney. *Numerical Analysis: Mathematics of Scientific Computing*. American Mathematical Society, Provedince, RI, U.S.A., 2002.

[101] D.A. Cox. *Applications of Polynomial Systems*, volume 134. CBMS Regional Conference Series in Mathematics, American Mathematical Society, Providence, RI, U.S.A., 2020.